Uncoded Space-Time Labeling Diversity with Three Transmit Antennas: Symbol Mapping Designs and Error Performance Analysis

Dauda Olayinka Ayanda

Supervisor: Professor Hongjun Xu

A thesis submitted in fulfillment of the requirement for the degree of

Doctor of Philosophy in Electronic Engineering

School of Engineering
University of KwaZulu-Natal
South Africa

June, 2020

As the candidate's supervisor, I have approved the submission of this thesis.

Signed.....

Date.....

Name: Professor Hongjun Xu

Declaration 1 - Plagiarism

I, **Dauda Olayinka Ayanda**, declare that;

1. The research reported in this thesis, except where otherwise indicated, is my original research.
2. This thesis has not been submitted for any degree or examination at any other university.
3. This thesis does not contain other persons' data, pictures, graphs or other information, unless specifically acknowledged as being sourced from other persons.
4. This thesis does not contain other persons' writing, unless specifically acknowledged as being sourced from other researchers. Where other written sources have been quoted, then:
   (a) Their words have been re-written but the general information attributed to them has been referenced,
   (b) Where their exact words have been used, then their writing has been placed in italics and inside quotation marks, and referenced.
5. This thesis does not contain text, graphics or tables copied and pasted from the Internet, unless specifically acknowledged, and the source being detailed in the thesis and in the references sections.

Signed.....Date.....

Declaration 2 - Publication

DETAILS OF CONTRIBUTION TO PUBLICATIONS that form part and/or include research presented in this thesis. The following journal papers emanating from this work have been either published or are *in preparation* for submission:

1. Uncoded M-ary quadrature amplitude modulation space-time labeling diversity with three transmit antennas. *Published in International Journal of Communication System.*
2. Performance Analysis of *M*-ary APSK Uncoded Space-time Labeling Diversity with Three Transmit Antennas in Rician Broadcast Channels. *In preparation for submission.*
3. Symbol Mapping Design and Error Analysis of Cross-QAM Uncoded Space-Time Labeling Diversity with Three Transmit Antennas. *In preparation for submission.*
4. Design and Analysis of Rectangular QAM Uncoded Space-Time Labeling Diversity with Three Transmit Antennas Scheme over Nakagami-*q* Fading Channels. *In preparation for submission to a letter.*

The following conference papers have been published or *in press* during this doctoral research:

1. A Unified Error Analysis of Uncoded Space-Time Labeling Diversity with Three Transmit Antennas in Rician Fading Channels. *Published as conference proceedings in Institute of Electrical and Electronic Engineers (IEEE) Xplore 2019.* **The paper won best paper award.**
2. Closed-form Analysis of Uncoded Space-Time Labeling Diversity Schemes over Downlink Nakagami-*q* Fading Channel. *Published as conference proceedings in Southern Africa Telecommunication Networks and Applications Conference (SATNAC) 2019.*
3. High-Density *M*-QAM Mapper Design for Uncoded Space-Time Labeling Diversity with Three Transmit Antennas over Nakagami-*m* Fading Channels. *in press for publication after presentation at IEEE AFRICON 2019.*

Dedication

Glory to thy, The Almighty Allah. .*Subhanaka Ya Allahu*

Glory to thy, The Compassionate... ...*Subhanaka Ya Hanan*

Glory to thy, The Benefactor .... *Subhanaka Ya Manan*

Glory to thy, The Discharged from Debt.. ..*Subhanaka Ya Dayan*

Glory to thy, The Supreme .... *Subhanaka Ya Sultan*

... in loving memory of my beautiful mother. You are so loved and missed!

... for loneliness of thoughts of my son - Sulaiman Akorede Ayanda.

... for sacrifices of unsung heroes and heroines of my adventures.

Acknowledgements

"*Blessed be all sorrow, hardships and endurance that demand courage. Blessed be these things: for of these things cometh the making of a man*". Peter - the hero of Hugh Walpole's novel entitled 'Fortitude'.

First, I am eternally grateful to the Lord of the world, Almighty Allah for the courage, inspiration and perseverance to complete this thesis. Indeed! I attest to His Majesty for all things bright and beautiful, all creatures great and small, all things wise and wonderful, the Lord God made them all.

My profound gratitude goes to my supervisor, Professor Hongjun Xu, for his selfless research guidance, dedication and invaluable advice that led to the success of my PhD thesis submission. I also want to acknowledge his humane personality of arriving at King Shaka International Airport thirty minutes before my flight landing to pick me up on my first coming to South Africa and to ensure my safety. Thank you Professor Xu for this kindness!

It is with pleasure that I thank Dr Narushan Pillay for his extensive and detailed reviews and useful suggestions that improve my academic writing skills. I am highly indebted to all my research colleagues and mentors with whom I enjoyed discussing problems and sharing ideals. Notably include Reggie Pillay, Buthanani Dlodlo, Ronald Tsvaki, Segun Oladoyinbo and Wamolambo Ramasila. Special appreciation to Dr Tahmid Quazi, Dr Peter Akuon, Dr Shoaib Mughal, Dr Sulaiman Patel and Dr Babatunde Adejumobi.

I acknowledge with immense gratitude the financial grants of the Centre for Radio Access and Rural Technologies (CRART), University of KwaZulu-Natal in support of 2019 SATNAC and 2019 IEEE AFRICON conferences attendance. I also acknowledge the College of Engineering Grant for participation at 2019 IEEE Wireless Africa conference in Pretoria.

I would like to acknowledge Dr Leigh Jarvis, the discipline academic leader as well as member of academic staff of Discipline of Electrical, Electronic and Computer Engineering for their tremendous support while serving IEEE South Africa Section as Executive Vice Chair and IEEE Eta Kappa Nu

(IEEE-HKN) as Mu Eta Chapter President. Special thanks to Professor Glen Bright, the Dean of College of Engineering, for his support and for sharing his leadership experience during 2018/19 Mu Eta Chapter induction ceremony as the guest speaker. Indeed! It was one of my most humbling experience to have worked with a team of distinguished experts in advancing IEEE mission in South Africa as well as the rare opportunity of leading a prestigious IEEE-HKN Electrical Engineering Honour Society's Chapter.

I deeply appreciate the support of member of academic community of University of Ibadan. I acknowledge the support of the current University Librarian, Dr Helen Komolafe-Opadeji, Dr Benedict Oladele (immediate past University Librarian), Professor Adeyinka Aderinto (immediate past Deputy Vice-Chancellor Academic), Professor AbdulRahman Oloyede (Chief Imam, Muslim Community), Dr Olubunmi Oyemade, Dr Babatunde Ajala, Dr Jeremiah Arowosegbe, Mr Reuben Ojo, Engineer Babatunde Adewolu, Mrs Aderinsola Kayode and Mrs Seun Egbodo.

I appreciate the immense moral and financial supports of Professor AbdulGaniy Raji, Dr Khadeejah AbdulSalam, Dr Lukman Akanbi, Sulaiman Taiwo, Shuaib Idris, AbdulKabeer Olalere and Qamardeen Olaniyan. Special thanks to Dr Babajide Afolayan, Dr Enoruwa Obayiuwana, Dr Efe Orumwense, Dr Adebayo Kutu, Dr Armeline Mafuta, Dr Steven Awilo, Dr Sibongukiphiwa L. Nene, Dr Sakhile Magadla, Adefolarin Bolaji, Akeem Abodunrin, Engineer Yunus Adejumo, Bamidele Kolawole, Bukola Ajewole, Korede Oluyide, Hammed Abass, Kazeem Aremu, AbdulRahman Mogbonjubola, Ajibola Adigun and Udoh James Akpan for their support and for showing that no one achieves greatness in isolation.

And finally, thanks to my family for their support. God bless you all!

Abstract

Uncoded space-time labeling diversity (USTLD) is a relatively new proposed multiple-input, multiple-output (MIMO) scheme for two transmit antennas. The fundamental idea of USTLD is to transmit two different mapped symbols pair in two consecutive time slots.

In this thesis, the first objective is to develop USTLD with three transmit antennas. Such a scheme has not been reported in open literature to date. Hence, a heuristic algorithm is proposed to design the second and third mappers for square quadratic amplitude modulation (QAM). An analytical expression for a tight bound of the average bit error probability (ABEP) of the proposed system with three transmit antennas over independent and identically distributed (i.i.d) Rayleigh fading channels is derived and the accuracy of this bound is verified by Monte Carlo simulation results which shows superior error performance compared with the existing two transmit antenna USTLD. Moreover, complexity reduction analysis of the low-complexity (LC) detector is proposed. It is shown that the proposed LC algorithm achieves near-maximum likelihood detection accuracy, while reducing complexity by 51% and 96.5% for 16QAM and 64QAM, respectively.

Motivated by the nonlinear channels typical of digital broadcasting systems, M-ary amplitude phase-shift keying (M-APSK) is a modulation scheme that has become widely adopted for the second generation of digital video broadcasting for satellites (DVB-S2) and its extension (DVB-S2X) which offers an attractive combination of spectral and energy efficiency. The second objective of this thesis is to investigate the design of labeling mappers for USTLD with three transmit antennas based on amplitude and phase shift keying (APSK) modulation. The proposed USTLD schemes are DVB-S2 and DVB-S2X standards compatible for both Rician fast frequency-flat fading and quasi-static frequency-flat fading channels. Numerical analysis of the proposed schemes are derived based on pairwise error probability. The analytical results are validated by Monte Carlo simulations, which converge accurately at high signal-to-noise ratio (SNR). Furthermore, by adapting constellation structure between square QAM modulations and concentric rings of APSK modulations, the authors proposed mapper design for 16-APSK, 32-APSK and 64-APSK modulations for USTLD scheme

using heuristic algorithm. Finally, the proposed USTLD schemes show bit error rate (BER) improvement over the existing two transmit USTLD schemes with error performance gain of 1.2 dB and 2.8 dB at a BER of 10^{-6} for 16-APSK and 64-APSK USTLD scheme, respectively.

In addition, square QAM USTLD scheme has been widely used due to its high power and bandwidth efficiency. However, square QAM does not provide satisfying requirements for a system where the number of bits per symbol is odd. In this scenario, the peak and the average power of transmission can be reduced by using cross QAMs (XQAMs) instead. The third objective of this thesis is to investigate the design of XQAM labeling mappers for USTLD with three transmit antennas over i.i.d. Nakagami-m fading channels. The theoretical ABEP is derived based on pairwise error probability. This expression is validated by Monte Carlo simulation results, which converge accurately at high SNR. Since channels are not i.i.d in practical sense, the authors further investigate XQAM USTLD scheme in correlated channels. The ABEP for the proposed system is derived and served to validate the Monte Carlo simulation results. Finally, the impact of channel correlation are demonstrated by comparing the BER results in correlated channels with that of i.i.d channels.

Contents

Declaration 1 - Plagiarism ii

Declaration 2 - Publication iii

Dedication iv

Acknowledgements v

Abstract vii

List of Figures xiv

List of Figures xiv

List of Tables xvi

List of Tables xvi

List of Acronyms xvii

Preface xxi

I Introduction 1

1 Introduction to Wireless Communication 2

1.1 Review of Fading Channel Models 3

1.1.1 The Rayleigh fading channel 3

1.1.2 The Nakagami-*q* fading channel 3

1.1.3 The Nakagami-*m* fading channel 4

1.1.4 The Nakagami-*n* fading channel 5

1.2 Wireless Channel Impairments 5

1.2.1 Noise 5

1.2.2 Path loss . . . 6
1.2.3 Shadowing . . . 6
1.2.4 Fading . . . 6
1.3 Diversity Techniques . . . 7
1.3.1 Space diversity . . . 7
1.3.2 Polarization diversity . . . 9
1.3.3 Frequency diversity . . . 9
1.3.4 Time diversity . . . 9
1.4 Classification of Diversity . . . 10
1.4.1 Macro diversity . . . 10
1.4.2 Micro diversity . . . 10
2 Space-time Coding . . . 10
2.1 Layered Space-Time Code . . . 11
2.2 Space-Time Trellis Code . . . 11
2.3 Super-Orthogonal Space-Time Trellis Code . . . 12
2.4 Space-Time Block Code . . . 12
2.5 Space-Time Labeling Diversity . . . 13
2.5.1 Coded STLD . . . 13
2.5.2 Uncoded STLD . . . 14
3 Research Motivation and Contributions . . . 14
3.1 Paper A: . . . 15
3.2 Paper B: . . . 16
3.3 Paper C: . . . 16
4 Structure of the Thesis . . . 17
References . . . 18

II Paper A **23**

A Uncoded M-ary Quadrature Amplitude Modulation Space-Time Labeling Diversity with Three Transmit Antennas **24**

1 Abstract . . . 25
2 Introduction . . . 26
3 System Model . . . 27
3.1 Existing USTLD system model . . . 27

3.2 Proposed USTLD system model 28
4 Error Performance analysis of USTLD with Three Transmit Antennas 30
5 Design of the Second and the Third M-QAM Mapper in USTLD with three transmit antennas 32
6 Detection Schemes 37
6.1 ML detection 37
6.2 Proposed LC detection scheme for USTLD 37
6.3 Complexity derivations of LC detection scheme for USTLD 38
6.4 Computational complexity comparison 39
7 Simulation and Discussion 39
8 Conclusion 42
9 Appendix A 43
References 44

III Paper B **46**

B Performance Analysis of *M*-ary APSK Uncoded Space-time Labeling Diversity with Three Transmit Antennas in Rician Broadcast Channels **47**
1 Abstract 48
2 Introduction 49
2.1 Contributions 51
2.2 Notations 52
3 System Model 52
3.1 Transmitter Model 52
3.2 Rician Channel Model 53
3.3 ML Detection 54
4 Error Performance Analysis 54
4.1 Rician fading error analysis 55
5 Mapper Design 56
6 Results and Discussion 58
6.1 Validation of Analytical Results in quasi-static and fast fading channels . . . 59
6.2 BER Comparison for Rate One with existing APSK USTLD $N_T = 2$ 61
7 Conclusion 62
8 Appendix B 63

References 65

IV Paper C **69**

C Symbol Mapping Design and Error Analysis of Cross-QAM Uncoded Space-Time Labeling Diversity with Three Transmit Antennas **70**

1 Abstract 71

2 Introduction 72

3 System Model 74

3.1 Uncorrelated Channel Modeling 74

3.2 Correlated Channel Modeling 75

3.3 Maximum Likelihood Detection (ML) 76

4 Error Performance Analysis 76

4.1 Uncorrelated Error Analysis 77

4.2 The special case of m = 1 for Nakagami-m in i.i.d channels 78

4.3 Correlated Error Analysis 79

5 Design of the Labeling Mappers 80

6 Numerical Results and Discussion 81

6.1 BER validation in uncorrelated USTLD Nakagami-m channel 82

6.2 Average BER in correlated channels with antenna spacing 82

7 Conclusion 84

8 Appendix C 85

References 87

V Conclusion **89**

1 Conclusion 90

2 Future Research 91

2.1 Higher Order Mapper Design for USTLD Scheme 91

2.2 Optimization Algorithm using Artificial Intelligence Concept 91

2.3 Large Scale Fading for USTLD Scheme with Transmit Antennas 91

2.4 Further Application of USTLD Scheme to Digital Broadcasting 91

2.5 Application of USTLD Scheme to Hybrid Satellite-Terrestrial MIMO 92

2.6 Application of Index Modulation for USTLD Scheme with three Transmit Antennas 92

2.7 Impact of Channel Estimation Error on USTLD Scheme with three Transmit Antennas 93
References 94

List of Figures

List of Figures

1 Space Diversity Reception with (A) SISO, (B) SIMO, (C) MISO, and (D) MIMO [31] 8

2 USTLD with two transmit antennas scheme [10] 14

A.1 System model of three transmit antenna uncoded space-time labeling diversity (USTLD). RF, radio frequency 29

A.2 Three transform of 4-ary pulse amplitude modulation 34

A.3 Mappers of 8-ary pulse amplitude modulation 34

A.4 16-quadrature amplitude modulation Gray-coded labeling map Ω_1^{16}, optimized maps Ω_2^{16}, and Ω_2^{16} 35

A.5 64-quadrature amplitude modulation Gray-coded labeling map Ω_1^{64}, optimized maps Ω_2^{64}, and Ω_2^{64} 36

A.6 Bit error rate (BER) performance of uncoded space-time labeling diversity (USTLD) systems for 16-quadrature amplitude modulation using maximum likelihood and low-complexity detectors. SNR, signal-to-noise ratio 41

A.7 Bit error rate (BER) performance of uncoded space-time labeling diversity (USTLD) systems for 64-quadrature amplitude modulation using maximum likelihood and low-complexity detectors 41

B.1 System model of the proposed A-USTLD 53

B.2 Constellation Mappers for: (A) existing 16-QAM, (B) proposed 16-APSK USTLD . 58

B.3 Constellation Mappers for: (A) 32-RQAM, (B) proposed 32-APSK USTLD 59

B.4 Constellation Mappers for: (A) one quadrant of 64-QAM, (B) equivalent one quadrant of 64-APSK, (C) proposed 64-APSK USTLD 60

B.5 Validation of BER for APSK modulation with *M*=16-APSK, 32-APSK and 64-APSK in Rician broadcast channel 61

B.6 BER Comparison for USTLD APSK modulation schemes with *M*=16-APSK and 64-APSK in Rician broadcast channel 62

C.1 System model of the proposed XQAM-USTLD 75

C.2 32-XQAM constellations and optimized mappers for three transmit antennas USTLD scheme 80

C.3 128-XQAM constellation and optimized mapper for three transmit antennas USTLD scheme 81

C.4 Validation of BER for CrossQAM modulation with *M*=32, 128-XQAM, in i.i.d Nakagami-*m* fading channel 82

C.5 Validation of BER for CrossQAM modulation with *M*=32, 128XQAM, *m*=2 in Correlated Nakagami-m fading channel 83

C.6 BER Comparison for CrossQAM modulation with *M*=32, 128-XQAM, *m*=2, $c = 0.2\lambda$ in i.i.d and Correlated Nakagami-*m* fading channel 84

List of Tables

List of Tables

A.1 Mapping for two transmit antenna systems 33
A.2 Mapping for three transmit antenna systems 35
A.3 Computational complexities between ML and proposed LC detectors for USTLD . . 40

B.1 USTLD APSK Modulation Scheme for DVB-S2X Standard [2] 57

List of Acronyms

1G	First Generation Communication Systems
4G	Fourth Generation Communication Systems
5G	Fifth Generation Communication Systems
6G	Sixth Generation Communication Systems
ABEP	Average Bit Error Probability
ADSL	Asymmetric Digital Subscriber Line
APSK	Amplitude and Phase Shift Keying
AWGN	Additive White Gaussian Noise
A-USTLD	Amplitude and Phase Shift Keying-based Uncoded Space-Time Labeling Diversity
BER	Bit Error Rate
BI-STCM	Bit-Interleaved Space-Time Coded Modulation
BPSK	Binary Phase Shift Keying
CR	Constellation Rearrangement
CSI	Channel State Information
DLST	Diagonally Layered Space-Time
DVB-C	Digital Video Broadcasting Cable
DVB-NGH	Digital Video Broadcasting - Next Generation Handheld
DVB-S2	Digital Video Broadcasting Second Generation
DVB-S2X	Digital Video Broadcasting Second Extensions Generation

DVB-T2	Digital Video Broadcasting Second Generation Terrestrial
ETSI	European Telecommunications Standards Institute
FDM	Frequency Division Multiplexing
i.i.d	Independent and Identically Distributed
IEEE	Institute of Electrical and Electronic Engineers
HLST	Horizontally Layered Space-Time
LOS	Line-of-Sight
MbM	Media-based Modulation
MED	Minimum Euclidean Distance
MGF	Moment Generating Function
MI	Mutual Information
MIMO	Multiple-input Multiple-output
MISO	Multiple-input Single-output
ML	Maximum Likelihood
MODCOD	Modulation and Coding
MRC	Maximum Ratio Combining
M-PSK	M-ary Phase Shift Keying
LC	Low Complexity
LDPC	Low Density Parity Check
LST	Layered Space-Time
OFDM	Orthogonal Frequency Division Multiplexing
OP	Orthogonal Projection
OSTBC	Orthogonal Space-Time Block Codes
PAM	Pulse Amplitude Modulation
PDF	Probability Density Function
QAM	Quadrature Amplitude Modulation

QPSK	Quadratic Phase Shift Keying
RF	Radio Frequency
RQAM	Rectangular Quadrature Amplitude Modulation
RVs	Random Variables
PAPR	Peak to Average Power Ratio
PED	Product Euclidean Distance
PEP	Pairwise Error Probability
SD	Sequential Decoding
SEP	Symbol Error Probability
SIMO	Single-input Multiple-output
SISO	Single-input Single-output
SNR	Signal-to-Noise Ratio
SOBC	Super-Orthogonal Block Coding
SOSTTC	Super-Orthogonal Space-Time Trellis Coding
STBC	Space-Time Block Codes
STBC-SM	Space-Time Block Codes Spatial Modulation
STC	Space-Time Coding
STCM	Space-Time Coded Modulation
STLD	Space-Time Labeling Diversity
STTC	Space-Time Trellis Coding
TAD	Transmit Antenna Diversity
TCM	Trellis Coded Modulation
USTLD	Uncoded Space-Time Labeling Diversity Scheme
USTLD-STCM	Uncoded Space-Time Labeling Diversity Space-Time Coded Modulation
VDSL	Very High Speed Digital Subscriber Line
Wi-Fi	Wireless Fidelity

WLAN Wireless Local Area Network

XQAM Cross Quadrature Amplitude Modulation

Preface

The research discussed in this thesis is carried out in the College of Agriculture, Engineering and Science of the University of Kwa-Zulu Natal, Durban, from January 2016 until November 2019 by Dauda Olayinka Ayanda under the supervision of Professor Hongjun Xu.

As the candidate's supervisor, I, Hongjun Xu, agree to the submission of this thesis.

Signed:..... Date:.....

I, Dauda Olayinka Ayanda, hereby declare that all the material incorporated in this thesis are my own original work, except where acknowledgement is made by name or in the form of a reference. The work contained in herein has not been submitted in any form for any degree or diploma to any other institution.

Signed:..... Date:.....

University of KwaZulu-Natal, June 25, 2020

Part I

Introduction

1 Introduction to Wireless Communication

The rapid growth in wireless communication technology has led to an increasing demand for high data rate communication systems. This is feasible in technological progression from first generation communication systems (1G) through fourth generation systems (4G) until the current fifth generation systems (5G) with gradual and substantial shift towards the use of higher, less congested frequencies band [1], [2], [3]. Besides, as 5G is currently in the final phase of developing and close to its massive commercialization as a result of increasing demand for cellular network [4], there is new research and industrial efforts towards development of the sixth generation (6G) wireless communication technologies [5].

Recent research in wireless communication systems have shown that large gains in the throughput and reliability of communication schemes over wireless channels can be achieved by utilizing multiple antennas in the transmission as well as reception of wireless communication systems, known as multiple-input multiple-output (MIMO) techniques. MIMO is an appealing technology that promises to achieve improved spectral efficiency and reliability without adding bandwidth and ultimately enhances system performance gains by reducing bit error rate [1] - [3], [6] [7] [8]. As a result, it has drawn much attention in both academia and industry.

MIMO schemes are efficient techniques for enhancing the error performance gain of a system, but in order to exploit the huge potential of MIMO techniques, it is necessary to resort to new transmit strategies, referred to as Space-Time Coding (STC), which utilize the spatial domain between the transmitter and the receiver in addition to the time and spectral domain [6].

STC is a relatively recent scheme that is broadly used in wireless communication systems as a result of enhancements in reliability and spectral efficiency of MIMO techniques [9]. STC transmits signal across the spatial and time domain concurrently in order to achieve diversity gain while conserving bandwidth resources. Hence, STC has been studied in both coded and uncoded wireless communications. Uncoded space-time labeling diversity scheme (USTLD) which is the main goal of this research has recently been introduced in the literature as a MIMO technique whereby two transmit signal paths with bit-to-constellation labeling mappers are created, each of which experiences independent fading paths [10].

In this thesis, we extend the original USTLD in [10] to a new USTLD scheme with three transmit antennas for square M-ary quadrature amplitude modulation (M-QAM) in Rayleigh fading channels in order to improve the error performance gain over the existing scheme. In addition, we present USTLD scheme with three transmit antennas for other transmission techniques in M-ary amplitude

and phase shift keying (APSK) modulation, Cross-QAM (XQAM) and Rectangular QAM for different modulation schemes that are applicable to next-generation wireless communication technology. Moreover, there are different small-scale fading distributions that describe the statistical behaviour of the multipath fading envelope. As such, we also investigate USTLD with three transmit antennas scheme in Nakagami (-q, $-m$, $-n$) fading channels.

1.1 Review of Fading Channel Models

Due to the existence of a great variety of fading environments, several statistical models are used to describe the probability distribution of the received signal amplitude. In this study, we consider Rayleigh fading, Nakagami (-q, $-m$, $-n$) fading channels. Nakagami-n is otherwise known as Rician fading channels.

1.1.1 The Rayleigh fading channel

The Rayleigh fading channel model is used to describe propagation paths where there is no strong line-of-sight (LOS) path between the transmitter and the receiver [11] [12]. This statistical distribution is often used to model multipath fading in urban areas where there exist a large number of reflectors with no LOS component. Based on central limit theorem, the fading coefficient of the in-phase and quadrature-phase components of the received signal in independent and identically distributed (i.i.d) Gaussian random variables (RVs) with unit variance and zero mean can be expressed as:

$$\alpha = \alpha^I + j\alpha^Q \tag{1}$$

where α^I denotes the in-phase component and α^Q represents the quadrature component. Both α^I and α^Q are Gaussian RVs with zero mean and variance of $\frac{1}{2}$. The fading amplitude is expressed as [13]:

$$A = \sqrt{|\alpha^I|^2 + |\alpha^Q|^2} \tag{2}$$

The fading amplitude A is said to be Rayleigh distributed with probability density function (PDF) which can be expressed as [13]:

$$f(A) = \frac{A}{\sigma^2} \exp\left(\frac{-A^2}{2\sigma^2}\right) \tag{3}$$

where σ^2 is the variance of A.

1.1.2 The Nakagami-q fading channel

The Nakagami-q fading channel is widely applied in the literature to model fading conditions more severe than Rayleigh distribution [14], [15]. Nakagami-q distribution shows good ability to describe

the statistics of real-world fading channels and models scintillation effects for signal propagation in satellite links. The fading parameter, q, lies in the range $0 \leq q \leq 1$. Thus, Nakagami-q fading distribution ranges from one sided Gaussian distribution (that is, $q = 0$) to Rayleigh distribution (that is, $q = 1$).

In Nakagami-q fading channels, the Gaussian RVs distributed with unit variance and zero mean is model as in-phase $a^I \sim \mathcal{N}(0, \frac{1}{1+q^2})$ and quadrature $a^Q \sim \mathcal{N}(0, \frac{q^2}{1+q^2})$. The PDF is defined as [13]:

$$f_\gamma(\gamma) = \frac{1+q^2}{2q\bar{\gamma}} \exp\left[-\frac{(1+q^2)^2\gamma}{4q^2\bar{\gamma}}\right] \mathbf{I}_o\left[\frac{(1-q^4)\gamma}{4q^2\bar{\gamma}}\right] \gamma \geq 0 \tag{4}$$

Note that $\mathbf{I}_o$ is the modified zeroth-order Bessel function of the first kind.

1.1.3 The Nakagami-*m* fading channel

Nakagami-*m* distribution was a novel fading channel first proposed in the 1940's to model rapid fading in long-distance wireless channels [16]. Nakagami-*m* channels model fading scenarios whereby the received signal has contributions from both scattered and specular components, that is, the electric field is the sum of a strong component (which is not necessarily LOS) and several components with less amplitude [17]. Both of these components are random, that is, circularly symmetric complex Gaussian RVs. The shape factor, *m*, refers to the relationship between the amplitudes of strong component and that of weak component, and ranges from $\frac{1}{2}$ to ∞. Rayleigh fading is obtained from the Nakagami-*m* model when *m*=1. In a single cluster, the phases of individual reflected waves are random, but the time delays are approximately equal for all waves. As a result, the envelope of each cluster signal is Rayleigh distributed given by [18]:

$$g(t) = \frac{1}{\sqrt{N_R}} \sum_{n=1}^{N_R} \exp[j(w_d t \cos\alpha_n + \varphi_n)] \tag{5}$$

where $g(t)$ is the baseband signal of the normalized Clarke's 2-D isotropic scattering Rayleigh fading models. N_R and w_d correspond to the number of propagation paths and the maximum angular Doppler frequency, respectively. α_n and φ_n denote the angle of arrival and initial phase of nth propagation path, respectively whereby α_n and φ_n are both uniformly distributed over $[-\pi, \pi]$.

Unlike most fading distributions that model certain conditions, the Nakagami-*m* fading model is capable of modeling a wide range of fading channel conditions and it fits well the empirical data [12]. Thus, Nakagami-*m* distribution is a generalized fading model that is very similar to Rician fading distribution. However, the specular (strong) component in the Rician distribution is deterministic. In addition, the Nakagami-*m* PDF has a closed-form analytical expression that is simpler to evaluate

numerically and fits better some measurements than Rician or Nakagami-*q* fading channels. It is to be noted that Nakagami-*m* PDF does not contain Bessel functions.

Moreover, there is a mathematical relationship which exists between the Rician distribution *K*-factor and Nakagami-*m* *m*-parameter, and is given as [11].

$$m = \frac{(K+1)^2}{(2K+1)} \tag{6}$$

1.1.4 The Nakagami-*n* fading channel

The Nakagami-*n* statistical distribution is frequently used to describe propagation paths which consists of one strong direct LOS component and many random weaker components [12]. The PDF for Nakagami-*n* fading amplitude is modelled as [16]:

$$f_\gamma(\gamma) = \frac{2(1+n^2)e^{-n^2}\gamma}{\bar{\gamma}} \exp\left[-\frac{(1+n^2)\gamma^2}{\bar{\gamma}}\right] \times \boldsymbol{I}_0\left(2n\gamma\sqrt{\frac{(1+n^2)}{\bar{\gamma}}}\right) \tag{7}$$

Note that *n* denotes the Nakagami-*n* fading parameter which ranges from 0 to ∞ and is related to Rician *K* factor by $K = n^2$. On the other hand, the *K*-factor refers to the ratio of the average signal power of dominant specular component for LOS and the average signal power of the weaker diffused component. Mathematically, *K*-factor could be expressed as [12]:

$$K = \frac{(h_D^I)^2 + (h_D^Q)^2}{2\sigma^2} \tag{8}$$

where h_D^I and h_D^Q are constant values for in-phase and quadrature component of LOS. Thus, Nakagami-*n* fading model is also known as Rician distribution.

1.2 Wireless Channel Impairments

Due to natural and constructive obstacles, the signals transmitted through radio propagation are restricted in bit error performance gain. Some of the impairments that affects the wireless communication systems are discussed in the subsections below:

1.2.1 Noise

Noise refers to the unwanted random components of an electrical signal that tend to disturb the transmission and processing of the signal [11]. Generally, noise arises from several natural phenomena, such as the fluctuation of electrical characteristics in physical components due to temperature (that is, thermal noise) and black body noise from celestial sources such as Sun [19]. On the other hand, noise also describes any signal present in the receiver other than the desired

signal [20]. Hence, thermal noise at the receiver is modelled as additive white Gaussian noise (AWGN).

1.2.2 Path loss

Path loss refers to the loss in power on the way of its propagation as the radio signal travels in the space [11]. In other words, path loss describes how the received signal power decreases with increasing distance between two communicating nodes of a wireless system, and this depends on the type of environment the radio signal is deployed [21]. Path loss could also be described as the mean attenuation of the radio signal and it happens due to the dissipation of power radiated by the transmitter between the mobile station and the base unit as well as the effects of propagation channel. In general, it is assumed that path loss is the same at a given transmit and receive distance whereby the effect of shadowing is not taken into consideration [22].

1.2.3 Shadowing

Shadowing is due to the presence of obstructions between the transmitter and the receiver in a radio signal path [23]. Shadowing is caused by obstructions as a result of absorption, reflection, scattering and diffraction of radio wave attenuated in the propagation path [11]. When the mean attenuation is strong, the signal is blocked. This shadowing behaviour is determined based on the nature of the terrain surrounding the base station, mobile unit and the height of the transmitting antenna. As a result, the received power variation due to path loss takes place over long distances, whereas variation as a result of shadowing takes place over distances that are proportional to the length of the obstructing object [24]. The variation in distances occur more in outdoor environments than in indoor environments.

1.2.4 Fading

Fading in a channel combines the effect of multiple propagation paths, high speed movement of mobile units and reflectors on both forward and reverse link [25]. Fading occurs in a channel whereby two or more variants of the radio signals propagated, that is multipath signals, arrive at the receiving nodes of the communication system at slightly different times interval while producing signals that vary significantly in amplitude and phase. The arriving signals reduce the received power to zero (or very near zero) by adding up destructively.

In other words, the multipath signals have a small-scale effect on propagation and cause a rapid change in signal strength, random frequency modulation and time echoes as a result of propagation delay [26]. Signal duplications due to different paths of wave propagation undergoes different mean attenuation

in terms of distortion, delays and phase shifts.

In fading channels, the received signal power varies randomly over distance or time as a result of shadowing for large-scale fading or multipath fading for small-scale effect [11]. The bit error performance gain of a wireless communication system can be severely degraded by fading. In order to combat fading, diversity techniques are applied.

1.3 Diversity Techniques

Signal power in a wireless channel fluctuates with time, frequency and space [27]. As a result of the fluctuation, the signal power drops dramatically and the channel is said to be in fade. Diversity technique is a communication scheme used to compensate for fading channel impairments by providing wireless link enhancements at a relatively low cost [28]. Diversity scheme is broadly used to reduce the depth and duration of the fades experienced by a receiver in a flat fading channel [29]. Diversity technique utilizes the random nature of signal transmission by finding independent path for radio signal communication. In other words, this techniques provides two or more inputs at the receiver such that the fading phenomena among these inputs are i.i.d, that is, the channel is uncorrelated. If one radio path undergoes deep fade, another i.i.d path may have a strong signal at that input. In this instance, the information that is transmitted several times will have the replicas that will not undergo severe fading. Generally, the mean power available for each branch in diversity techniques are approximately equal [30]. Examples of diversity techniques include:

1.3.1 Space diversity

Space diversity is a technique for multiple antennas transmission or reception, or both, whereby the effects of fading are minimized by physical separation of the antennas by one half or more wavelengths [31], [32], [33]. This physical distance of antennas separation determines the channel correlation among the branch signals and the amount of mutual coupling between the adjacent branch antennas, and the main goal is to avoid both criteria in wireless system. **Fig. 1** is a space diversity scheme for different antenna configurations where both $T\times$ and $R\times$ correspond to the transmitter and the receiver, respectively. Spatial diversity provides significant error performance gain without sacrificing any extra bandwidth on the transmitted power resources and is best suitable for wireless system because it is cost effective, very simple and easy to implement [29], [34].

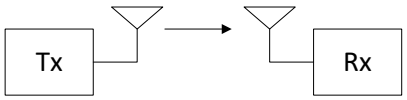

(A)

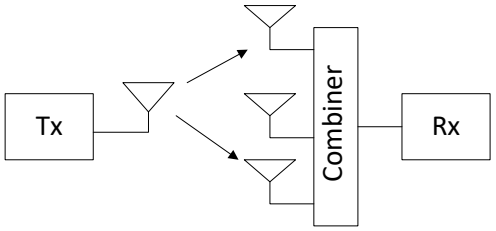

(B)

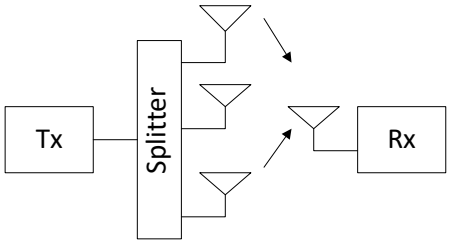

(C)

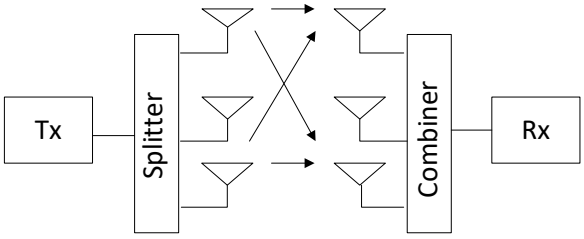

(D)

Figure 1: Space Diversity Reception with (A) SISO, (B) SIMO, (C) MISO, and (D) MIMO [31]

1.3.2 Polarization diversity

This scheme describes diversity technique whereby two radio signals are propagated or received with orthogonal polarization, and the fading in the radio signals is partially correlated or uncorrelated [35]. Polarization diversity uses two antennas of different polarization in both horizontal and vertical direction to constitute two-branched diversity schemes [36], [37]. Polarization diversity has an advantage over space diversity in terms of small size design and cost reduction as a single dual-polarized can be used to achieve polarization diversity, whereas more than one antenna separated by spaces are required for implementation of space diversity [38], [39]. Another advantage is that polarization diversity performs well as compared to space diversity in a non LOS scenario with random terminals orientation [40].

1.3.3 Frequency diversity

Fading is also frequency dependent since the effects of reflection, refraction and diffraction on signal propagation are frequency dependent. Thus, frequency diversity is sometimes used to combat the likelihood of deep fade by taking advantage of the frequency-dependent nature of fading, and transmitting multiple duplicates of information signal at different frequency bands [41], [42].

In general, the information signals are modulated through different carriers in frequency diversity scheme. It is important that different replicas of the radio signals undergo independent fading and this requires extra energy to transmit the signals over different frequency bands [31]. In this scenarios, the probability of simultaneous fading is the product of the separate antenna fading probabilities that employs frequency division multiplexing mode (FDM) [43].

1.3.4 Time diversity

Time diversity exploits coding of channel and interleaving to combat fading at a cost of added delay and loss of bandwidth efficiency [44], [45]. In this diversity scheme, information is transmitted at the time spacing that exceeds the coherence time of the channel. Multiple replicas of the signals are received with independent fading version of the same transmitted signals in different time slots, thereby providing full diversity advantages [31]. If the interval between the time slots is sufficient, the sequential amplitude samples of the fading signals will be i.i.d, that is uncorrelated, and the time interval should be at least the reciprocal of the fading bandwidth [46]. Redundancy could also be introduced into the transmitted signals in order to achieve time diversity in the temporal domain by repetition of channel coding.

1.4 Classification of Diversity

Diversity techniques can be classified into two schemes based on the antenna separation, namely macro diversity and micro diversity [31].

1.4.1 Macro diversity

Macro diversity is used to combat the slower fading variations caused by shadowing in large-scale fading [47]. The mitigation of shadowing requires the use of multiple base stations, that is, the use of a group of geographically distributed base stations in the cell [48]. Since each base station applies a micro diversity technique to combat fading, the concurrent application of multiple base stations coupled with the processing radio signals from these multiple base stations provides an advantage in macro diversity scheme for improved bit error rate in shadowed fading channels [49].

1.4.2 Micro diversity

Micro diversity is a diversity technique employed to mitigate rapid fading variations in the received signals caused by multipath fading whereby multiple antennas are used at the base stations [50]. Small-scale fading results from multipath fading propagation and is characterized by deep and high speed amplitude fluctuations that occur as the mobiles moves over distances of just a few wavelengths. Micro diversity technique has been very efficient to mitigate small-scale fadings [51]. The most popular microdiversity techniques in the literature are equal gain combining, selection combining and maximal ratio combining.

2 Space-time Coding

STC is a power and spectrally efficient channel code that is widely adopted for MIMO schemes without sacrificing the diversity gains over wireless channels. This coding scheme employs the combination of conventional channel coding techniques, modulation schemes and MIMO diversity schemes in their design criteria.

Space–time coded scheme introduces spatial and temporal correlation into signals propagated from different antennas in order to provide diversity gain at the receiver as well as coding gain over an uncoded scheme without sacrificing additional bandwidth resources [52]. Space-time coded scheme also gives an improved error performance rate as compared with an uncoded space-time scheme [53]. However, uncoded scheme avoids delay involved in frame-by-frame detection since no interleaving is required thereby minimizing system computational complexity [10]. Various forms of STC schemes

that can be adopted for MIMO techniques are highlighted below.

2.1 Layered Space-Time Code

The layered space-time (LST) architecture is a technique for processing space-time signals whereby a layered transmission scheme is combined with iterative multi-user detection techniques [54].

The LST scheme is a channel code that is constructed and processed according to the LST architecture and is designed by assembling one-dimensional constituent coding technology. The constituent channel codes can be separated and then detected using conventional detection algorithm designed for one-dimensional constituent codes based on the use of interference suppression and interference cancellation in the receiver. This approach leads to a much lower detection complexity as compared to maximum likelihood detection. Other possible methods with low detection complexity techniques include sequential detection (SD) [55] and multistage detection [53], [56]. The encoded codewords used in the LST architecture can either be assigned diagonally, that is, diagonally layered space-time (DLST) or assigned horizontally, that is, horizontally layered space-time (HLST) [57], [58]. Based on truncated multi-dimensional effective code length and the truncated multi-dimensional product distance of the constituent code, DLST codes can achieve improved error performance gain as compared to HLST [57].

2.2 Space-Time Trellis Code

Space-time trellis code (STTC) is a simple and effective signaling technique of error control coding, modulation, transmit and receive diversity, which is able to mitigate the impacts of channel fading. STTC was proposed in [53] as a type of STC scheme employed in MIMO wireless systems. This kind of codes combines signal processing with a multiple antenna system to produce a scheme with a better error performance gain over the previously proposed transmit diversity schemes in the literature [59]. STTC scheme transmits multiple, redundant replicas of a generalized Trellis Coded Modulation (TCM) signal distributed over successive time interval and a number of space. TCM is a spectrally efficient scheme that combines coding and modulation techniques, without sacrificing extra bandwidth resources [60].

The multiple data transmitted in STTC are used by the receiver to attempt to reconstruct the actual data being propagated. For the STC scheme to be applied, there should be multiple transmit antennas, but only a single receive antennas is required. However, multiple receive antennas can often be used since the error performance of the system is improved by the resulting spatial diversity [52]. STTC takes advantage of the coding gain provided by trellis codes and the advantage

of diversity gain provided by STC for an improved error performance gain. STTCs are difficult to design at both the encoder and decoder due to the fact that the scheme combine single channel successive time coding with the signaling protocol being used, and extend that with a multi-antenna framework [61]. This technique depends on a Viterbi decoder for detection at the receiver whereby STBCs require only linear processing.

For STTC, therefore, the decoder uses Viterbi algorithm to perform maximum likelihood detection and select the path with the minimum path metric as decoded sequence based on the assumption that perfect CSI is available at the receiver. STTC concatenating with STBC provides improved coding gain as well as a reasonable increase in detection complexity.

2.3 Super-Orthogonal Space-Time Trellis Code

Super-orthogonal space-time trellis code (SOSTTC) is a class of STCs that employs sets of super-orthogonal block code (SOBC) and sets of partitioning technique in its construction [62] [63] [64]. These codes are improvements over both STTC and STBC in order to provide full diversity and better coding gain. The transmission matrices of SOSTTC for two transmit antenna can be expressed as [53].

$$\mathbf{C}(x_1, x_2, \theta) = \begin{bmatrix} x_1 e^{j\theta} & x_2 \\ -x_2^* e^{j\theta} & x_1^* \end{bmatrix} \tag{9}$$

where signals x_1 and x_2 are selected by input bits and can be represented by $e^{(j2\pi/M)}$ for M-PSK signal constellations. θ is the rotation angle which can be expressed as $\theta = \frac{2\pi l}{M}$, where $l = 0, 1, \ldots, M-1$. $\theta = 0$ or π for BPSK signal constellation and $\theta = 0$ or $\frac{\pi}{2}$ or π or $\frac{3\pi}{2}$ for QPSK signal constellation. Alamouti STBC is obtained when $\theta = 0$. In equation (9), the two rows correspond to the symbols transmitted in two time slots, that is, time slots 1 and 2, respectively. Likewise, the two columns correspond to the symbols transmitted by two antennas, that is, antennas 1 and 2, respectively.

2.4 Space-Time Block Code

Space-time block coding (STBC) is a relatively simple technique used in wireless communication systems to combat the effects of channel impairments due to multipath fading, and hence enhance the link reliability of MIMO systems.

STBC exploits the redundancy for several transmission between the transmitter and receiver by sending diverse versions of information signals with high probability that some of the signals are less attenuated than the others [65]. Thus, the system provides higher chances of being able to use one or more copies of the received signals for improved data rate and link reliability.

A simple and novel transmit diversity scheme was proposed by Alamouti [41]. The Alamouti STBC scheme is a full-rate two antennas scheme that transmit symbols in two consecutive time slots. Also, Alamouti achieves full-diversity error performance with symbol rate of one.

The modulated radio signal is propagated with additive white Gaussian noise (AWGN) over quasi-static multipath fading channels, while constant fading coefficients are assumed over the pair of time slots and different values from one pair of time slots to another. In this scheme, there is no channel state information (CSI) at the transmitter but perfect CSI is assumed at the receiver. Mathematically, Alamouti STBC transmission matrix can be expressed as [41]:

$$\mathbf{X} = \begin{bmatrix} x_1 & x_2 \\ -x_2^* & x_1^* \end{bmatrix} \tag{10}$$

where x_1 and x_2 are either M-QAM or M-PSK constellation symbols. These symbols pair imply that STBC transmit symbols both in space, that is, across two antennas and also in time, that is, two successive transmission intervals. In the first time slot, antenna one transmits symbols x_1 and antenna two transmits symbols x_2. In the second time slot, antenna one transmits symbols $-x_2^*$ and antenna two transmits symbols x_1^*. The Alamouti STBC is the only orthogonal full-rate STBC, such that $\mathbf{X}^H\mathbf{X} = (|x_1|^2 + |x_2|^2)\mathbf{I}_2$ [41].

2.5 Space-Time Labeling Diversity

Space-time labeling diversity (STLD) is a relatively new scheme broadly used in wireless communication systems due to the enhancements in spectral efficiency and link reliability of MIMO techniques [9]. STLD has been studied in both coded and uncoded communication systems.

2.5.1 Coded STLD

In coded communication systems, research on maximizing the asymptotic coding gain has attracted significant interest in the literature [9], [66], [67], [68], [69]. Huang and Ritcey [9] proposed an optimal constellation diversity technique for $N_R \times N_T$ bit-interleaved STCM (BI-STCM). Furthermore, Huang and Ritcey [9] investigated a labeling design criterion for BI-STCM. Besides, Huang and Ritcey [66] introduced an enhanced 16-ary quadrature amplitude modulation (QAM) labeling diversity scheme for BI-STCM iterative decoding using Alamouti STBC. In the time, STLD has been applied to 2×2 wireless local area network (WLAN) coded networks [67]. An improved version of the labeling diversity scheme has been introduced in Krasicki and Szulakiewicz [68] - [69] that maximizes the asymptotic coding gain. Coded modulation scheme requires ID for channel modeling and thus incurs high system complexity which results in increased energy consumption and higher latencies. This

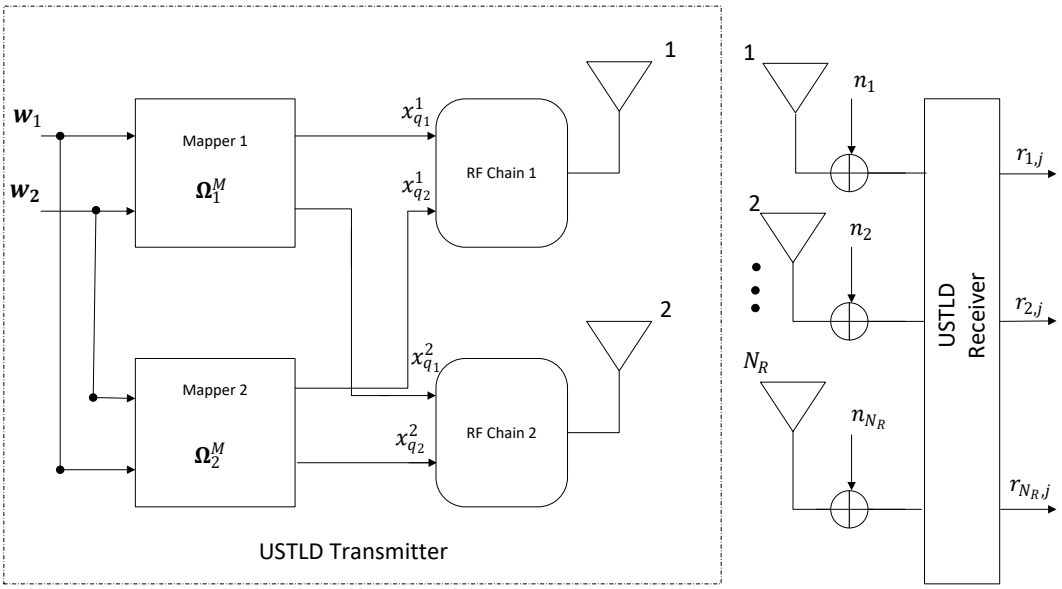

Figure 2: USTLD with two transmit antennas scheme [10]

motivated application of labeling diversity to uncoded modulation scheme which has become more attractive in the literature.

2.5.2 Uncoded STLD

In uncoded communication systems, the same concept of labeling mapping using constellation rearrangement was adopted to enhance bit error rate of STLD systems by mapping same information bits into different signal constellations for transmissions and has been adopted in multiple packet transmission systems [70], OFDM [71] and wireless relay networks [72].

In the recent time, authors in [10] applied labeling diversity to STBC systems, which was named as uncoded space-time labeling diversity (USTLD) as shown in **Fig. 2**. USTLD achieves a significant signal-to-noise ratio (SNR) gain in comparing to STBC scheme. Nonetheless, there exist a significant high detection complexity for the optimal detector used in performing joint symbol detection for the two transmit antennas USTLD scheme.

3 Research Motivation and Contributions

Uncoded space-time labeling diversity (USTLD) is a recently proposed two transmit MIMO scheme [73] that achieves improved error performance compared to Alamouti STBC [41]. In this scheme,

the basic idea is to map a block of data bits to symbols using two labeling mappers without the need for coding and bit-interleaving thereby allowing for more flexibility, low complexity detection and bandwidth optimization.

Motivated by error performance gains of USTLD scheme as a bandwidth efficient wireless communication scheme over STBC, the major focus of the research presented in this thesis is to enhance the link reliability of the conventional USTLD for square M-QAM transmission by developing a new three transmit antennas USTLD scheme for square M-QAM transmission for improved error performance rate and robustness in the presence of noise and multipath fading. Since the existing USTLD scheme is carried out in Rayleigh fading distributions and limited to i.i.d channels, this study further derives analytical expressions for three transmit antennas schemes in M-APSK schemes for fast frequency-flat and quasi-static frequency-flat Rician fading channels that are well suited for digital broadcasting systems as well as X-QAM three transmit antennas schemes in Nakagami-*m* channels for both i.i.d and correlated channels. Therefore, the major contributions of this research are detailed in paper A, paper B and paper C as follows:

3.1 Paper A:

D. Ayanda, H. Xu and N. Pillay, "Uncoded M-ary quadrature amplitude modulation space-time labeling diversity with three transmit antennas" *International Journal of Communication Systems*,vol. 31, no. 18: e3818, Dec. 2018. The summary of this paper is as follows:

Uncoded space-time labeling diversity (USTLD) is a recent scheme that improves the error performance of space-time block-coded wireless communication links. However, the existing space-time labeling diversity technique used in USTLD only employs two transmit antennas. To further improve error performance in USTLD systems, this paper investigates USTLD systems with three transmit antennas. A heuristic approach is proposed to design the second and third mappers. Simulation results show superior error performance compared with the existing two transmit antenna USTLD. Furthermore, an analytical expression for a tight bound of the average bit error probability of the proposed system with three transmit antennas is derived. Moreover, complexity reduction analysis of the low-complexity (LC) detector is proposed. It is shown that the proposed LC algorithm achieves near-maximum likelihood detection accuracy, while reducing complexity by 51% and 96.5% for 16QAM and 64QAM, respectively.

3.2 Paper B:

Performance Analysis of *M*-ary APSK Uncoded Space-time Labeling Diversity with Three Transmit Antennas in Rician Broadcast Channels (in preparation for submission to a journal). The summary of this paper is as follows:

This paper investigates the design of labeling mappers for uncoded space-time labeling diversity with three transmit antennas (USTLD) based on amplitude and phase shift keying (APSK) modulation. The proposed USTLD schemes are DVB-S2 and DVB-S2X standards compatible in both Rician frequency-flat fast and quasi-static fading channels. Numerical analysis of the proposed schemes are derived based on pairwise error probability. The analytical results are validated by Monte Carlo simulations, which converge accurately at high SNR. Furthermore, by adapting constellation structure between square QAM modulations and concentric rings of APSK modulations, the authors proposed mapper design for 16-APSK, 32-APSK and 64-APSK modulations for USTLD using heuristic algorithm. Finally, the proposed USTLD schemes show bit error rate (BER) improvement over the existing two transmit USTLD schemes with error performance gain of 1.2 dB and 2.8 dB at a BER of 10^{-6} for 16-APSK and 64-APSK USTLD scheme, respectively.

3.3 Paper C:

Symbol Mapping Design and Error Analysis of Cross-QAM Uncoded Space-Time Labeling Diversity with Three Transmit Antennas (in preparation for submission to a journal). The summary of this paper is as follows:

Uncoded space-time labeling diversity (USTLD) is a recent scheme that improves the error performance of space-time block code by using labeling mappers to transmit information bits. In this scheme, square quadratic amplitude modulation (QAM) has been widely used due to its high power and bandwidth efficiency. However, square QAM does not provide satisfying requirements for a system where the number of bits per symbol is odd. In this scenario, the peak and the average power of transmission can be reduced by using cross QAMs (XQAMs) instead. Hence, authors in this paper investigate the design of XQAM labeling mappers for USTLD with three transmit antennas over independent and identically distributed (i.i.d) Nakagami-*m* fading channels. The analytical average bit error probability (ABEP) are derived based on pairwise error probability. This expression is validated by Monte Carlo simulation results, which converge accurately at high signal-to-noise ratio. Since channels are not i.i.d in practical sense, the authors further investigate XQAM USTLD scheme in correlated channels. The ABEP for the proposed system are derived and served to validate the Monte-Carlo simulation results. Finally, the impact of channel correlation are demonstrated by

comparing the BER results with BER of i.i.d channels.

4 Structure of the Thesis

The work covered in this thesis has been detailed in paper A, paper B and paper C and are presented in Part II, Part III and Part IV. Part V is the conclusion and suggestions for possible future research directions.

References

[1] M. R. Bhalla and A. V. Bhalla, "Generations of mobile wireless technology: A survey," *International Journal of Computer Application*, vol. 5, no. 4, pp. 26–32, Aug. 2010.

[2] A. Kumar, Y. Liu, J. Sengupta *et al.*, "Evolution of mobile wireless communication networks: 1G to 4G," *International Journal of Electronic and Communication Technologies*, vol. 1, no. 1, pp. 68–72, Dec. 2010.

[3] F. Boccardi, R. W. Heath, A. Lozano, T. L. Marzetta, and P. Popovski, "Five disruptive technology directions for 5G," *IEEE Commun. Mag.*, vol. 52, no. 2, pp. 74–80, Feb. 2014.

[4] M. R. Akdeniz, Y. Liu, M. K. Samimi, S. Sun, S. Rangan, T. S. Rappaport, and E. Erkip, "Millimeter wave channel modeling and cellular capacity evaluation," *IEEE J. Sel. Areas Commun.*, vol. 32, no. 6, pp. 1164–79, Jun. 2014.

[5] M. Katz, M. Matinmikko-Blue, and M. Latva-Aho, "6Genesis Flagship Program: Building the Bridges Towards 6G-Enabled Wireless Smart Society and Ecosystem," in *IEEE 10th Latin-American Conference on Communications (LATINCOM)*, Nov. 2018, pp. 1–9.

[6] S. N. Diggavi, N. Al-Dhahir, A. Stamoulis, and A. R. Calderbank, "Great expectations: the value of spatial diversity in wireless networks," *Proc. of IEEE*, vol. 92, no. 2, pp. 219–270, Feb. 2004.

[7] D. Gesbert, M. Shafi, D. S. Shiu, P. J. Smith, and A. Naguib, "From theory to practice: an overview of MIMO space-time coded wireless systems," *IEEE J. Select Area Comm.*, vol. 21, no. 3, pp. 281–302, Apr. 2003.

[8] A. J. Paulraj, D. A. Gore, R. U. Nabar, and H. Bolcskei, "An overview of MIMO communications - a key to gigabit wireless," *Proc. of IEEE*, vol. 92, no. 2, pp. 198 – 218, Feb. 2004.

[9] Y. Huang and J. A. Ritcey, "Optimal constellation labelling for iteratively decoded bit-interleaved space-time coded modulation," *IEEE Trans Inf. Theory.*, vol. 51, no. 5, p. 1865- 1871, Apr. 2005.

[10] H. Xu, K. Govindasamy, and N. Pillay, "Uncoded space-time labelling diversity," *IEEE Communications Letters*, vol. 20, no. 8, pp. 1511–1514, Jun. 2016.

[11] A. Goldsmith, *Wireless Communications*. Cambridge University Press, Aug.,2005.

[12] M. K. Simon and M.-S. Alouini, *Digital Communication over Fading Channels*. 2nd ed., J. Wiley Sons, 2005.

[13] E. G. Larsson and P. Stoica, *Space-time block coding for wireless communications*. Cambridge University Press, 2008.

[14] J. F. Paris, "Nakagami-q (Hoyt) distribution function with applications," *Electronic Letters*, vol. 45, no. 4, p. 210–211, Feb. 2009.

[15] N. Hajri, N. Youssef, T. Kawabata, M. Pätzold, and W. Dahech, "Statistical properties of double Hoyt fading with applications to the performance analysis of wireless communication systems," *IEEE Access*, vol. 6, pp. 19 597–19 609, Apr. 2018.

[16] M. Nakagami, "The *m*-distribution – A general formula of intensity distribution of rapid fading," Jan. 1960, pp. 3–36.

[17] ——, "Statistical studies on fading, diversity effects and characteristics of diversity receiving systems," *Shukyo—sha, Kobe*, 1947.

[18] G. K. Karagiannidis, D. A. Zogas, and S. A. Kotsopoulos, "On the multivariate Nakagami-*m* distribution with exponential correlation," *IEEE Trans. Commun.*, vol. 51, no. 8, p. 1240–1244, Aug. 2003.

[19] S. Haykin Simon and M. Michael, "Communication systems," 2010.

[20] S. Haykin, *An introduction to analog and digital communication*. John Wiley, 1994.

[21] J. Karedal, N. Czink, A. Paier, F. Tufvesson, and A. F. Molisch, "Path loss modeling for vehicle-to-vehicle communications," *IEEE transactions on vehicular technology*, vol. 60, no. 1, pp. 323–328, Nov. 2010.

[22] C. Phillips, D. Sicker, and D. Grunwald, "A survey of wireless path loss prediction and coverage mapping methods," *IEEE Communications Surveys & Tutorials*, vol. 15, no. 1, pp. 255–270, Mar. 2012.

[23] R. Parasuraman, K. Kershaw, and M. Ferre, "Experimental investigation of radio signal propagation in scientific facilities for telerobotic applications," *International Journal of Advanced Robotic Systems*, vol. 10, no. 10, p. 364, Oct. 2013.

[24] R. He, Z. Zhong, and B. Ai, "Path loss measurements and analysis for high-speed railway viaduct scene," in *Proceedings of the 6th International Wireless Communications and Mobile Computing Conference*. ACM, Jun. 2010, pp. 266–270.

[25] R. Esmailzadeh and M. Nakagawa, *TDD-CDMA for wireless communications*. Artech House, 2003.

[26] E. Biglieri, J. Proakis, and S. Shamai, "Fading channels: Information theoretic and communication aspects," *IEEE Transactions on Information Theory*, vol. 44, no. 6, p. 2619–2692, Oct. 1998.

[27] C.-B. Chae, A. Forenza, R. W. Heath, M. R. McKay, and I. B. Collings, "Adaptive mimo transmission techniques for broadband wireless communication systems [topics in wireless communications]," *IEEE Communications Magazine*, vol. 48, no. 5, pp. 112–118, May 2010.

[28] P.-S. Kildal, K. Rosengren, J. Byun, and J. Lee, "Definition of effective diversity gain and how to measure it in a reverberation chamber," *Microwave and Optical Technology Letters*, vol. 34, no. 1, pp. 56–59, Jul. 2002.

[29] R. G. Vaughan and J. B. Andersen, "Antenna diversity in mobile communications," *IEEE Transactions on Vehicular Technology*, vol. 36, no. 4, pp. 149–172, Nov. 1987.

[30] I. Ahamed and M. Vijay, "Comparison of different diversity techniques in MIMO antennas," in *2017 2nd International Conference on Communication and Electronics Systems (ICCES), IEEE*, Oct. 2017, pp. 47–50.

[31] B. Vucetic and J. Yuan, *Space-time coding*. John Wiley & Sons, Jun. 2003.

[32] P. L. Perini and C. L. Holloway, "Angle and space diversity comparisons in different mobile radio environments," *IEEE Transactions on Antennas and Propagation*, vol. 46, no. 6, pp. 764–775, Jun. 1998.

[33] Z. Li and M. Latva-aho, "Spatial transmit diversity techniques for mc-cdma systems," in *IEEE Seventh International Symposium on Spread Spectrum Techniques and Applications,*, vol. 1, Sep. 2002, pp. 155–159.

[34] W. C. Jakes and D. C. Cox, *Microwave mobile communications*. Wiley-IEEE Press, 1994.

[35] J. Shapira and S. Miller, "A novel polarization smart antenna," in *IEEE VTS 53rd Vehicular Technology Conference, Spring 2001. Proceedings (Cat. No. 01CH37202)*, vol. 1. IEEE, May 2001, pp. 253–257.

[36] J. J. Lempiainen and J. K. Laiho-Steffens, "The Performance of Polarization Diversity Schemes at a Base Station in Small/Micro Cells at 1800 MHz," *IEEE Transactions on Vehicular Technology*, vol. 47, no. 3, pp. 1087–1092, Aug. 1998.

[37] J. F. Valenzuela-Valdes, A. M. Martinez-Gonzalez, and D. Sanchez-Hernandez, "Reduction of 3×3 MIMO volume requirements by using true polarization diversity techniques," in *Proceedings of the 10th European Conference on Wireless Technology*, Oct. 2007, pp. 166–168.

[38] W. Lee and Y. Yeh, "Polarization diversity system for mobile radio," *IEEE Transactions on Communications*, vol. 20, no. 5, pp. 912–923, Oct. 1972.

[39] A. M. Turkmani, A. A. Arowojolu, P. Jefford, and C. Kellett, "An experimental evaluation of the performance of two-branch space and polarization diversity schemes at 1800 mhz," *IEEE Transactions on Vehicular Technology*, vol. 44, no. 2, pp. 318–326, May 1995.

[40] C. B. Dietrich, K. Dietze, J. R. Nealy, and W. L. Stutzman, "Spatial, polarization, and pattern diversity for wireless handheld terminals," *IEEE Transactions on Antennas and Propagation*, vol. 49, no. 9, pp. 1271–1281, Sep. 2001.

[41] S. M. Alamouti, "A simple transmit diversity technique for wireless communications," *IEEE J. Select in Commun.*, vol. 16, no. 8, pp. 1451–1458, Oct. 1998.

[42] M. Leabman, "Multi-connection, non-simultaneous frequency diversity in radio communication systems," Aug. 28 2007, US Patent 7,263,335.

[43] U. Kesavan, I. M. Rafiqul, A. Khaizuran, and A. Tharek, "Frequency Diversity Improvement Factor for Rain Fade at Terrestrial Link in Tropical Region," in *International Conference on Computer and Communication Engineering (ICCCE)*, Jul. 2016, pp. 62–65.

[44] W. Wong, R. Steele, B. Glance, and D. Horn, "Time diversity with adaptive error detection to combat rayleigh fading in digital mobile radio," *IEEE Transactions on Communications*, vol. 31, no. 3, pp. 378–387, Mar. 1983.

[45] L.-F. Wei, "Coded m-dpsk with built-in time diversity for fading channels," *IEEE Transactions on Information Theory*, vol. 39, no. 6, pp. 1820–1839, Nov. 1993.

[46] E. Biglieri, G. Taricco *et al.*, "Transmission and reception with multiple antennas: Theoretical foundations," *Foundations and Trends® in Communications and Information Theory*, vol. 1, no. 2, pp. 183–332, Sep. 2004.

[47] V. V. Milenkovic, N. M. Sekulovic, M. C. Stefanovic, and M. B. Petrovic, "Effect of microdiversity and macrodiversity on average bit error probability in gamma-shadowed rician fading channels," *ETRI Journal*, vol. 32, no. 3, pp. 464–467, Jun. 2010.

[48] J. Zhang and V. Aalo, "Effect of macrodiversity on average-error probabilities in a rician fading channel with correlated lognormal shadowing," *IEEE Transactions on Communications*, vol. 49, no. 1, pp. 14–18, Jan. 2001.

[49] P. Shankar, "Analysis of microdiversity and dual channel macrodiversity in shadowed fading channels using a compound fading model," *AEU-International Journal of Electronics and Communications*, vol. 62, no. 6, pp. 445–449, Jun. 2008.

[50] A. Annamalai, "Microdiversity reception of spread-spectrum signals on nakagami fading channels," *IEEE transactions on communications*, vol. 47, no. 11, pp. 1747–1756, Nov. 1999.

[51] S. Mukherjee and D. Avidor, "Effect of microdiversity and correlated macrodiversity on outages in a cellular system," *IEEE Transactions on Wireless Communications*, vol. 2, no. 1, pp. 50–58, Feb. 2003.

[52] A. F. Naguib and R. Calderbank, "Space-time coding and signal processing for high data rate wireless communications," *Wireless communication technologies: new multimedia systems*, pp. 23–59, Jan. 2002.

[53] V. Tarokh, N. Seshadri, and A. R. Calderbank, "Space-Time Codes for High Data Rate Wireless Communication: Performance Criterion and Code Construction," *IEEE transactions on information theory*, vol. 44, no. 2, pp. 744–765, Mar. 1998.

[54] G. J. Foschini, "Layered space-time architecture for wireless communication in a fading environment when using multi-element antennas," *Bell Labs Technical Journal*, vol. 1, no. 2, pp. 41–59, Jun. 1996.

[55] S. Lin and D. J. Costello, *Error Control Coding: Fundamentals and Applications*. Prentice Hall, New Jersey, 1983.

[56] A. R. Calderbank, "Multilevel Codes and Multistage Decoding," *IEEE Transactions on Communications*, vol. 37, no. 3, pp. 222–229, Mar. 1989.

[57] D. Shiu and M. Kahn, "Layered Space-Time Codes for Wireless Communications Using Multiple Transmit Antennas," in *Proc. of IEEE Intl. Conf. on Communication*, vol. 1, Jun. 1999, pp. 436–440.

[58] W. Firmanto, J. Yuan, K. L. Lo, and B. Vucetic, "Layered space-time coding: performance analysis and design criteria," in *GLOBECOM'01. IEEE Global Telecommunications Conference*, vol. 2, Nov. 2001, pp. 1083–1087.

[59] V. Tarokh, A. Naguib, N. Seshadri, and A. R. Calderbank, "Space–time codes for high data rate wireless communication: performance criteria in the presence of channel estimation errors, mobility, and multiple paths," *IEEE Transactions on Communications*, vol. 47, no. 2, p. 199–207, Feb. 1999.

[60] V. Tarokh, H. Jafarkhani, and A. R. Calderbank, "Space-time block codes from orthogonal designs," *IEEE Transactions on Information theory*, vol. 45, no. 5, pp. 1456–1467, Jul. 1999.

[61] N. Seshadri and J. H. Winters, "Two signaling schemes for improving the error performance of frequency division duplex (FDD) transmission systems using transmit antenna diversity," *International Journal of Wireless Information Networks*, vol. 1, no. 1, p. 49–60, Jan. 1994.

[62] H. Jafarkhani and N. Seshadri, "Super-orthogonal space-time trellis codes," *IEEE Transactions on Information Theory*, vol. 49, no. 4, pp. 937–950, Apr. 2003.

[63] J. N. Pillai and S. H. Mneney, "Super Orthogonal Space Time Trellis Codes in Rapid Rayleigh Fading Channels," in *proc, SATNAC*, 2005.

[64] S. Siwamogsatham and M. P. Fitz, "Improved High –rate Space Time codes via Concatenation of expanded orthogonal Block code and MTCM," in *2002 IEEE International Conference on Communications. Conference Proceedings. ICC 2002 (Cat. No. 02CH37333)*, vol. 1, Apr. 2002, pp. 636–640.

[65] M. Wennström, "On MIMO Systems and Adaptive Arrays for Wireless Communication: Analysis and Practical Aspects," Ph.D. dissertation, Signaler och System, 2002.

[66] Y. Huang and J. A. Ritcey, "Improved 16-QAM constellation labeling for BI-STCM-ID with the Alamouti scheme," *IEEE Communications Letters*, vol. 9, no. 2, pp. 157–159, Jan. 2005.

[67] S. Ejaz, Y. FengFan, and H. Xu, "Labeling Diversity for 2 x 2 WLAN Coded-Cooperative Networks," vol. 24, no. 9, pp. 695–697, Jun. 2015.

[68] M. Krasicki and P. Szulakiewicz, "Boosted space-time diversity scheme for wireless communications," *Electronics letters*, vol. 45, no. 16, p. 843–845, Jul. 2009.

[69] M. Krasicki, "Essence of 16-QAM labelling diversity," *Electronics Letters*, vol. 49, no. 8, p. 567–569, Apr. 2013.

[70] H. Samra, Z. Ding, and P. M. Hahn, "Symbol mapping diversity design for multiple packet transmission," *IEEE Transactions on Communications*, vol. 53, no. 5, pp. 810–807, May 2005.

[71] H. Samra and Z. Ding, "Retransmission diversity schemes for multicarrier modulations," *IEEE transactions on wireless communications*, vol. 5, no. 5, pp. 1142–1147, Jun. 2006.

[72] K. G. Seddik, A. S. Ibrahim, and K. R. Liu, "Trans-modulation in wireless relay networks," *IEEE Communications Letters*, vol. 12, no. 3, pp. 170–173, Mar. 2008.

[73] Xu, Hongjun and Govindasamy, Kyle, "A space-time labelling technique for wireless communication systems," Jul. 12 2018, US Patent App. 15/740,364.

Part II

Paper A

Paper A

Uncoded M-ary Quadrature Amplitude Modulation Space-Time Labeling Diversity with Three Transmit Antennas

1 Abstract

Uncoded space-time labeling diversity (USTLD) is a recent scheme that improves the error performance of space-time block–coded wireless communication links. However, the existing space-time labeling diversity technique used in USTLD only employs two transmit antennas. To further improve error performance in USTLD systems, this paper investigates USTLD systems with three transmit antennas. A heuristic approach is proposed to design the second and third mappers. Simulation results show superior error performance compared with the existing two transmit antenna USTLD. Furthermore, an analytical expression for a tight bound of the average bit error probability of the proposed system with three transmit antennas is derived. Moreover, complexity reduction analysis of the low-complexity (LC) detector is proposed. It is shown that the proposed LC algorithm achieves near-maximum likelihood detection accuracy, while reducing complexity by 51% and 96.5% for 16QAM and 64QAM, respectively.

2 Introduction

Space-time coded modulation (STCM) is a recent scheme widely employed in wireless communication systems as a result of improvements in reliability and spectral efficiency of multiple-input multiple-output (MIMO) techniques [1]. This coding scheme provides three forms of error performance enhancement - labeling diversity, time diversity, and antenna diversity. Labeling diversity has been studied in both coded and uncoded communication systems.

In coded communication systems, research effort on maximizing the asymptotic coding gain has gained attention [1], [2], [3], [4], [5], [6], [7]. Huang and Ritcey [1] proposed an optimal constellation diversity technique for $N_R \times N_T$ bit-interleaved STCM (BI-STCM). Huang and Ritcey [1] further discussed a labeling design criterion for BI-STCM. Meanwhile, Huang and Ritcey [2] proposed an improved 16-ary quadrature amplitude modulation (QAM) labeling diversity scheme for BI-STCM iterative decoding using Alamouti space-time block coding (STBC). Recently, labeling was also discussed for 2×2 wireless local area network (WLAN) coded networks [3]. An improved version of the labeling diversity scheme has been introduced in Krasicki and Szulakiewicz [4] - [7] that maximizes the asymptotic coding gain.

In uncoded communication systems, the constellation rearrangement (CR), which is the same concept of labeling diversity was used to improve the error performance of systems that employ transmissions of the same information bits in multiple packet transmission systems and relay networks [8], [9] [10]. The labeling diversity technique maps the same information bits into different constellations for transmissions and has been employed in multiple packet transmission systems, [8] OFDM, [9] and wireless relay networks [10].

Very recently, Xu et al [11] applied labeling diversity to STBC systems, which was named as uncoded space-time labeling diversity (USTLD). USTLD achieves a significant signal-to-noise ratio (SNR) gain in comparing with STBC scheme. However, the optimal maximum likelihood (ML) detection principle has the highest computational complexity, since the detector performs joint symbol detection for USTLD.

Govindasamy et al [12] also applied labeling diversity scheme to STBC spatial modulation (STBC-SM), named as STBC-SM labeling diversity (STBC-SM-LD). STBC-SM-LD shows improved bit error rate (BER) when compared with the conventional STBC-SM. Also, Pillay and Xu [13] further applied media-based modulation (MbM) with radio frequency (RF) mirrors to USTLD, which is termed USTLD-STCM. USTLD-STCM exhibits a significant performance in BER over USTLD [11] and space-time channel modulation [14].

In this paper, we focus on USTLD systems. The USTLD systems in both Xu et al [11] and Govindasamy et al [12] are limited to only two transmit antennas. To further improve error performance of USTLD, we propose to extend the USTLD system to three transmit antennas. In the proposed system, the main work is to find the second and third mappers, which maximize the minimum product distance. A heuristic approach is adopted to design the second and third mappers in the proposed system. In addition, we also employ the union bound to derive the analytical error performance of the system. Since the complexity of ML detection is very high, the orthogonal projection (OP) detection algorithm used in Govindasamy et al [12] is also employed in the proposed system to reduce the detection complexity.

The remainder of this paper is structured as follows: Section 3 describes the existing system model of two transmit antenna USTLD and presents the proposed three transmit antenna USTLD system model. The analytical expression for error performance is presented in Section 4. Section 5 proposes a new mapper design based on a heuristic algorithm. In Section 6, detection schemes, computational complexities, and analysis are presented. Section 7 discusses numerical results. The final conclusion is discussed in Section 8.

In terms of notation, N_T and N_R denote the number of transmit and receive antennas, respectively. Boldface letters represent the vectors and matrices, and italics are used for scalars. $|\cdot|$, $[\cdot]^T$, $(\cdot)^H$, and $\|\cdot\|_F$ denote the Euclidean norm, transpose, transpose and conjugate, and Frobenius norm, respectively. $Q(\cdot)$, $(\cdot)!$ and $E\{\cdot\}$ denote Gaussian Q-function, factorial, and statistical expectation operator, respectively. $argmax_w(\cdot)$ and $argmin_w(\cdot)$ are used for maximum and minimum of the argument with respect to *w*. *j* is a complex number.

3 System Model

In this section, we first describe the system model of existing $2 \times N_R$ USTLD MIMO scheme. On the basis of increase in number of transmit antennas, we then discuss the proposed system model.

3.1 Existing USTLD system model

The conventional USTLD is a MIMO technique [11] with transmit and receive antennas N_T and N_R where $N_T = 2$. Message bits are partitioned into two bit streams, $\mathbf{m}_1 = [m_{1,1}, m_{1,2}, \cdots, m_{1,r}]$ and $\mathbf{m}_2 = [m_{2,1}, m_{2,2}, \cdots, m_{2,r}]$ each of length $r = \log_2 M$. The two bit streams are fed into two USTLD mappers - Mapper 1 (Ω_1^M) and Mapper 2 (Ω_2^M). Mapper 1 uses Gray-coded M-ary QAM (MQAM) constellation points in the Argand plane and maps $\mathbf{m}_1$ onto two symbols, $x_{q_1}^1 = \Omega_1^M(\mathbf{m}_1)$

and $x^1_{q_2} = \Omega^M_1(\mathbf{m}_2)$, where $q_i \in [1:M]\,, i \in [1:2]$

Mapper 2 uses optimized labeling maps in the Argand plane and maps $\mathbf{m}_2$ onto two symbols, $x^2_{q_1} = \Omega^M_2(\mathbf{m}_1)$ and $x^2_{q_2} = \Omega^M_2(\mathbf{m}_2)$. Assume $E(|x^k_{q_i}|^2) = 1$, $k \in [1:2]$. After the mapping, two symbols $x^1_{q_1}$ and $x^1_{q_2}$ are transmitted by antenna 1 simultaneously in the first time slot. Likewise, two symbols $x^2_{q_2}$ and $x^2_{q_1}$ are transmitted by antenna 2 simultaneously in the second time slot.

The received signal vector as given as $N_R \times 1$ in time slot k, is thus defined as:

$$\mathbf{y}_k = \sqrt{\frac{\rho}{2}}\mathbf{H}_k\mathbf{x}_k + \boldsymbol{\eta}_k, \quad k \in [1:2] \tag{A.1}$$

where $\mathbf{x}_1 = [x^1_{q_1} x^1_{q_2}]^T$, $\mathbf{x}_2 = [x^2_{q_2} x^2_{q_1}]^T$. $\mathbf{y}_k = [\,y_{1,k}, y_{2,k}, \cdots, y_{N_R,k}]^T$ $\frac{\rho}{2}$ is the average SNR of the transmission antenna. On the whole, labeling diversity codeword is defined as $\mathbf{X} = [\mathbf{x}_1\,\mathbf{x}_2]$ and the set of symbol pairs of $(\mathbf{x}_1, \mathbf{x}_2)$ is contained in χ_2. $\mathbf{H}_k$ is the $N_R \times 2$ channel fading for time slot *k* defined as $\mathbf{H}_k = [\mathbf{h}^1_k\,\mathbf{h}^2_k]$, and $\boldsymbol{\eta}_k$ is an $N_R \times 1$ additive white Gaussian noise (AWGN) vector. $\mathbf{h}_k$ and $\boldsymbol{\eta}_k$ are independent and identically distributed (i.i.d) complex Gaussian random variables (RVs) distribution according to $CN(0,1)$ and $CN(0,\sigma^2)$, respectively.

At the receiver, optimal maximum-likelihood (ML) detection principle is used to estimate the transmitted symbols, thus given by

$$[x^1_{\hat{q}_1},\ x^1_{\hat{q}_2},\ x^2_{\hat{q}_2},\ x^2_{\hat{q}_1}] = \underset{(\mathbf{x}_1,\mathbf{x}_2)\in\chi_2}{\operatorname{argmin}} \Big(\sum_{k=1}^{2} \Big\| \mathbf{y}_k - \sqrt{\frac{\rho}{2}}\mathbf{H}_k\mathbf{x}_k \Big\|^2_F \Big) \tag{A.2}$$

3.2 Proposed USTLD system model

In this subsection, the authors consider $N_R \times N_T$ USTLD MIMO system, as shown in **Figure A.1**, which is an extension of the system in Xu et al, [11] where $N_T = 3$. Information bits are partitioned into three bit streams, $\mathbf{m}_i = [\,m_{i,1}, \cdots, m_{i,r}]\,, i \in [1:3]$, where $r = \log_2 M$, where $M = 16$ or 64.

Let $q_i = 1 + \sum_{k=1}^{r} 2^{k-1} m_{i,k}$, which is the index of bit stream $\mathbf{m}_i$. Bit stream $\mathbf{m}_i$ is fed into three mappers, mapper 1 (Ω^M_1), mapper 2 (Ω^M_2) and mapper 3 (Ω^M_3). $\Omega^M_1(\mathbf{m}_i)$ maps bit stream $\mathbf{m}_i$ into MQAM constellation points in the Argand plane and gives $x^k_{q_i} = \Omega^M_k(\mathbf{m}_i)\,, i \in [1:3]$ and $k \in [1:3]\,$.

In the proposed system, mapper 1 Ω^M_1 is Gray mapper; mappers 2 and 3 will both be designed with the objective of maximizing the minimum product distance. It is assumed that $E[|x^l_{q_i}|^2] = 1$. After the mapping, symbol transmission takes place simultaneously in antennas 1, 2 and 3. In antenna 1, $x^1_{q_1}$, $x^1_{q_2}$, and $x^1_{q_3}$ are transmitted in the first time slot; in antenna 2, $x^2_{q_1}$, $x^2_{q_2}$, and $x^2_{q_3}$ are transmitted in the second time slot; and in antenna 3, $x^3_{q_1}$, $x^3_{q_2}$, and $x^3_{q_3}$ are transmitted in the third time slot. Let

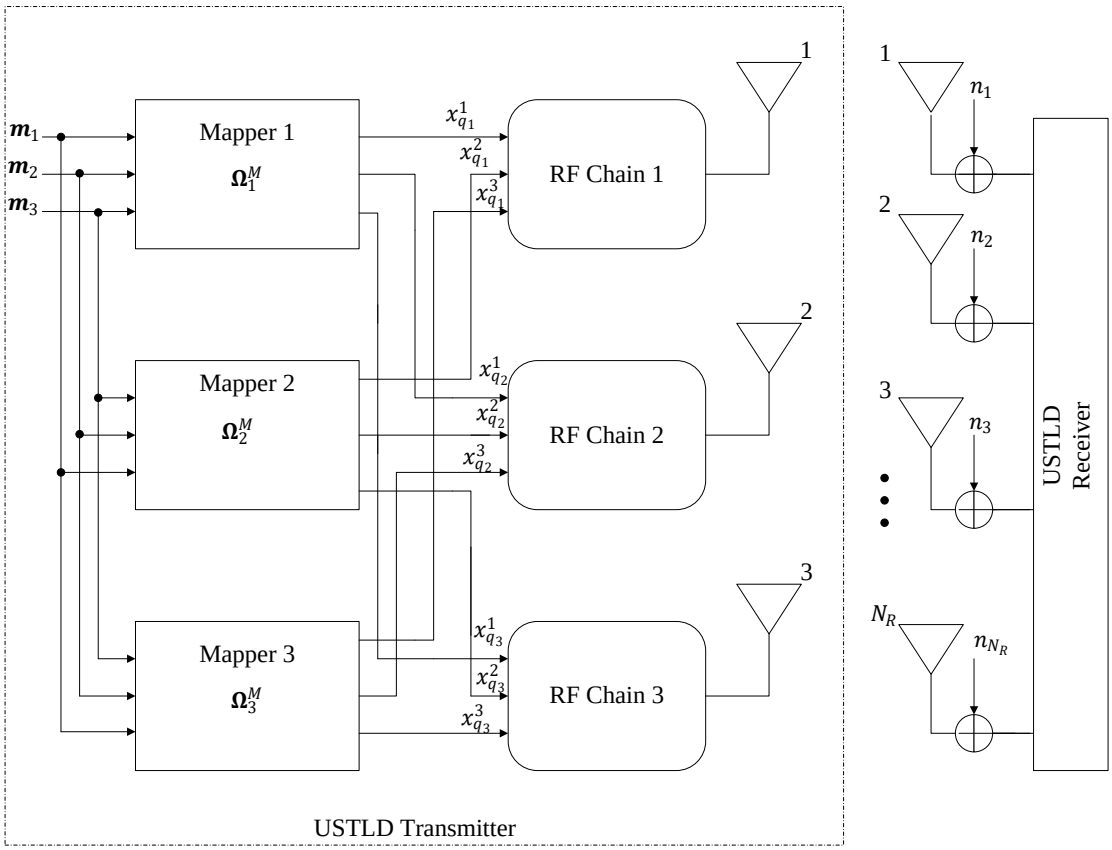

Figure A.1: System model of three transmit antenna uncoded space-time labeling diversity (USTLD). RF, radio frequency

the overall transmitted USTLD codeword vector be defined as $\mathbf{x}_k = [\, x_{q_1}^k, x_{q_2}^k, x_{q_3}^k \,]^T$, $k \in [1:3]$. For convenience of the following discussion, let χ be the set of symbol pair combinations of $(\mathbf{x}_1, \mathbf{x}_2, \mathbf{x}_3)$.

Then, the received signal vector in time slot k, $k \in [1:3]$ is given by

$$\mathbf{y}_k = \sqrt{\frac{\rho}{3}} \mathbf{H}_k \mathbf{x}_k + \mathbf{n}_k, \quad k \in [\,1:3] \tag{A.3}$$

where $\mathbf{y}_k \in C^{N_R \times 1}$ is the kth received signal vector. $\frac{\rho}{3}$ is the total average SNR of the transmission antenna. $\mathbf{H}_k = [\, \mathbf{h}_k^1, \mathbf{h}_k^2, \mathbf{h}_k^3]$, where $\mathbf{h}_k^i \in C^{N_R \times 1}$ is the kth channel fading vector for the ith transmit antenna. $\mathbf{n}_k \in C^{N_R \times 1}$ is an $N_R \times 1$ AWGN vector. The authors assumed that $\mathbf{h}_k^i$ and $\mathbf{n}_k$ are i.i.d complex Gaussian RVs according to $CN(0,1)$ and $CN(0,1)$, respectively.

4 Error Performance analysis of USTLD with Three Transmit Antennas

The bit error performance of USTLD with two transmit antennas has been studied in Xu et al. [11]. In the derivation of error performance of USTLD in Xu et al. [11], it is assumed that only one pair of symbols is detected with errors while the other pair of symbols is detected correctly at high SNR. In this paper, we extend above assumption to three transmit antennas and also assume that only one triad of symbols is detected with errors, while the other two triads of symbols are detected correctly at high SNR. Assuming at high SNR, two triads of symbols, $x_{q_i}^k$, $i \in [\,2:3]$, $k \in [\,1:3]$ are detected correctly while $x_{q_1}^k$ is detected with errors. Based on the above assumption, (A.3) can equivalently be written as

$$\mathbf{y}_k = \sqrt{\frac{\rho}{3}} \mathbf{h}_k^1 x_{q_1}^k + \mathbf{n}_k, \qquad k \in [\,1:3] \tag{A.4}$$

Based on the equivalent model in (A.4), the average bit error probability (ABEP) is defined as [13]:

$$ABEP(\rho) \leq \frac{1}{Mr} \sum_{q_1=1}^{M} \sum_{\hat{q}_1 \neq q_1}^{M} \Delta(q_1, \hat{q}_1) P(\mathbf{X} \rightarrow \hat{\mathbf{X}}) \tag{A.5}$$

where $\Delta(q_1, \hat{q}_1)$ is the number of bit errors for the associated pairwise error probability (PEP) event $P(\mathbf{X} \rightarrow \hat{\mathbf{X}})$ between the transmitted codeword $\mathbf{X}$ and the received codeword $\hat{\mathbf{X}}$, represented as $\mathbf{X} = [\, x_{q_1}^1 x_{q_1}^2 x_{q_1}^3]$ and $\hat{\mathbf{X}} = [\, \hat{x}_{q_1}^1 \hat{x}_{q_1}^2 \hat{x}_{q_1}^3]$.

The conditional PEP on $\mathbf{h}_k^1$, $k \in [\,1:3]$ can be formulated as

$$P(\mathbf{X} \rightarrow \hat{\mathbf{X}} | \mathbf{h}_1^1,\ \mathbf{h}_2^1,\ \mathbf{h}_3^1) = P\left(\sum_{k=1}^{3} \left\| \mathbf{y}_k - \sqrt{\frac{\rho}{3}} \mathbf{h}_k^1 \hat{x}_{q_1}^k \right\|_F^2 < \sum_{k=1}^{3} \left\| \mathbf{y}_k - \sqrt{\frac{\rho}{3}} \mathbf{h}_k^1 x_{q_1}^k \right\|_F^2 \right) \tag{A.6}$$

Substituting (A.4) into (A.6), (A.6) becomes

$$P(\mathbf{X} \to \hat{\mathbf{X}}|\mathbf{h}_1^1,\ \mathbf{h}_2^1,\ \mathbf{h}_3^1) = P\left(\sum_{k=1}^{3} \left\|\mathbf{n}_k + \sqrt{\frac{\rho}{3}}\mathbf{h}_k^1(x_{q_1}^k - \hat{x}_{q_1}^k)\right\|_F^2 < \sum_{k=1}^{3} \left\|\mathbf{n}_k\right\|_F^2\right) \tag{A.7}$$

Let $d_k = x_{q_1}^k - \hat{x}_{q_1}^k$. (A.7) can be further simplified as

$$P(\mathbf{X} \to \hat{\mathbf{X}}|\mathbf{h}_1^1,\ \mathbf{h}_2^1,\ \mathbf{h}_3^1) = P\left(\sum_{k=1}^{3} Re\left\{\sqrt{\frac{\rho}{3}}\mathbf{h}_k^1 d_k \mathbf{n}_i^H\right\} > \frac{1}{2}\sum_{k=1}^{3}\delta_k\right) \tag{A.8}$$

where $\delta_k = \left\|\sqrt{\frac{\rho}{3}}\mathbf{h}_k^1 d_k\right\|_F^2$. δ_k can be further simplified as $\delta_k = \frac{\rho}{3}|d_k|^2\left\|\mathbf{h}_k^1\right\|_F^2$.

Since $\mathbf{h}_k^1$, $x_{q_1}^k$ and $\hat{x}_{q_1}^k$ are given in (A.8), $\sqrt{\frac{\rho}{3}}\mathbf{h}_k^1(x_{q_1}^k - \hat{x}_{q_1}^k)\mathbf{n}_k^H$ is also a complex Gaussian RV with zero mean and variance of δ_k.

$$P(\mathbf{X} \to \hat{\mathbf{X}}|\mathbf{h}_1^1,\ \mathbf{h}_2^1,\ \mathbf{h}_3^1) = Q\left(\sqrt{\frac{1}{2}(\delta_1 + \delta_2 + \delta_3)}\right) \tag{A.9}$$

where δ_k, $k \in [\,1 : 3\,]$, are central chi-squared RVs with the probability density function (PDF) in (A.10).

$$f_{\delta_k}(v_k) = \frac{1}{(2\sigma_{\alpha_k}^2)^{N_R}(N_R - 1)!}\exp\Big(-\frac{v_k}{2\sigma_{\alpha_k}^2}\Big) \tag{A.10}$$

where $\sigma_{\alpha_k}^2 = \frac{\rho}{12}|d_k|^2$.

By averaging three i.i.d RVs δ_k, $k \in [\,1 : 3]$ the PEP can be expressed as

$$P(\mathbf{X} \to \hat{\mathbf{X}}) = \int_0^\infty \int_0^\infty \int_0^\infty P(\mathbf{X} \to \hat{\mathbf{X}}|\mathbf{h}_1^1,\ \mathbf{h}_2^1,\ \mathbf{h}_3^1) f_{\delta_1}(v_1) f_{\delta_2}(v_2) f_{\delta_3}(v_3) dv_1 dv_2 dv_3 \tag{A.11}$$

Using trapezoidal transformation of the Q-function

$$\int_a^b f(x)dx = \frac{b-a}{n}\left[\frac{f(a) + f(b)}{2} + \sum_{k=1}^{n-1} f\Big(a + \frac{k(b-a)}{n}\Big)\right] \tag{A.12}$$

PEP can be verified as

$$P(\mathbf{X} \to \hat{\mathbf{X}}) = \frac{1}{2n}\Big[\frac{1}{2}\prod_{k=1}^{3} M_k\Big(\frac{1}{2}\Big) + \sum_{l=1}^{n-1}\prod_{k=1}^{3} M_k\Big(\frac{1}{2\sin^2(\frac{l\pi}{2n})}\Big)\Big] \tag{A.13}$$

where $M_k(s)$ is the moment generating function defined as:

$$M_k(s) = \int_0^\infty f_{\delta_k}(v_k)(\gamma)e^{-sv_k}dv_k = \Big(\frac{1}{1 + 2\sigma_{\alpha_k}^2 s}\Big)^{N_R} \tag{A.14}$$

We finally have the PEP:

$$P(\mathbf{X} \to \hat{\mathbf{X}}) = \frac{1}{2n}\Big[\frac{1}{2}\prod_{k=1}^{3}\Big(1 + \frac{\rho}{12}\delta_k\Big)^{-N_R} + \sum_{l=1}^{n-1}\prod_{k=1}^{3}\Big(1 + \frac{\rho}{12}\delta_k\frac{1}{\sin^2(\frac{l\pi}{2n})}\Big)^{-N_R}\Big] \tag{A.15}$$

At high SNR, $\frac{\rho}{12}\delta_k \gg 1$, $P(\mathbf{X} \to \hat{\mathbf{X}})$ can be approximated as

$$P(\mathbf{X} \to \hat{\mathbf{X}}) \approx \frac{1}{2n}\Big[\frac{1}{2}\prod_{k=1}^{3}\Big(\frac{\rho}{12}\delta_k\Big)^{-N_R} + \sum_{l=1}^{n-1}\prod_{k=1}^{3}\Big(\frac{\rho}{12}\delta_k\frac{1}{\sin^2(\frac{l\pi}{2n})}\Big)^{-N_R}\Big] \tag{A.16}$$

Equation (A.16) will be used to guide the design of mappers. The overall diversity gain *d* attained by the scheme in Equation (A.16) can be defined as [15]

$$\lim_{SNR\to\infty}\frac{\log P_e(SNR)}{\log(SNR)} = -d, \tag{A.17}$$

where $P_e(SNR)$ denotes overall probability of error as a function of SNR.

Given $P_e(SNR) = P(\mathbf{X} \to \hat{\mathbf{X}})$ as given in (A.16), Equation (A.17) becomes

$$-d = \lim_{SNR\to\infty}\frac{\log(P(\mathbf{X} \to \hat{\mathbf{X}}))}{\log(SNR)} \tag{A.18}$$

On the basis of (A.18), we can derive the diversity gain *d* as

$$d = 3N_R$$

Detail of the derivation is shown in Appendix A.

5 Design of the Second and the Third M-QAM Mapper in USTLD with three transmit antennas

It is shown in (A.16) that the error performance of USTLD system depends on the minimum product distance $\prod_{k=1}^{3}\delta_k$. Maximizing the minimum product distance will minimize the error performance of USTLD system. Maximizing the minimum product distance can be achieved through the design of three mappers in USTLD system. Since Mapper 1 is Gray mapper the optimization can be formulated as

$$(\Omega_2^M, \Omega_3^M) = \underset{(x_{q1}^k, \hat{x}_{q1}^k)\in\chi}{\operatorname{argmax}}\Big\{\min_{x_{q1}^k \neq \hat{x}_{q1}^k \in\chi}\prod_{k=1}^{3}\delta_k\Big\} \tag{A.19}$$

In designing the mappers, research efforts have been focused towards maximizing the minimum product distance [4], [5], [8] - [11]. In Krasicki and Szulakiewicz, [4], [5], for instance, a pair of labels assigned to adjacent symbols in one mapping is fed to symbols spaced further apart in subsequent mappings. In Xu et al [11], a heuristic approach is proposed to design the mappers. The approach first regards 16QAM or 64QAM constellation points as a 4×4 or 8×8. This method is then followed by rearranging the rows and the columns of the matrix to ensure that any two adjacent rows in the source constellation matric are nonadjacent. The approach finally swaps constellation

Table A.1: Mapping for two transmit antenna systems

$s_1 = s_1^I + js_1^Q$	Transform	$s_2 = s_2^I + js_2^Q$	$s_1 = s_1^I + js_1^Q$	Transform	$s_2 = s_2^I + js_2^Q$
$-3+j3$		$1-j$	$-1+j3$		$-3+j$
$3+j3$	$s_2^I = f_1(s_1^I)$	$-1-j$	$1+j3$	$s_2^I = f_3(s_1^I)$	$3+j$
$-3-j3$	$s_2^Q = f_1(s_1^Q)$	$1+j$	$-1-j3$	$s_2^Q = f_3(s_1^Q)$	$-3-j$
$3-j3$		$-1+j$	$1-j3$		$3-j$
$-3+j$		$1+j3$	$-1+j$		$-3-j3$
$3+j$	$s_2^I = f_1(s_1^I)$	$-1+j3$	$1+j$	$s_2^I = f_3(s_1^I)$	$3-j3$
$-3-j$	$s_2^Q = f_3(s_1^Q)$	$1-j3$	$-1-j$	$s_2^Q = f_1(s_1^Q)$	$-3+j3$
$3-j$		$-1-j3$	$1-j$		$3+j3$

points in different quadrature. In this paper, we also propose another heuristic approach to design the mappers. In the MQAM constellation, the Euclidean distance between any two different symbols $x_i$and x_k is defined as

$$d_{ED} = (x_i^I - x_k^I)^2 + (x_i^Q - x_k^Q)^2 \tag{A.20}$$

where $x_i = x_i^I + jx_i^Q$ and $x_k = x_k^I + jx_k^Q$, $x_i \neq x_k$, d_{ED} is the sum of $(x_i^I - x_k^I)^2$, and $(x_i^Q - x_k^Q)^2$, which are the real part distance and imaginary part distance. Since squared MQAM constellation is symmetric in terms of real and imaginary parts, the mapper design of squared MQAM in USTLD is equivalent to the real component mapper design or the imaginary component mapper design.

For example, the real or imaginary component of 16QAM is 4-ary pulse amplitude modulation (4PAM) while the real or imaginary component of 64QAM is 8PAM. The proposed approach to design mappers is based on swapping different amplitude in symmetric way. There are three different mappers in 4PAM. These three mappers are shown in **Figure A.2**$(A - C)$. For convenience discussion, we regard these three mappers as different transforms, f_1,f_2 and f_3. For two transmit antenna systems, one of the mappers in Krasicki and Szulakiewicz, [4], [5] is selected for the second mapper, which provides the best error performance, to the best knowledge of the authors. This mapper can be designed based on transform f_1 and f_3, which is shown in **Table A.1**. For three transmit antenna systems, the third mapper is also designed based on transform f_1 and f_3 which is shown in **Table A.2**.

For 64QAM, there are three different mappers shown as **Figure A.3**$(A - C)$, which can also be regarded as f_4, f_5 and f_6. Transforms f_4 and f_5 can be combined as a single transform, while f_6 is selected as the second mapper. For ease of analysis, each quadrant is partitioned into a single 16QAM equivalent with two and three transmit antennas, respectively.

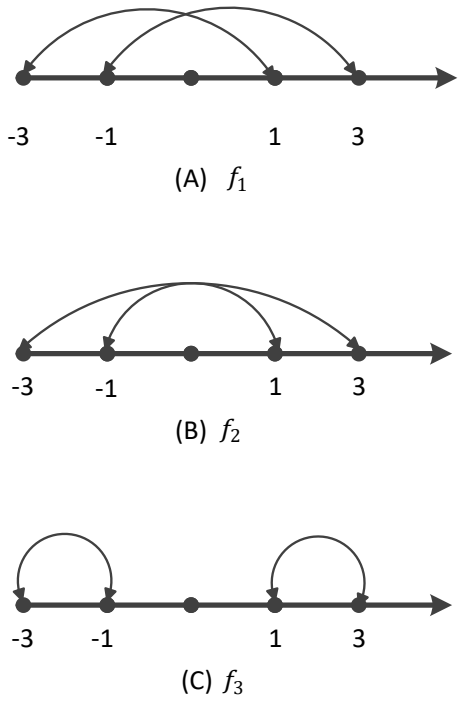

Figure A.2: Three transform of 4-ary pulse amplitude modulation

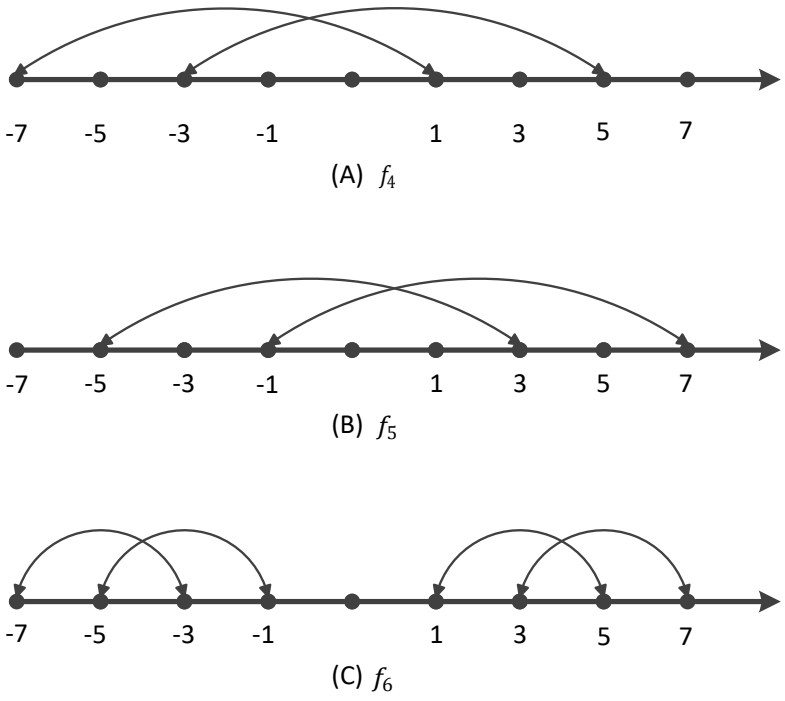

Figure A.3: Mappers of 8-ary pulse amplitude modulation

Table A.2: Mapping for three transmit antenna systems

$s_1 = s_1^I + js_1^Q$	Transform	$s_3 = s_3^I + js_3^Q$	$s_1 = s_1^I + js_1^Q$	Transform	$s_3 = s_3^I + js_3^Q$
$-3+j3$		$1-j$	$-1+j3$		$-3+j$
$3+j3$	$s_3^I = f_1(s_1^I)$	$-1-j$	$1+j3$	$s_3^I = f_3(s_1^I)$	$3+j$
$-3-j3$	$s_3^Q = f_1(s_1^Q)$	$1+j$	$-1-j3$	$s_3^Q = f_3(s_1^Q)$	$-3-j$
$3-j3$		$-1+j$	$1-j3$		$3-j$
$-3+j$		$-1-j3$	$-1+j$		$3-j3$
$3+j$	$s_3^I = f_3(s_1^I)$	$1-j3$	$1+j$	$s_3^I = f_1(s_1^I)$	$-3-j3$
$-3-j$	$s_3^Q = f_1(s_1^Q)$	$-1+j3$	$-1-j$	$s_3^Q = f_1(s_1^Q)$	$3+j3$
$3-j$		$1+j3$	$1-j$		$-3+j3$

Based on design of mappers in **Tables A.1** and **A.2**, we illustrate Gray-coded labeling map Ω_1^M,optimized maps Ω_2^M and Ω_3^M for 16-QAM in **Figure A.4** and for 64-QAM in **Figure A.5**.

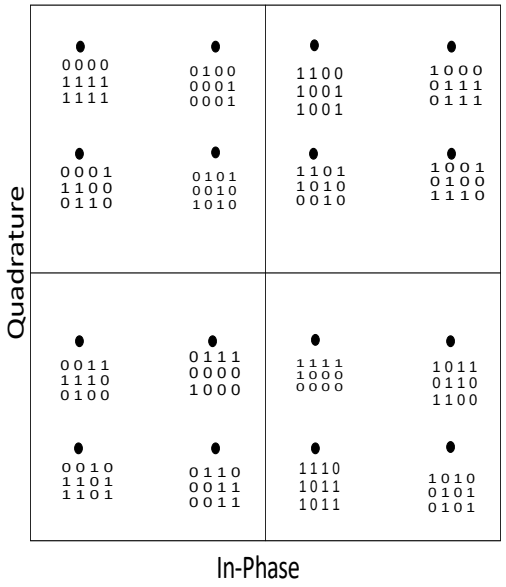

Figure A.4: 16-quadrature amplitude modulation Gray-coded labeling map Ω_1^{16}, optimized maps Ω_2^{16}, and Ω_2^{16}

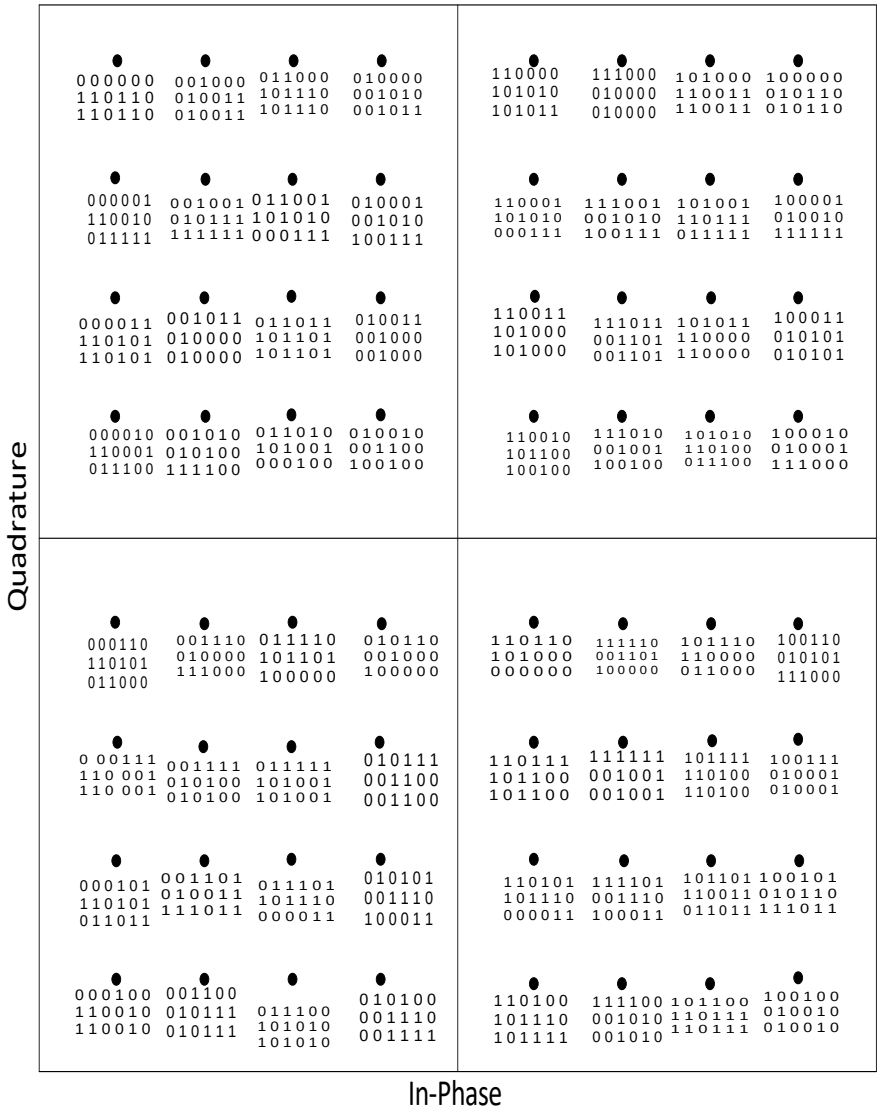

Figure A.5: 64-quadrature amplitude modulation Gray-coded labeling map Ω_1^{64}, optimized maps Ω_2^{64}, and Ω_2^{64}

6 Detection Schemes

6.1 ML detection

Assuming that perfect channel state information (CSI) at the receiver, the transmitted symbols are estimated by minimizing the ML expression as given by

$$[\hat{q}_1,\ \hat{q}_2,\ \hat{q}_3] = \underset{\substack{q_k \in [1:M],\\ k \in [1:3]}}{\operatorname{argmin}} \Big(\sum_{k=1}^{3} \Big\| \mathbf{y}_k - \sqrt{\frac{\rho}{3}} \mathbf{H}_k \mathbf{x}_k \Big\|_F^2 \Big) \tag{A.21}$$

The complexity of the optimal detection is proportional to $\prime(M^3)$, which is very high-order modulation. In the next subsection, we will discuss a low complexity (LC) detection scheme for the proposed USTLD with three transmit antennas.

6.2 Proposed LC detection scheme for USTLD

To reduce the computational complexity of the optimal ML USTLD detector, this section proposes a near-ML LC detector based on OP [16]. First, we express the received signal vector in time slot *k*, $k \in [1:3]$ as (A.3). The algorithm for the OP has four steps as

Step 1 – Compute the projection matrices $\mathbf{P}_k^i$ and projection spaces $\mathbf{r}_{k,q_i}^i$.

We define projection matrices $\mathbf{P}_k^i$, $i,k \in [1:3]$ that project a signal on the subspace orthogonal to $\mathbf{h}_k^i$, respectively, such that $\mathbf{P}_k^i$ is given by

$$\mathbf{P}_k^i = \mathbf{I}_{N_R} - \mathbf{T}_k^i \tag{A.22}$$

where $\mathbf{I}_{N_R}$ is an identity matrix, $\mathbf{T}_k^i = \mathbf{H}_k^i((\mathbf{H}_k^i)^H \mathbf{H}_k^i)^{-1}(\mathbf{H}_k^i)^H$ and $\mathbf{H}_k^i = [\mathbf{h}_k^1\, \mathbf{h}_k^2\, \mathbf{h}_k^3] \backslash [\mathbf{h}_k^i]$, where $[\mathbf{h}_k^1\, \mathbf{h}_k^2\, \mathbf{h}_k^3] \backslash [\mathbf{h}_k^i]$ denotes excluding $\mathbf{h}_k^i$ from $[\mathbf{h}_k^1\, \mathbf{h}_k^2\, \mathbf{h}_k^3]$. For example, $\mathbf{H}_1^2 = [\mathbf{h}_1^1\, \mathbf{h}_1^2\, \mathbf{h}_1^3] \backslash [\mathbf{h}_1^2] = [\mathbf{h}_1^1\, \mathbf{h}_1^3]$. Let the projection spaces be $\mathbf{r}_{k,q_i}^i$, which is given by

$$\mathbf{r}_{k,q_i}^i = \mathbf{y}_k - \sqrt{\frac{\rho}{3}} \mathbf{h}_k^i x_{q_i}^k, \quad i,k \in [1:3] \tag{A.23}$$

Step 2 - Based on OP, compute the metric for given $i, i \in [1:3]$.

$$\mathbf{z}_{q_i} = \sum_{k=1}^{3} \Big\| \mathbf{P}_k^i(\mathbf{r}_{k,q_i}^i) \Big\|_F^2, \qquad q_i \in [1:M], i \in [1:3] \tag{A.24}$$

Step 3 - Determine the indices of l possible transmitted symbols for each $i, i \in [1:3]$.

Sort the metric sets $\mathbf{z}_{q_1} = \{z_{q_{1,1}},\, z_{q_{1,2}}, \cdots, z_{q_{1,M}}\}$, $\mathbf{z}_{q_2} = \{z_{q_{2,1}},\, z_{q_{2,2}}, \cdots, z_{q_{2,M}}\}$ and $\mathbf{z}_{q_3} = \{z_{q_{3,1}},\, z_{q_{3,2}}, \cdots, z_{q_{3,M}}\}$ in ascending order, where $q_{i,j}, i \in [1:3], j \in [1:3]$. For convenience, let $\Phi_{i,l} = \{q_{i,1},\, q_{i,2}, \cdots, q_{i,l}\}$, where $\hat{q}_i$, $i \in [1:3]$, is the estimated indices for the

transmitted symbols.

Step 4 - Perform joint detection.

Finally, the joint detection is given by

$$[\hat{q}_1,\ \hat{q}_2,\ \hat{q}_3] = \underset{q_{i,v}\in\Phi_{i,l}}{\operatorname{argmin}}\Big(\sum_{k=1}^{3}\Big\|\mathbf{y}_k - \sqrt{\frac{\rho}{3}}\mathbf{h}_k^i x_{q_{i,v}}^k\Big\|_F^2\Big) \tag{A.25}$$

6.3 Complexity derivations of LC detection scheme for USTLD

The authors carry out complexity derivation of optimal ML USTLD in this subsection by analyzing and evaluating the decision metric similar to Rajashekar [17] using the number of floating point operations for each of $\mathbf{M}^{N_T}$ possible vector pairs. For a given vector $x_{q_i}^k$, $i,k \in [1:3]$, the following three steps derive the complexity of calculating vector norm $\left\|\mathbf{y}_k - \mathbf{h}_k^i x_{q_i}^k\right\|_F^2$.

Step 1 - Matrix product $\mathbf{h}_k^i x_{q_i}^k$: $N_T N_R$ complex multiplications, $N_T N_R - N_R$ complex additions.

Step 2 - Vector subtraction $\mathbf{y}_k - \mathbf{h}_k^i x_{q_i}^k$: N_R complex subtractions.

Step 3 - Vector norm $\left\|\mathbf{y}_k - \mathbf{h}_k^i x_{q_i}^k\right\|_F^2$: $4N_R - 1$ real operations.

Matrix product $\mathbf{h}_k^i x_{q_i}^k$ is given for $\mathbf{h}_k^1 x_{q_1}^k$, $\mathbf{h}_k^2 x_{q_2}^k$, and $\mathbf{h}_k^3 x_{q_3}^k$ with adding effective real operations $3(7N_T N_R - N_R) + 2$. Vector norm is performed for three real operations with two additions. The number of possible combinations of $x_{q_1}^1$, $x_{q_1}^2$ and $x_{q_1}^3$ is dependent on the size of the constellation used, M. Each of the N_T elements in the transmitted vector could take one of M possible values. Therefore, the overall complexity of ML detection is given as

$$\sigma_{USTLD-ML} = M^{N_T}(63N_T N_R + 9N_R + 5) \tag{A.26}$$

Since the complexity of LC near-ML detector scheme for STLD is an extension of two mappers design in Govindasamy et al, [12] the algorithm for $3 \times N_R$ USTLD scheme is analyzed in three steps:

Step 1 – Computing the projection matrices.

The number of complex operations required in evaluating and computing the projection matrices are based on (A.22). The argument of the inverse operation is a real scalar quantity R, where quantity $R = |\mathbf{H}_k^i|_F^2 = ((\mathbf{H}_k^i)^H \mathbf{H}_k^i)$. Since the argument operates on a quantity R, the authors ignore the inverse operation. The analysis requires N_R complex multiplications and $(N_R - 1)$ complex additions. Furthermore, the second term becomes $\mathbf{H}_k^i . \frac{1}{R} . (\mathbf{H}_k^i)^H$, which requires only $N_R^2 + N_R$ complex multiplications. Finally, the remaining complex operation is the subtraction of an $N_R \times N_R$ matrix resulting in N_R^2 complex additions. Given that we require nine projection matrices, the overall number of complex operations required for computation is thus

$$\sigma_{pm} = 9N_R^2 + 14N_R + 6 \tag{A.27}$$

Step 2 - Computing the metric sets $\mathbf{z}_{q_i}$, where $q_i \in [1:M]$, $i \in [1:3]$.

The number of complex operations required in evaluating and computing the metric for given $i, i \in [1:3]$. Given the complex operation in (A.24) that are equal, each of the computation of $\mathbf{P}_1^1(\mathbf{r}_{1,q_1}^1)$, $\mathbf{P}_1^2(\mathbf{r}_{1,q_1}^2)$, and $\mathbf{P}_1^3(\mathbf{r}_{1,q_1}^3)$ is a multiplication of a $N_R \times N_R$ matrix and a $N_R \times 1$ vector. This gives a $N_R \times 1$ vector, which requires N_R^2 complex multiplications and $N_R(N_R-1)$ complex addition. The computation of $\mathbf{r}_{1,q_1}^1$, $\mathbf{r}_{1,q_1}^2$ and $\mathbf{r}_{1,q_1}^3$ contain redundant calculations $\sqrt{\frac{\rho}{3}}\mathbf{h}_1^1$, $\sqrt{\frac{\rho}{3}}\mathbf{h}_2^1$, and $\sqrt{\frac{\rho}{3}}\mathbf{h}_3^1$, respectively, that can be evaluated and stored. Thus, the overall metric sets gives

$$\sigma_{set} = M(21N_R^2 + 36N_R - 4) \tag{A.28}$$

Step 3 - Computing the joint ML detection The final step requires performing joint ML search through the candidate sets in (A.25) and determining the number of complex operations σ_{ML-LC} performed through the search. The argument of each operator in the Frobenius norm is $2N_R$ complex multiplications and N_R complex additions. In the said (A.25), each Frobenius norm requires N_R complex multiplications and $(N_R - 1)$ complex additions. Given that the norm operator contains three norms and is evaluated over l^3 possible transmitted symbol combination, we arrive at

$$\sigma_{ML-LC} = 45l^3N_R - 6l^3 - 4 \tag{A.29}$$

The overall computational complexity for LC is

$$\sigma_{USTLD-LC} = \sigma_{pm} + \sigma_{set} + \sigma_{ML-LC} \tag{A.30}$$

$$\sigma_{USTLD-LC} = N_R^2(9 + 21M) + N_R(14 + 36M + 45l^3) + (2 - 4M - 6l^3)$$

6.4 Computational complexity comparison

The computational complexities for ML and LC OP detectors for the proposed three mappers are evaluated and compared in this section. The tabulated result in **Table A3** outlines complexity comparison for 16QAM and 64QAM. The percentage reduction in complexity between the two detectors is thus given as

$$\%\ \textit{Reduction}\ \sigma_{USTLD-LC} = 1 - \frac{\sigma_{USTLD-LC}}{\sigma_{USTLD-ML}} \times 100\% \tag{A.31}$$

7 Simulation and Discussion

The Monte Carlo simulation outputs and the theoretical BER expressions for the proposed $3 \times N_R$ USTLD scheme for 16-QAM and 64-QAM are presented in this section. We consider simulation

Table A.3: Computational complexities between ML and proposed LC detectors for USTLD

Configuration	ML Detector	Proposed LC Detector	Percentage Drop in Complexity
M = 16, L=9	201728	98854	51%
M = 64, L=9	3227648	112918	96.5%

using Monte Carlo techniques in this research since the average BER performance is plotted against the average SNR per received antenna for different systems configuration. In this study, we assume $N_R = 4$ received antennas in all cases.

Further, the authors assume perfect CSI at the receiver and an ideal feedback link to the transmitter exists. N_T antennas are separated wide enough from N_R antennas in order to avoid correlation, while maximal ration combining reception is considered with N_R received signal. We also assume that the total N_T power is the same at the transmitter.

Performance comparisons for 16QAM are made for proposed $3 \times N_R$ mappers USTLD, existing $2 \times N_R$ mappers USTLD [11] and Samra [8]. However, performance comparisons for 64QAM are made only for proposed $3 \times N_R$ mappers USTLD and $2 \times N_R$ mappers USTLD [11], since Samra [8] is limited to 16QAM simulation. The results for 16QAM USTLD and 64QAM $2 \times N_R$ and $3 \times N_R$ USTLD and are depicted in **Figure A6** and **Figure A7**, respectively.

In the first set of investigation, performance comparisons for 16QAM model for existing USTLD [11], proposed USTLD and 16QAM mapping proposed by Samra [8] are evaluated at a BER gain of 10^{-5}. The proposed $3 \times N_R$ USTLD exhibits an SNR performance gain of approximate value $0.8\,dB$ when compared with Samra [8] and $3\,dB$ over USTLD of existing Xu et al. [11].

Secondly, the simulation outputs and analytical expression for the proposed USTLD BER at 64QAM match very closely at high SNR and show an approximate SNR gain of $4.8\,dB$ when compared with existing USTLD [11] at a BER value of 10^{-5}.

The ABEP expression is evaluated for a tight analytical bound with the simulation results for USTLD. Again, the formulated LC detector for both 16QAM and 64QAM USTLD approach near ML performance with considerable lower complexity than the ML detector.

The labeling maps design in this paper are based on heuristic algorithm whose determination has the merit of requiring an exhaustive computer search.

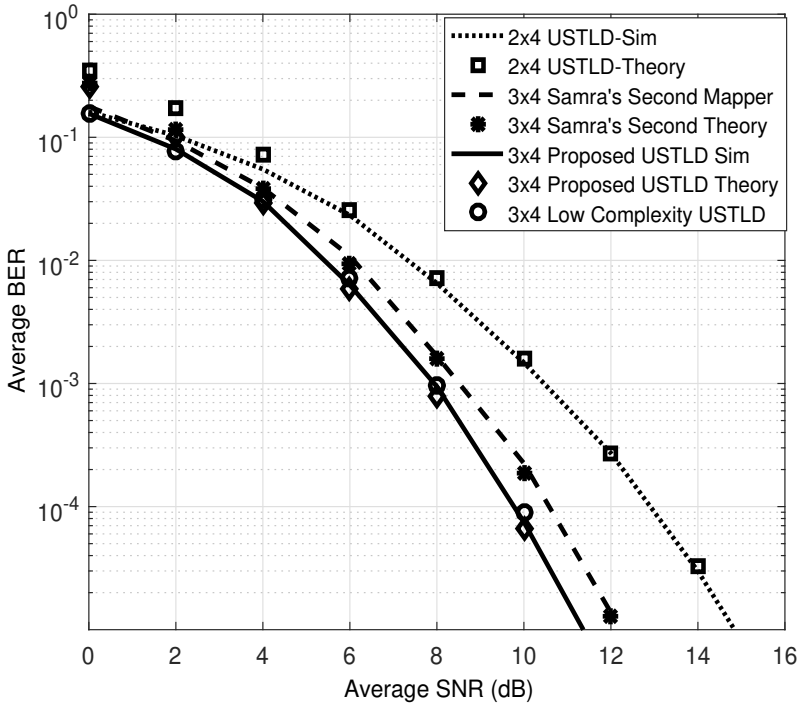

Figure A.6: Bit error rate (BER) performance of uncoded space-time labeling diversity (USTLD) systems for 16-quadrature amplitude modulation using maximum likelihood and low-complexity detectors. SNR, signal-to-noise ratio

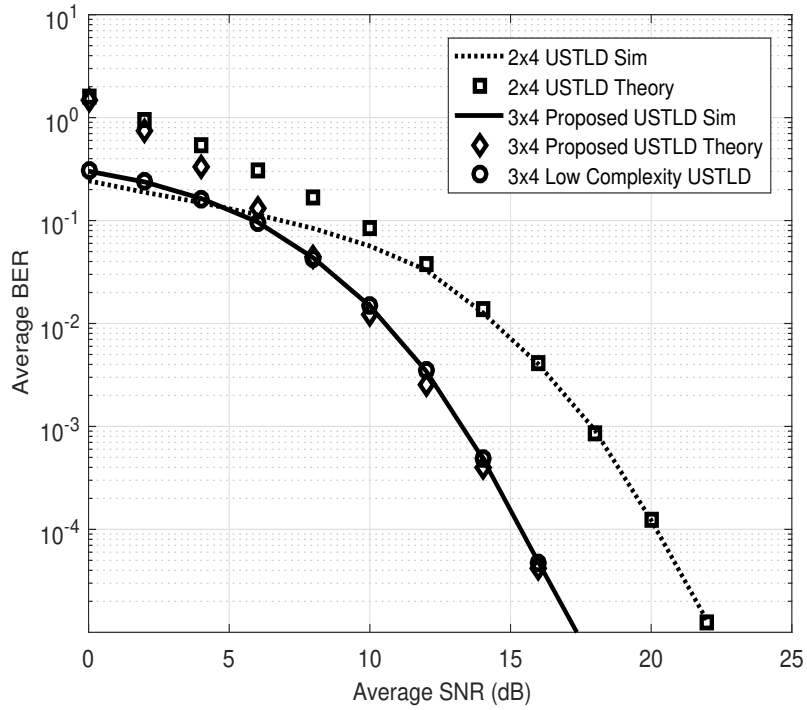

Figure A.7: Bit error rate (BER) performance of uncoded space-time labeling diversity (USTLD) systems for 64-quadrature amplitude modulation using maximum likelihood and low-complexity detectors

8 Conclusion

This paper introduces three transmit antennas USTLD scheme to further improve error performance of the existing two transmit antennas USTLD scheme. The scheme requires designing a new mapper for the third symbol mapping using heuristic approach to mapper design. The heuristic algorithm is designed to maximize the minimum product distance.

The analytical union bound was derived that tightly matched the Monte Carlo simulation results for different M-ary constellation systems. Moreover, the effect of high computational payload, which exists in the ML detection scheme, was mitigated by proposing a near-ML OP LC scheme. Compared with the existing two mapper USTLD, the performance of the proposed three-mapper USTLD improved significantly while reducing computational complexity by 51% and 96.5% for 16QAM and 64QAM respectively.

9 Appendix A

$P(\mathbf{X} \to \hat{\mathbf{X}})$ DIVERSITY GAIN DERIVATION

Where $\rho = SNR$, Equation (A.18) becomes

$$-d = \lim_{\rho\to\infty} \frac{\log\left(\frac{1}{2n}\left[\frac{1}{2}\prod_{k=1}^{3}\left(\frac{\rho}{12}\delta_k\right)^{-N_R} + \sum_{l=1}^{n-1}\left(\frac{1}{\sin^2\left(\frac{l\pi}{2n}\right)}\right)^{-3N_R}\prod_{k=1}^{3}\left(\frac{\rho}{12}\delta_k\right)^{-N_R}\right]\right)}{\log(\rho)} \tag{A.32}$$

Simplify further, $-d$ is given as

$$-d = \lim_{\rho\to\infty} \frac{\log(\beta\rho^{-3N_R})}{\log(\rho)} \tag{A.33}$$

where $\beta = \frac{1}{2n}\left[\frac{1}{2} + \sum_{l=1}^{n-1}\left(\frac{1}{\sin^2\left(\frac{l\pi}{2n}\right)}\right)^{-3N_R}\right]\prod_{k=1}^{3}\left(\frac{\delta_k}{12}\right)^{-N_R}$

Since $\lim_{\rho\to\infty}\frac{\log(\beta)}{\log(\rho)} = 0$, therefore, $d = 3N_R$.

The diversity order d of the system in Equation (A.16) with three transmit antennas is $3N_R$.

References

[1] Y. Huang and J. A. Ritcey, "Optimal constellation labeling for iteratively decoded bit-interleaved space-time coded modulation," *IEEE Transactions on Information Theory*, vol. 51, no. 5, pp. 1865–1871, Apr. 2005.

[2] ——, "Improved 16-QAM constellation labeling for BI-STCM-ID with the Alamouti scheme," *IEEE Communications Letters*, vol. 9, no. 2, pp. 157–159, Jan. 2005.

[3] S. Ejaz, Y. FengFan, and H. Xu, "Labeling Diversity for 2 x 2 WLAN Coded-Cooperative Networks." *Radioengineering*, vol. 24, 2015.

[4] M. Krasicki and P. Szulakiewicz, "Boosted space-time diversity scheme for wireless communications," *Electronics letters*, vol. 45, no. 16, pp. 843–845, Jul. 2009.

[5] M. Krasicki, "Improved labelling diversity for iteratively-decoded multi-antenna systems," in *2011 7th International Wireless Communications and Mobile Computing Conference*, Jul. 2011, pp. 359–364.

[6] ——, "Comments on "Optimal constellation labeling for iteratively decoded bit-interleaved space-time coded modulation"," *IEEE Transactions on Information Theory*, vol. 58, no. 7, pp. 4967–4968, Apr. 2012.

[7] ——, "Essence of 16-QAM labelling diversity," *Electronics Letters*, vol. 49, no. 8, pp. 567–569, Apr. 2013.

[8] H. Samra, Z. Ding, and P. M. Hahn, "Symbol mapping diversity design for multiple packet transmissions," *IEEE Transactions on Communications*, vol. 53, no. 5, pp. 810–817, May 2005.

[9] H. Samra and Z. Ding, "Retransmission diversity schemes for multicarrier modulations," *IEEE transactions on wireless communications*, vol. 5, no. 5, pp. 1142–1147, Jun. 2006.

[10] K. G. Seddik, A. S. Ibrahim, and K. R. Liu, "Trans-modulation in wireless relay networks," *IEEE Communications Letters*, vol. 12, no. 3, pp. 170–172, Mar. 2008.

[11] H. Xu, K. Govindasamy, and N. Pillay, "Uncoded space-time labeling diversity," *IEEE Communications Letters*, vol. 20, no. 8, pp. 1511–1514, Jun. 2016.

[12] K. Govindasamy, H. Xu, and N. Pillay, "Space-time block coded spatial modulation with labeling diversity," *International Journal of Communication Systems*, vol. 31, no. 1, p. e3395, Jan. 2018.

[13] N. Pillay and H. Xu, "Uncoded space-time labeling diversity—Application of media-based modulation with RF mirrors," *IEEE Communications Letters*, vol. 22, no. 2, pp. 272–275, Nov. 2017.

[14] E. Basar and I. Altunbas, "Space-time channel modulation," *IEEE Transactions on Vehicular Technology*, vol. 66, no. 8, pp. 7609–7614, Feb. 2017.

[15] L. Zheng and D. N. C. Tse, "Diversity and multiplexing: A fundamental tradeoff in multiple-antenna channels," *IEEE Transactions on information theory*, vol. 49, no. 5, pp. 1073–1096, 2003.

[16] S. Bahng, S. Shin, and Y.-O. Park, “ML approaching MIMO detection based on orthogonal projection,” *IEEE communications letters*, vol. 11, no. 6, pp. 474–476, Jul. 2007.

[17] R. Rajashekar, K. Hari, and L. Hanzo, “Reduced-complexity ML detection and capacity-optimized training for spatial modulation systems,” *IEEE Transactions on Communications*, vol. 62, no. 1, pp. 112–125, Dec. 2013.

Part III

Paper B

Paper B

Performance Analysis of *M*-ary APSK Uncoded Space-time Labeling Diversity with Three Transmit Antennas in Rician Broadcast Channels

1 Abstract

This paper investigates the design of labeling mappers for uncoded space-time labeling diversity with three transmit antennas (USTLD) based on amplitude and phase shift keying (APSK) modulation. The proposed USTLD schemes are DVB-S2 and DVB-S2X standards compatible and provide robustness against nonlinear distortion for both Rician fast frequency-flat fading and quasi-static frequency-flat fading channels. Numerical analysis of the proposed schemes are derived based on pairwise error probability. The analytical results are validated by Monte Carlo simulations, which converge accurately at high SNR. Furthermore, by adapting constellation structure between square QAM modulations and concentric rings of APSK modulations, the authors proposed mapper design for 16-APSK, 32-APSK and 64-APSK modulations for USTLD using heuristic algorithm. Finally, the proposed USTLD schemes show bit error rate (BER) improvement over the existing two transmit USTLD schemes with error performance gain of 1.2 dB and 2.8 dB at a BER of 10^{-6} for 16-APSK and 64-APSK USTLD scheme, respectively.

2 Introduction

The growing demand for higher spectral efficiency and receiver error performance has led to evolution of standards for digital communications. By exploiting efficient transmission techniques, new standards for digital broadcasting are emerging. The second-generation digital video broadcasting for satellites (DVB-S2) has been improved upon and extended without fundamentally changing its original structure [1]. This updated standard with the name DVB-S2 extensions (DVB-S2X) is an improvement in data rates over a wide range of signal-to-noise ratios (SNRs) to DVB-S2 standard [2].

Specifically, these extensions to DVB-S2X include the design of new high order constellations up to 256-APSK as opposed to 32-APSK of DVB-S2, the design of new low density parity check (LDPC) codes, the adoption of advanced receiver architectures, the application of the faster-than-Nyquist technique, or its extension known as time packing, and an optimization of the bandwidth and the baud rate of the transmitted signals [3].

On the other hand, the design of higher order modulation scheme for improved spectral efficiency in digital broadcasting has received a significant attention in the recent time. Modulation and coding configurations adopting constellations of orders 64-APSK, 128-APSK and 256-APSK are employed in DVB-S2X standard [2]. There is a foreseeable demands for larger constellations in near future knowing fully well that the traffic demand for satellite broadband is expected to grow six-fold by 2020 [4].

Several modern wireless communication schemes use M-ary quadrature amplitude modulation (M-QAM) constellations as transmission techniques as a result of their square structure. However, M-QAM do not provide satisfying robustness to amplitude and phase noise distortion effects due to the increase in the number of constellation points. This leads to increasing peak to average power ratio (PAPR) that is not well suited for long distance satellite communications [5]. Also, M-QAM requires a cost ineffective power amplifier and oscillator at the transmitter in order to guarantee low distortion which complicate the application of dense transmission techniques in realistic high-data rate digital broadcasting systems.

Due to its nonlinear channels typical of digital broadcasting communications, M-ary amplitude phase-shift keying (M-APSK) is a modulation technique that has become widely adopted for DVB-S2 and DVB-S2X that offers an attractive combination of spectral and energy efficiency. The APSK constellation design approaches considered recently in the literature follow two main optimization criteria [6], [7], [8]. These criteria are maximization of the minimum Euclidean distance

(MED), and maximization of the channel mutual information (MI). Unlike the former optimization criterion which refers to the high SNR asymptotic case, channel MI provides an optimum M-APSK constellation for each SNR operating point.

Constellation labeling design for M-APSK scheme in coded and uncoded modulations have become an attractive research topic for digital broadcasting [6], [7], [8], [9], [10], [11], [12], [13], [14], [15], [16]. In this area, maximizing the MI between the channel input and output signals is a popular criterion. Based on MI criterion, both the radii and phases of each concentric circle as well as the number of points on each circle can be optimized for high capacity error performance and robustness to phase noise.

Authors in [9] showed that M-APSK performs better in terms of MI, particularly for the cases of 16-APSK and 64-APSK considering the peak power limited Gaussian complex channels. MI provides the maximum transmission rate (in bits per channel use) at which error-free transmission is possible with a given signal set. The design optimization analysis and results obtained for 64-APSK modulation schemes based on the MI maximization criterion are presented in [8]. Optimization of 64-APSK constellation was made by maximizing MI criteria, which ensures that the maximum amount of information par symbol is transmitted over communication channel.

The problem of designing constellations that maximize the MI of a memoryless phase noise channel was addressed in the literature [13]. In this study, the approximate MI for the channel was derived, and optimal constellations were obtained by maximizing the MI using a simulated annealing algorithm. The author in [14] proposed two methods of improving the average MI based on phase and amplitude in bit-interleaved coded modulation and the improvement were verified by bit error rate. Other authors have proposed multi-level coded modulation scheme with low detection complexity and competitive error performance [5].

The impact of nonlinear distortion in the framework of single-carrier signal has been investigated and a new modeling approach for its compensation proposed in uncoded and coded modulation [15]. For coded modulation, recently developed metrics that can be adjusted to the statistical characteristics of nonlinear channel distortion was proposed in [15]. For uncoded modulation, optimal decision region as well as suboptimal ones that may exhibit error performance gains close to the optimal in the case of low SNR was equally developed in [15]. Also, authors in [16] derived error rate bounds for 16-APSK and 32-APSK in DVB-S2 standard in uncoded modulation scheme and determined the optimal input power level for the soft-limiter channel.

Recently, multiple-input multiple-output (MIMO) scheme has been considered as one of the key next-

generation technologies for hybrid satellite-terrestrial broadcasting systems [17], [18], [19], [20], [20]. Due to its potential multiplexing gain or diversity gain and increased coverage area, or a trade-off between them, MIMO can provide higher data rates than single antenna systems without any extra bandwidth consumption or propagation power usage. For instance, the second generation Digital Video Broadcasting - Terrestrial (DVB-T2) [21] has recently employed multiple-input single-output (MISO) scheme, while Digital Video Broadcasting - Next Generation Handheld (DVB-NGH) [22] employed 2×2 MIMO scheme.

Uncoded space-time labeling diversity is a MIMO scheme that achieves improved diversity gain over Alamouti STBC [23]. The majority of transmission scheme applied for USTLD both in coded [24], [25], [26], [27] and uncoded modulation [28], [29], [30], [31], [32] has been M-QAM constellation. A new mapper design using heuristic algorithm for USTLD in Nakagami-q fading channel has been proposed for APSK digital broadcasting [33]. The authors derive a set of possible metrics based on MED for evaluating mappers design in two transmit antennas USTLD scheme. In addition, authors in [34] proposed a new genetic algorithm for USTLD applicable to M-QAM, M-ary Phase Shift Keying (M-PSK) and M-APSK.

In this study, we introduce APSK-based USTLD scheme for three transmit antennas (A-USTLD) in nonlinear Rician fading channel where the transmission of line-of-sight (LOS) component is not obstructed by obstacles [35] [36]. Moreover, Rician fading channel has attracted interest in digital broadcast channels recently [37], [38], [39]. Therefore, the significance of this research lies in the study of bit error rate analysis of the proposed A-USTLD scheme for broadcast communication in independent and identically distributed channel (i.i.d) for fast frequency-flat Rician fading and quasi-static frequency-flat Rician fading channel.

2.1 Contributions

The adaptation of MIMO USTLD scheme for digital broadcasting system using APSK transmission model has just been introduced in the literature [33] [34]. Motivated by the transmit diversity gain and spectrally efficient error performance of three transmit antennas USTLD scheme [31] over two transmit antennas USTLD scheme [23] in M-QAM constellations, this paper introduces the design of new constellation mappers for 16-APSK, 32-APSK and 64-APSK USTLD with three transmit antennas and its application to DVB-S2 and DVB-S2X satellite standards.

Therefore, the original contributions of this study are as follows: (1) An APSK-based USTLD with three transmit antennas (A-USTLD) for a digital broadcasting is proposed for Rician fast and quasi-static fading channel. (2) Closed-form error performance analysis of the proposed A-USTLD are

derived based on trapezoidal approximation and Gaussian Q-function. The numerical expressions converge accurately in the high SNR range. (3) In addition, designing the first and second optimized mappers that is well suited to nonlinear digital broadcasting schemes for DVB-S2 and DVB-S2X is a major factor. Thus, a heuristic algorithm that explores the similarity in structure between the square M-QAM and concentric rings M-APSK constellations are adapted for this study taking into consideration the nonlinear effect that models amplitude and phase distortions on the input signals. (4) Moreover, error performance comparison of the proposed schemes are carried out with the existing USTLD APSK with two transmit antennas based on rate one for link reliability.

2.2 Notations

Throughout this paper, vectors are denoted in bold small letters, while matrices are denoted in bold capital letters. $[\cdot]^T$, $(\cdot)^H$, $\| \cdot \|_F$ and $| \cdot |$ are used for the transpose, Hermitian transpose, Frobenius norm and Euclidean norm, respectively. $E(\cdot)$ is the expectation operator. $Q(\cdot)$ is the Gaussian Q-function. $(\cdot)!$ represents factorial. $I_{N_R}()$ is the modified N_R-order Bessel functions of the first kind. *j* is the complex number. The superscript operators $(\cdot)^I/(\cdot)^Q$ correspond to the in-phase/quadrature components. The minimum and maximum of the argument with respect to *w* are denoted by operators $argmin_w(\cdot)$ and $argmax_w(\cdot)$.

3 System Model

This section discusses the transmitter model, channel model and maximum likelihood (ML) detection for the nonlinear ASPK signals in Rician fading USTLD with three transmit antennas.

3.1 Transmitter Model

The M-ary APSK constellation are composed of L concentric contours, each with uniformly spaced PSK points. Mathematically, the set on the ℓth ring, for $\ell = 0, 1, \cdots, L-1$, can be expressed as [7]:

$$\Psi_\ell = \left\{ r_\ell e^{j\left(\phi_\ell + k\frac{2\pi}{N_\ell}\right)} : k \in [0 : N_\ell - 1] \right\}, \tag{B.1}$$

where r_ℓ and ϕ_ℓ correspond to the radius and phase shift, respectively. N_ℓ is used for the number of points on the ℓth ring. It is assumed that Ψ_0, Ψ_1,$\cdots$,Ψ_{L-1} are mutually exclusive. Thus, the entire set of signal constellations can be expressed as $\Psi = \bigcup_{\ell=0}^{L-1} \Psi_\ell$ and $N = |\Psi| = \sum_{\ell=0}^{L-1} N_\ell$ [15]. For gray code, the radii of APSK rings r_ℓ are arranged in a descending order, that is, $r_{\ell-1} < r_\ell < r_{\ell+1}$, and are defined as $r_\ell = \rho_\ell r_0$ with $r_0 = \sqrt{\frac{N}{(N_0 + \sum_{\ell=1}^{L-1} \rho_\ell^2 N_\ell)}}$, where $\rho_\ell = \frac{r_\ell}{r_0}$ is the ring ratio of the ℓ^{th} ring. It is assumed that r_0 is chosen such that the average energy is normalized to unity.

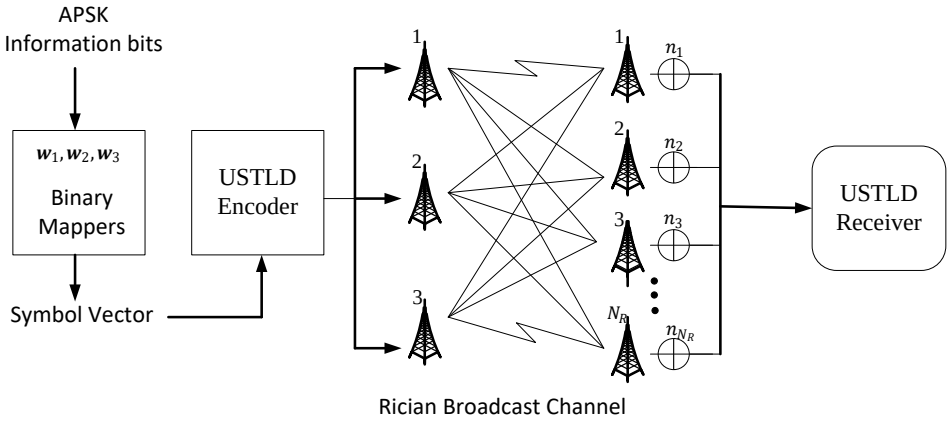

Figure B.1: System model of the proposed A-USTLD

The authors propose A-USTLD MIMO system equipped with $N_T = 3$ and N_R transmit and receive antennas, respectively as shown in **Figure B.1**. At the beginning of a transmission interval, a block of $c = 3\log_2 M$ bits, where *M*=16, 32 or 64 is the order of *M*-ary APSK modulation (*M*-APSK), is split into three $w = \log_2 M$-tuple vectors $\mathbf{w}_u = [w_{u,1}\, w_{u,2} \cdots w_{u,w}]$, $u \in [1:3]$, which are injected into Mapper 1, Mapper 2 and Mapper 3 simultaneously. Mappers $\Omega_v^M(\mathbf{w}_u)$, $u \in [1:3]$ and $v \in [1:3]$ map bit stream $\mathbf{w}_u$ into *M*-APSK constellation points in the Argand plane that produces $x_{q_u}^v = \Omega_v^M(\mathbf{w}_u)$. q_u is an index of $\mathbf{w}_u$ given as $q_u = 1 + \sum_{v=1}^{w} 2^{v-1} w_{u,v}$.

3.2 Rician Channel Model

In the proposed A-USTLD scheme, the authors represent Mapper 1 Ω_1^M as a Gray coded mapper, while Mapper 2 and Mapper 3 are the optimized labeling mappers designed to MED [31]. It is assumed that $E(|x_{q_u}^v|^2) = 1$. After the mapping, antennas 1, 2 and 3 simultaneously transmit the modulated symbols $x_{q_1}^1$, $x_{q_2}^1$ and $x_{q_3}^1$ in time slot 1. Symbols $x_{q_2}^2$, $x_{q_3}^2$ and $x_{q_1}^2$ are simultaneously transmitted by antennas 1, 2 and 3 in time slot 2 and in time slot 3, antennas 1, 2 and 3 simultaneously transmit $x_{q_3}^3$, $x_{q_1}^3$ and $x_{q_2}^3$, respectively. The $N_R \times 1$ received signal vector over Rician fading channels in time slots

1, 2 and 3 may be expressed as:

$$\mathbf{z}_1 = \sqrt{\frac{\tau}{3}}(\mathbf{h}_1^1 x_{q_1}^1 + \mathbf{h}_1^2 x_{q_2}^1 + \mathbf{h}_1^3 x_{q_3}^1) + \mathbf{n}_1 \tag{B.2a}$$

$$\mathbf{z}_2 = \sqrt{\frac{\tau}{3}}(\mathbf{h}_2^1 x_{q_2}^2 + \mathbf{h}_2^2 x_{q_3}^2 + \mathbf{h}_2^3 x_{q_1}^2) + \mathbf{n}_2 \tag{B.2b}$$

$$\mathbf{z}_3 = \sqrt{\frac{\tau}{3}}(\mathbf{h}_3^1 x_{q_3}^3 + \mathbf{h}_3^2 x_{q_1}^3 + \mathbf{h}_3^3 x_{q_2}^3) + \mathbf{n}_3 \tag{B.2c}$$

where $\mathbf{z}_v \in C^{N_R \times 1}$, $v \in [1:3]$ are received signal vector. $\frac{\tau}{3}$ are the average SNR at each receive antenna. $\mathbf{h}_v^u$, $u \in [1:3]$ are the $N_R \times 1$ channel matrix modeled as a fast frequency-flat Rician distribution, where it is assumed that the channel gains remain constant during a time slot, but assume independent values from one time slot to another defined as $\mathbf{h}_v^u = [h_v^{1,u}\, h_v^{2,u} \cdots h_v^{N_R,u}]^T$. A quasi-static frequency-flat Rician distribution is also taken into consideration in this study which corresponds to the case of $\mathbf{h}_1^1 = \mathbf{h}_2^1 = \mathbf{h}_3^1,\ \mathbf{h}_1^2 = \mathbf{h}_2^2 = \mathbf{h}_3^2$ and $\mathbf{h}_1^3 = \mathbf{h}_2^3 = \mathbf{h}_3^3$. The entries of fading matrix $\mathbf{h}_v^u$ can be modeled as:

$$h_v^{p,u} = \sqrt{\frac{K}{1+K}}\bar{\bar{h}}_v^{p,u} + \sqrt{\frac{1}{1+K}}\bar{h}_v^{p,u}, \quad [p \in 1:N_R], [u \in 1:3] \tag{B.3}$$

where K is the Rician factor defined as the ratio of the power of the dominant specular components to the average power of the random components. $\bar{\bar{h}}_v^{p,u}$ are entries of normalized constant vectors that represent the LOS components, and $\bar{h}_v^{p,u}$ are entries of symmetric Gaussian random variables. Note that $\bar{h}_v^{p,u}$ entries are i.i.d Gaussian distribution $CN(0,1)$. $\mathbf{n}_v \in C^{N_R \times 1}$ is an $N_R \times 1$ additive white Gaussian noise (AWGN) vector and $\mathbf{n}_v$ entries are i.i.d complex Gaussian random variables (RVs) according to $CN(0,1)$.

3.3 ML Detection

In this study, the authors assume complete knowledge of the channel at the receiver. The A-USTLD receiver uses an ML detector, which may be expressed as:

$$[\hat{q}_1,\ \hat{q}_2,\ \hat{q}_3] = \underset{q_1,q_2,q_3 \in [1:M]}{\operatorname{argmin}} \Big(\Big\| \mathbf{z}_1 - (\mathbf{h}_1^1 x_{q_1}^1 + \mathbf{h}_1^2 x_{q_2}^1 + \mathbf{h}_1^3 x_{q_3}^1) \Big\|_F^2 + \Big\| \mathbf{z}_2 - (\mathbf{h}_2^1 x_{q_2}^2 + \mathbf{h}_2^2 x_{q_3}^2 + \mathbf{h}_2^3 x_{q_1}^2) \Big\|_F^2 + \Big\| \mathbf{z}_3 - (\mathbf{h}_3^1 x_{q_3}^3 + \mathbf{h}_3^2 x_{q_1}^3 + \mathbf{h}_3^3 x_{q_2}^3) \Big\|_F^2 \Big) \tag{B.4}$$

4 Error Performance Analysis

In this section, the authors present a closed-form analysis of A-USTLD for Rician fading channels by using conditional pairwise error probability (PEP) and the trapezoidal approximation to Q-function.

We assume two triads of symbols are correctly detected while only one triad of symbols is erroneously detected at high SNR [31].

4.1 Rician fading error analysis

It is to be noted that two triads of symbols, $x_{q_u}^v$, $u \in [2:3]$, $v \in [1:3]$ are correctly detected in the high SNR, while $x_{q_1}^v$ is detected with errors. Therefore, (B.2a) - (B.2c) can be further expressed as:

$$\mathbf{z}_1 = \sqrt{\frac{\tau}{3}}\mathbf{h}_1^1 x_{q_1}^1 + \mathbf{n}_1 \tag{B.5a}$$

$$\mathbf{z}_2 = \sqrt{\frac{\tau}{3}}\mathbf{h}_2^3 x_{q_1}^2 + \mathbf{n}_2 \tag{B.5b}$$

$$\mathbf{z}_3 = \sqrt{\frac{\tau}{3}}\mathbf{h}_3^2 x_{q_1}^3 + \mathbf{n}_3 \tag{B.5c}$$

by applying the transmit model in (B.5a) - (B.5c), the average bit error probability (ABEP) can be expressed as:

$$P_{ABEP}(\tau) \leq \frac{1}{Mw}\sum_{q_1=1}^{M}\sum_{\hat{q}_1 \neq q_1}^{M} \Delta(q_1, \hat{q}_1) P(\mathbf{X} \rightarrow \hat{\mathbf{X}}) \tag{B.6}$$

where $\Delta(q_1, \hat{q}_1)$ is the number of bit errors for the associated pairwise error probability (PEP) event. $P(\mathbf{X} \rightarrow \hat{\mathbf{X}})$ is the PEP when $\mathbf{X}$ is transmitted and $\hat{\mathbf{X}}$ is detected, represented as $\mathbf{X} = [x_{q_1}^1 x_{q_1}^2 x_{q_1}^3]$ and $\hat{\mathbf{X}} = [x_{\hat{q}_1}^1\ x_{\hat{q}_1}^2\ x_{\hat{q}_1}^3]$. The conditional PEP $P(\mathbf{X} \rightarrow \hat{\mathbf{X}}|\mathbf{h}_1^1,\ \mathbf{h}_2^3,\ \mathbf{h}_3^2)$ may be formulated as:

$$\begin{aligned} P(\mathbf{X} \rightarrow \hat{\mathbf{X}}|\mathbf{h}_1^1,\ \mathbf{h}_2^3,\ \mathbf{h}_3^2) =& P\Bigg(\left\|\mathbf{z}_1 - \sqrt{\frac{\tau}{3}}\mathbf{h}_1^1 x_{\hat{q}_1}^1\right\|_F^2 + \left\|\mathbf{z}_2 - \sqrt{\frac{\tau}{3}}\mathbf{h}_2^3 x_{\hat{q}_1}^2\right\|_F^2 + \left\|\mathbf{z}_3 - \sqrt{\frac{\tau}{3}}\mathbf{h}_3^2 x_{\hat{q}_1}^3\right\|_F^2 \\ <& \left\|\mathbf{z}_1 - \sqrt{\frac{\tau}{3}}\mathbf{h}_1^1 x_{q_1}^1\right\|_F^2 + \left\|\mathbf{z}_2 - \sqrt{\frac{\tau}{3}}\mathbf{h}_2^3 x_{q_1}^2\right\|_F^2 + \left\|\mathbf{z}_3 - \sqrt{\frac{\tau}{3}}\mathbf{h}_3^2 x_{q_1}^3\right\|_F^2 \Bigg) \end{aligned} \tag{B.7}$$

The PEP can be given as (refer to Appendix B):

$$P(\mathbf{X} \rightarrow \hat{\mathbf{X}}|\mathbf{h}_1^1,\ \mathbf{h}_2^3,\ \mathbf{h}_3^2) = Q\left(\sqrt{\sum_{v=1}^{3}\delta_v}\right) \tag{B.8}$$

where $\delta_1 = \frac{\tau}{6}\|\mathbf{h}_1^1\|_F^2|d_1|^2$, $\delta_2 = \frac{\tau}{6}\|\mathbf{h}_2^3\|_F^2|d_2|^2$ and $\delta_3 = \frac{\tau}{6}\|\mathbf{h}_3^2\|_F^2|d_3|^2$. Note that $d_v = x_{q_1}^v - x_{\hat{q}_1}^v$, $v \in [1:3]$. δ_v can be simplified in terms of p^{th}-received antennas as:

$$\delta_v = \frac{\tau}{6}|d_v|^2\sum_{p=1}^{N_R}|h_v^{p,1}|^2 \tag{B.9}$$

For MRC with N_R diversity branches, the combiner output is given as: $\gamma_v = \sum_{p=1}^{N_R}\gamma_p$, where γ_p is the instantaneous SNR given as: $\gamma_p = \frac{\tau}{6}|h_v^{p,1}|^2$. The average SNR is then computed as:

$$\bar{\gamma}_p = E[\gamma_p] = \frac{\tau}{6}E[|h_v^{p,1}|^2] \tag{B.10}$$

Further computation of $\bar{\gamma}_p$ in terms of $\bar{\bar{h}}_v^{p,1}$ and $\bar{h}_v^{p,1}$ gives:

$$\bar{\gamma}_p = \frac{\tau}{6} E\left[\left|\sqrt{\frac{K}{1+K}}\bar{\bar{h}}_v^{p,1} + \sqrt{\frac{1}{1+K}}\bar{h}_v^{p,1}\right|^2\right] \tag{B.11}$$

Since $E[|\bar{h}_v^{p,1}|^2] = 1$ and $E[|\bar{h}_v^{p,1}|] = 0$, the average SNR can then be computed as:

$$\bar{\gamma}_p = \frac{\tau}{6}\left|\sqrt{\frac{K}{1+K}}\bar{\bar{h}}_v^{p,1}\right|^2 + \frac{\tau}{6}\left|\sqrt{\frac{1}{1+K}}\right|^2$$

The probability density function (pdf) of instantaneous SNR for v^{th}-transmit antennas over i.i.d Rician fading channel can be written as [40]:

$$f_{\delta_v}(\delta_v) = \left(\frac{N_R+K}{\bar{\gamma}_p}\right)\left[\frac{(N_R+K)\delta_v}{K\bar{\gamma}_p}\right]^{\frac{N_R-1}{2}} \times \exp\left[-\frac{(N_R+K)\delta_v + K\bar{\gamma}_p}{\bar{\gamma}_p}\right] \times \boldsymbol{I}_{N_R-1}\left[2\sqrt{\frac{K(N_R+K)\delta_v}{\bar{\gamma}_p}}\right] \tag{B.12}$$

where $f_{\delta_v}(\delta_v)$ is the combined pdf for N_R-diversity. By averaging the conditional PEP over RVs δ_v, the expression becomes:

$$P(\mathbf{X} \to \hat{\mathbf{X}}) = \int_0^\infty \int_0^\infty \int_0^\infty P(\mathbf{X} \to \hat{\mathbf{X}}|\mathbf{h}_1^1,\ \mathbf{h}_2^3,\ \mathbf{h}_3^2) \prod_{v=1}^{3} f_{\delta_v}(\delta_v) d\delta_v \tag{B.13}$$

based on trapezoidal approximation to Q-function in (B.8), we obtain:

$$P(\mathbf{X} \to \hat{\mathbf{X}}|\mathbf{h}_1^1,\ \mathbf{h}_2^3,\ \mathbf{h}_3^2) = \frac{1}{2g}\left[\frac{1}{2}\prod_{v=1}^{3}\exp\Big(-\frac{\delta_v}{2}\Big) + \sum_{l=1}^{g-1}\prod_{v=1}^{3}\exp\Big(-\frac{\delta_v}{2\sin^2\left(\frac{l\pi}{2g}\right)}\Big)\right] \tag{B.14}$$

where g is the total number of iterations. In terms of moment generating function (MGF), the final PEP for Rician fading channels can be expressed as:

$$P(X \to \hat{X}) = \frac{1}{2g}\left[\frac{1}{2}\prod_{v=1}^{3} M_{\delta_v}\Big(\frac{1}{2}\Big) + \sum_{l=1}^{g-1}\prod_{v=1}^{3} M_{\delta_v}\left(\frac{1}{2\sin^2(\frac{l\pi}{2g})}\right)\right] \tag{B.15}$$

where $M_{\delta_v}(\cdot)$ is the MGF defined as $M_{\delta_v}(\delta_v)E(e^{-\delta_v\gamma})$ [36], the corresponding MGF for Rician fading channels is given as [36]:

$$M_{\delta_v}(\delta_v) = \left[\frac{1+K}{1+K+\bar{\gamma}\delta_v}\exp\left(-\frac{K\bar{\gamma}\delta_v}{1+K+\bar{\gamma}\delta_v}\right)\right]^{N_R},\ K \geq 0 \tag{B.16}$$

5 Mapper Design

In this section, we discuss the designs of labeling mappers for 16-APSK, 32-APSK and 64-APSK USTLD schemes with three transmit antennas based on heuristic algorithm. The choice of APSK modulation schemes for this study are from the latest draft standard for DVB-S2X [2] as indicated in **Table B.1**.

Table B.1: USTLD APSK Modulation Scheme for DVB-S2X Standard [2]

Modulation Order	Structure	Definition in Draft Standard
16	4+12-APSK	Tables 11a and 11b, pg. 26
32	4+12+16-APSK	Tables 12a, 12b and 12c, pg. 29
64	4+12+20+28-APSK	Tables 13e and 13f, pg. 33

A heuristic algorithm is a technique in Mathematical optimization for finding an approximate solution for a class of NP-complete decision problems [41]. A heuristic algorithm for USTLD mapper design has been applied in square M-QAM constellation for the second and third mappers and the optimization metric to mapper design formulated as [31]:

$$(\Omega_2^M, \Omega_3^M) = argmax\Big\{ \min_{x_{q_1}^v \neq \hat{x}_{q_1}^v} \prod_{v=1}^{3} \delta_v \Big\} \tag{B.17}$$

By applying three different transforms which represent three mappers for designing second and third mappers in [31], the symmetric-based heuristic algorithms re-arranged the rows as well as the columns of the matrices to ensure two adjacent rows in the constellation matrices are non-adjacent and finally swaps alternate pairs of diametrically opposite constellation points across the origin. In this instance, 16-QAM constellation points are considered as 4×4 matrix with three different modulo values as indicated in **Figure B2**(A). In this Figure, the constellation points 0 and 5 are swapped with 15 and 10. Likewise, constellation points 8 and 13 are swapped with points 7 and 2.

By adapting the square 16-QAM constellations for USTLD with three transmit antennas, the constellations of 16-APSK USTLD can be designed by re-positioning the symbols as concentric rings with two kinds of different modulo values as shown in **Figure B2**(B) where square constellation points 5, 4, 0 and 1 are designed as ring structures 5 for the first ring and 4, 0 and 1 for the second ring. The 16-APSK constellation diagram and the associated bit allocation for USTLD with three transmit antennas discussed here refers to 4+12-APSK in which 4 symbols are uniformly spaced on the inner ring with radius R_1, and 12 symbols are uniformly spaced on the outer ring with radius R_2. The ratio of the outer and inner radii can be expressed as: $\beta_0 = \frac{R_2}{R_1}$.

On the other hand, 32-QAM is constructed as a Rectangular QAM which is an adaptive modulation with square QAM constellations as shown in **Figure B3**(A). Similarly, heuristic algorithms are applied for the second and third mappers for 32-QAM USTLD where constellation points 4 and 13 are swapped with diametrically opposite constellation points 31 and 22. Likewise, constellation points 20 and 29 are swapped with opposite constellation points 15 and 6. The constellations

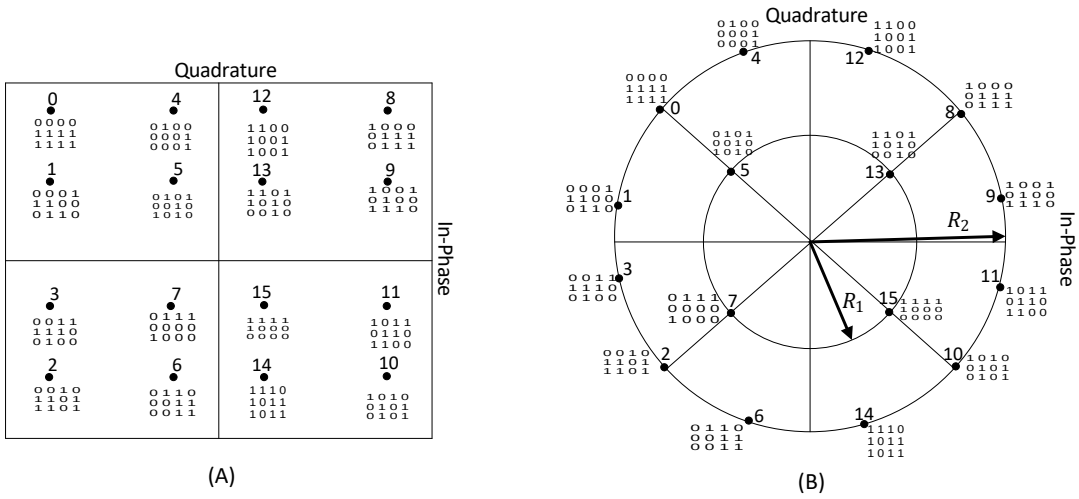

Figure B.2: Constellation Mappers for: (A) existing 16-QAM, (B) proposed 16-APSK USTLD

structure for 32-APSK USTLD are designed from 32-QAM USTLD by arranging the symbols in circles as shown **Figure B3**(B). The 32-APSK discussed here is 4+12+16-APSK and the ratios in the 32-APSK constellation are represented as: $\beta_1 = \frac{R_2}{R_1}$ and $\beta_2 = \frac{R_3}{R_1}$.

For square 64-QAM USTLD, the constellation points are considered as 8-ary pulse amplitude modulation represented as a quadrant in **Figure B4**(A). Following similar patterns for designing 16-APSK, 64-APSK concentric rings equivalent of a single quadrant as four different rings is shown in **Figure B4**(B). In 64-APSK constellation models, the concentric rings combinations are 4+12+20+28-APSK as indicated in **Figure B4**(C). The radii are denoted as: $\beta_1 = \frac{R_2}{R_1}$, $\beta_2 = \frac{R_3}{R_1}$ and $\beta_3 = \frac{R_3}{R_1}$. The modulation scheme consists of 4 rings where 4, 12, 20 and 28 symbols are allocated in the first to the fourth rings, respectively. The radii are: $\beta_1 = 2, 4$, $\beta_2 = 4, 3$ and $\beta_3 = 7$, respectively. The phase angle is $\phi = \frac{\pi}{28}$, according to the standard Draft ETSI [2].

6 Results and Discussion

This section presents Monte Carlo simulation outputs of the proposed A-USTLD schemes in nonlinear Rician fading channels for 16-APSK, 32-APSK and 64-APSK, respectively in i.i.d channels. We set the number of iterations $g = 10$, Rician factor, $K = 2$ and number of received antennas, $N_R = 4$. In both proposed models, we assume a complete channel state information at the receiver. The first Monte Carlo simulations are performed to validate the tightness of the proposed closed-form error performance for Rician broadcast channels in (B.15) for both fast frequency-flat fading and quasi-static frequency-flat fading channels. We also present simulation results for error performance comparison of the proposed A-USTLD with the existing two transmit antennas APSK-based USTLD scheme [33].

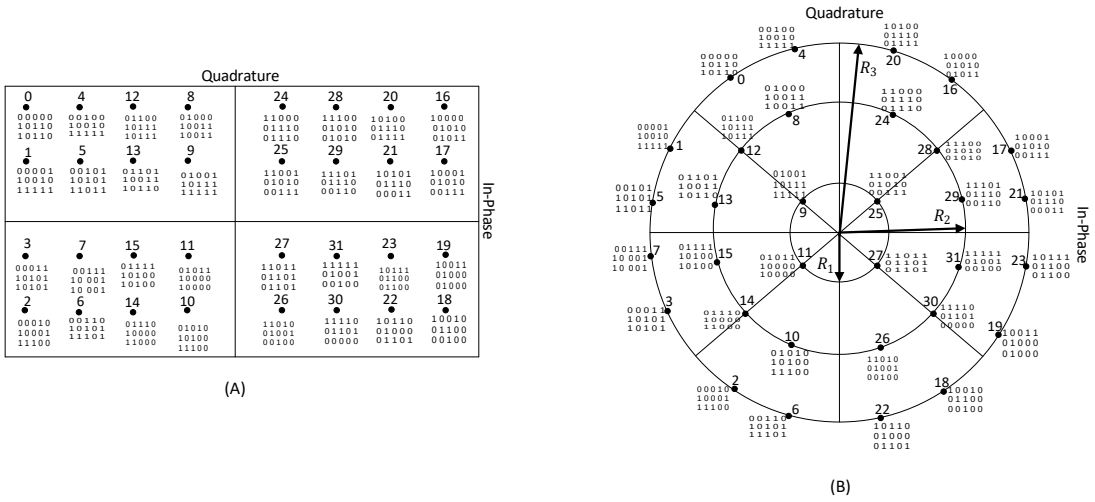

Figure B.3: Constellation Mappers for: (A) 32-RQAM, (B) proposed 32-APSK USTLD

It is to be noted that only 16-APSK and 64-APSK simulation results are considered as standards for DVB-S2X in the existing two transmit antennas APSK USTLD scheme.

6.1 Validation of Analytical Results in quasi-static and fast fading channels

The results for analytical expressions in (B.15) and the Monte Carlo simulation outputs are shown in **Figure B.5** for Rician fast frequency-flat fading and quasi-static frequency-flat fading channels. The modulation order are 16-APSK, 32-APSK and 64-APSK for A-USTLD where 16-APSK and 32-APSK are modulation schemes for DVB-S2 standard while 16-APSK and 64-APSK represent modulation order for DVB-S2X standard. In **Figure B.5**, simulation results tightly match the derived numerical expressions for Rician fast fading channels. On the other hand, Rician quasi-static fading channels exhibit slightly inferior simulation outputs at high SNRs.

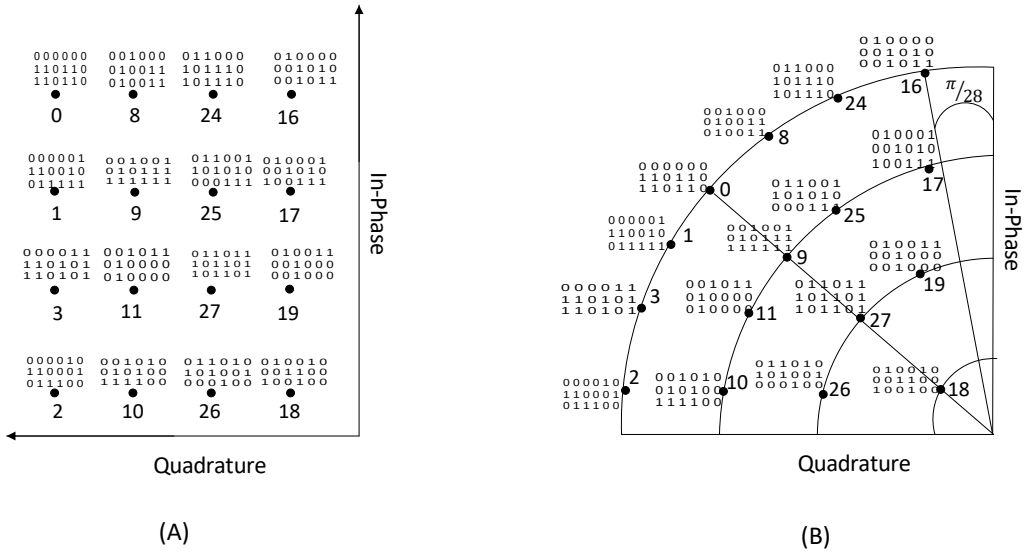

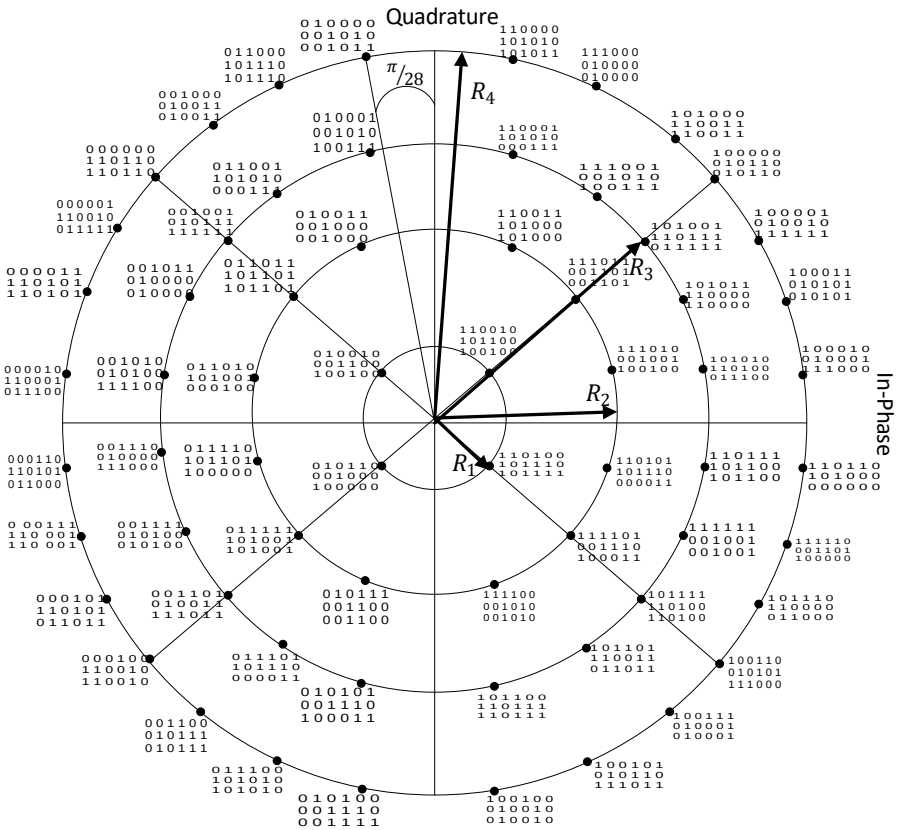

Figure B.4: Constellation Mappers for: (A) one quadrant of 64-QAM, (B) equivalent one quadrant of 64-APSK, (C) proposed 64-APSK USTLD

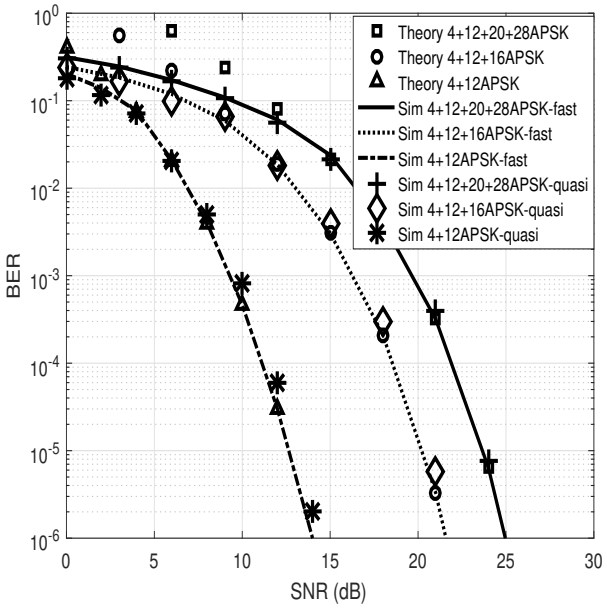

Figure B.5: Validation of BER for APSK modulation with *M*=16-APSK, 32-APSK and 64-APSK in Rician broadcast channel

6.2 BER Comparison for Rate One with existing APSK USTLD $N_T = 2$

In this subsection, three transmit antennas A-USTLD scheme is compared with the existing APSK-based USTLD with two transmit antennas [33]. For simplicity of explanation, we compare modulation order of 16-APSK and 64-APSK with concentric rings combination 4+12APSK and 4+12+20+28APSK, respectively as shown in **Figure B.6**. For 16-APSK, the proposed A-USTLD exhibits SNR gain of 1.2 dB gain over $2 \times N_R$ APSK-based USTLD at a BER of 10^{-6}. Also, an exact SNR gain of 2.8 dB could be observed for A-USTLD scheme as compared to $2 \times N_R$ APSK-based USTLD for 64-APSK. It can be inferred from the simulation outputs that BER of the system can be improved by introducing more transmit antennas from the existing two transmit APSK-based USTLD scheme to a new three transmit antennas A-USTLD scheme in order to improve the robustness of the scheme in the presence of noise and multipath fading. Hence, link reliability of the existing USTLD can be further enhanced with the proposed A-USTLD system.

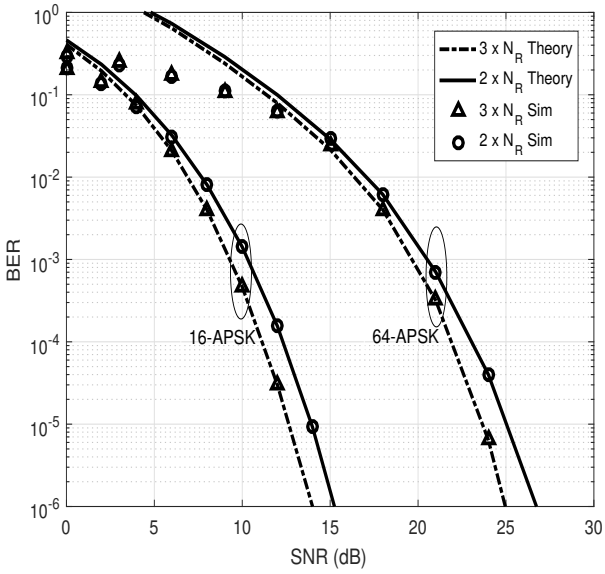

Figure B.6: BER Comparison for USTLD APSK modulation schemes with *M*=16-APSK and 64-APSK in Rician broadcast channel

7 Conclusion

The recent technical advancement in digital broadcasting has necessitated the exploitation of spectrally efficient and optimal power modulation schemes designed to operate in nonlinear fading channel environments. As a result, this paper introduced APSK transmission techniques for three transmit antennas USTLD scheme in nonlinear Rician distributions for fast frequency-flat fading and quasi-static frequency-flat fading channels. The modulation order are 16-APSK, 32-APSK and 64-APSK which are the specifications adopted by DVB-S2 and DVB-S2X standards.

Monte Carlo simulation and theoretical results further showed that the proposed A-USTLD with three transmit antennas can achieve error performance gain of 1.2 dB and 2.8 dB at a BER of 10^{-6} for 16-APSK and 64-APSK as compared to the existing two transmit antennas USTLD schemes under the same channel conditions.

8 Appendix B

The conditional PEP on $\mathbf{h}_1^1$, $\mathbf{h}_2^3$ and $\mathbf{h}_3^2$ is given as:

$$P(\mathbf{X}\rightarrow\hat{\mathbf{X}}|\mathbf{h}_1^1,\ \mathbf{h}_2^3,\ \mathbf{h}_3^2) = P\Bigg(\left\|\mathbf{z}_1-\sqrt{\frac{\tau}{3}}\mathbf{h}_1^1 x_{\hat{q}_1}^1\right\|_F^2+\left\|\mathbf{z}_2-\sqrt{\frac{\tau}{3}}\mathbf{h}_2^3 x_{\hat{q}_1}^2\right\|_F^2+\left\|\mathbf{z}_3-\sqrt{\frac{\tau}{3}}\mathbf{h}_3^2 x_{\hat{q}_1}^3\right\|_F^2 \\ < \left\|\mathbf{z}_1-\sqrt{\frac{\tau}{3}}\mathbf{h}_1^1 x_{q_1}^1\right\|_F^2+\left\|\mathbf{z}_2-\sqrt{\frac{\tau}{3}}\mathbf{h}_2^3 x_{q_1}^2\right\|_F^2+\left\|\mathbf{z}_3-\sqrt{\frac{\tau}{3}}\mathbf{h}_3^2 x_{q_1}^3\right\|_F^2\Bigg) \tag{B.17}$$

Based on the assumption that $(x_{q_1}^1, x_{q_1}^2, x_{q_1}^3)$ are detected in error while other symbols are detected correctly, (B.17) becomes:

$$P(\mathbf{X}\rightarrow\hat{\mathbf{X}}|\mathbf{h}_1^1,\ \mathbf{h}_2^3,\ \mathbf{h}_3^2) = P\Bigg(\left\|\sqrt{\frac{\tau}{3}}\mathbf{h}_1^1(x_{q_1}^1-x_{\hat{q}_1}^1)+\mathbf{n}_1\right\|_F^2+\left\|\sqrt{\frac{\tau}{3}}\mathbf{h}_2^3(x_{q_1}^2-x_{\hat{q}_1}^2)+\mathbf{n}_2\right\|_F^2 \\ +\left\|\sqrt{\frac{\tau}{3}}\mathbf{h}_3^2(x_{q_1}^3-x_{\hat{q}_1}^3)+\mathbf{n}_3\right\|_F^2 < \left\|\mathbf{n}_1\right\|_F^2+\left\|\mathbf{n}_2\right\|_F^2+\left\|\mathbf{n}_3\right\|_F^2\Bigg) \tag{B.18}$$

Let $\mathbf{A}=\sqrt{\frac{\tau}{3}}\mathbf{h}_1^1(x_{q_1}^1-x_{\hat{q}_1}^1)$, $\mathbf{B}=\sqrt{\frac{\tau}{3}}\mathbf{h}_2^3(x_{q_1}^2-x_{\hat{q}_1}^2)$, and $\mathbf{C}=\sqrt{\frac{\tau}{3}}\mathbf{h}_3^2(x_{q_1}^3-x_{\hat{q}_1}^3)$. By expanding the square of the Frobenius as a binomial expressions yields:

$$P(\mathbf{X}\rightarrow\hat{\mathbf{X}}|\mathbf{h}_1^1,\ \mathbf{h}_2^3,\ \mathbf{h}_3^2) = P\Big(\|\mathbf{A}\|_F^2+2Re\{\mathbf{n}_1^H\mathbf{A}\}+\|\mathbf{n}_1\|_F^2+\|\mathbf{B}\|_F^2+2Re\{\mathbf{n}_2^H\mathbf{B}\}+\|\mathbf{n}_2\|_F^2 \\ +\|\mathbf{C}\|_F^2+2Re\{\mathbf{n}_3^H\mathbf{C}\}+\|\mathbf{n}_3\|_F^2 < \|\mathbf{n}_1\|_F^2+\|\mathbf{n}_2\|_F^2+\|\mathbf{n}_3\|_F^2\Big) \tag{B.19}$$

$$= P\Big(Re\{\mathbf{n}_1^H\mathbf{A}\}+Re\{\mathbf{n}_2^H\mathbf{B}\}+Re\{\mathbf{n}_3^H\mathbf{C}\} > \frac{\|\mathbf{A}\|_F^2+\|\mathbf{B}\|_F^2+\|\mathbf{C}\|_F^2}{2}\Big) \tag{B.20}$$

Let $d_v = x_{q_1}^v - x_{\hat{q}_1}^v$, further simplification gives:

$$P(\mathbf{X}\rightarrow\hat{\mathbf{X}}|\mathbf{h}_1^1,\ \mathbf{h}_2^3,\ \mathbf{h}_3^2) = P\Bigg(Re\left\{\mathbf{n}_1^H\sqrt{\frac{\tau}{3}}\mathbf{h}_1^1 d_1\right\}+Re\left\{\mathbf{n}_2^H\sqrt{\frac{\tau}{3}}\mathbf{h}_2^3 d_2\right\}+Re\left\{\mathbf{n}_3^H\sqrt{\frac{\tau}{3}}\mathbf{h}_3^2 d_3\right\} \\ > \frac{1}{2}\left\{\left\|\sqrt{\frac{\tau}{3}}\mathbf{h}_1^1 d_1\right\|_F^2+\left\|\sqrt{\frac{\tau}{3}}\mathbf{h}_2^3 d_2\right\|_F^2+\left\|\sqrt{\frac{\tau}{3}}\mathbf{h}_3^2 d_3\right\|_F^2\right\}\Bigg) \tag{B.21}$$

Let $\tilde{n}_1 = \mathbf{n}_1^H\sqrt{\frac{\tau}{3}}\mathbf{h}_1^1 d_1$, $\tilde{n}_2 = \mathbf{n}_2^H\sqrt{\frac{\tau}{3}}\mathbf{h}_2^3 d_2$ and $\tilde{n}_3 = \mathbf{n}_3^H\sqrt{\frac{\tau}{3}}\mathbf{h}_3^2 d_3$. Given $\mathbf{h}_1^1$, $\mathbf{h}_2^3$ and $\mathbf{h}_3^2$, then $\tilde{n}_1$, $\tilde{n}_2$ and $\tilde{n}_3$ are Gaussian RVs with independent entries according to:

$$\tilde{n}_1 \sim CN(0, \frac{\tau}{3}\left\|\mathbf{h}_1^1\right\|_F^2|d_1|^2) \tag{B.22}$$

$$\tilde{n}_2 \sim CN(0, \frac{\tau}{3}\left\|\mathbf{h}_2^3\right\|_F^2|d_2|^2) \tag{B.23}$$

$$\tilde{n}_3 \sim CN(0, \frac{\tau}{3}\left\|\mathbf{h}_3^2\right\|_F^2|d_3|^2) \tag{B.24}$$

Let the decision variable $\tilde{n}$ be defined as:

$$\tilde{n} = \tilde{n}_1 + \tilde{n}_2 + \tilde{n}_3 \tag{B.25}$$

The decision variable $\tilde{n}$ is distributed according to:

$$\tilde{n} \sim CN(0, \frac{\tau}{3}\left\|\mathbf{h}_1^1\right\|_F^2|d_1|^2 + \frac{\tau}{3}\left\|\mathbf{h}_2^3\right\|_F^2|d_2|^2 + \frac{\tau}{3}\left\|\mathbf{h}_3^2\right\|_F^2|d_3|^2) \tag{B.26}$$

Note that $Re\{\tilde{n}\} = Re\{\tilde{n}_1\} + Re\{\tilde{n}_2\} + Re\{\tilde{n}_3\}$, where $Re\{\tilde{n}\}$ is distributed according to:

$$Re\{\tilde{\mathbf{n}}\} \sim \mathcal{N}(0, \frac{\tau}{6}\left\|\mathbf{h}_1^1\right\|_F^2|d_1|^2 + \frac{\tau}{6}\left\|\mathbf{h}_2^3\right\|_F^2|d_2|^2 + \frac{\tau}{6}\left\|\mathbf{h}_3^2\right\|_F^2|d_3|^2) \tag{B.27}$$

Thus, (B.21) becomes:

$$P(\mathbf{X} \to \hat{\mathbf{X}}|\mathbf{h}_1^1,\ \mathbf{h}_2^3,\ \mathbf{h}_3^2) = P\left(Re\{\tilde{n}\} > \frac{1}{2}\left\{\frac{\tau}{3}\left\|\mathbf{h}_1^1\right\|_F^2|d_1|^2 + \frac{\tau}{3}\left\|\mathbf{h}_2^3\right\|_F^2|d_2|^2 + \frac{\tau}{3}\left\|\mathbf{h}_3^2\right\|_F^2|d_3|^2\right\}\right) \tag{B.28}$$

It is to be noted that for a Gaussian RVs Z with zero mean and unit variance, the expression becomes:

$$P(Z > z) = \frac{1}{\sqrt{2\pi}}\int_z^\infty e^{\frac{-t^2}{2}}dt \tag{B.29}$$

$$= Q(z)$$

Hence,

$$P(\mathbf{X} \to \hat{\mathbf{X}}|\mathbf{h}_1^1,\ \mathbf{h}_2^3,\ \mathbf{h}_3^2) = Q\left(\frac{\left\{\frac{\tau}{6}\left\|\mathbf{h}_1^1\right\|_F^2|d_1|^2 + \frac{\tau}{6}\left\|\mathbf{h}_2^3\right\|_F^2|d_2|^2 + \frac{\tau}{6}\left\|\mathbf{h}_3^2\right\|_F^2|d_3|^2\right\}}{\sqrt{\frac{\tau}{6}\left\|\mathbf{h}_1^1\right\|_F^2|d_1|^2 + \frac{\tau}{6}\left\|\mathbf{h}_2^3\right\|_F^2|d_2|^2 + \frac{\tau}{6}\left\|\mathbf{h}_3^2\right\|_F^2|d_3|^2}}\right) \tag{B.30}$$

$$= Q\left(\sqrt{\frac{\tau}{6}\|\mathbf{h}_1^1\|_F^2|d_1|^2 + \frac{\tau}{6}\|\mathbf{h}_2^3\|_F^2|d_2|^2 + \frac{\tau}{6}\|\mathbf{h}_3^2\|_F^2|d_3|^2}\right) \tag{B.31}$$

Let $\delta_1 = \frac{\tau}{6}\|\mathbf{h}_1^1\|_F^2|d_1|^2$, $\delta_2 = \frac{\tau}{6}\|\mathbf{h}_2^3\|_F^2|d_2|^2$, $\delta_3 = \frac{\tau}{6}\|\mathbf{h}_3^2\|_F^2|d_3|^2$. Hence:

$$P(\mathbf{X} \to \hat{\mathbf{X}}|\mathbf{h}_1^1,\ \mathbf{h}_2^3,\ \mathbf{h}_3^2) = Q\left(\sqrt{\delta_1 + \delta_2 + \delta_3}\right) \tag{B.32}$$

$$= Q\left(\sqrt{\sum_{v=1}^{3}\delta_v}\right)$$

where δ_v are central chi-squared RVs with $2N_R$ degrees of freedom, defined as:

$$\delta_v = \sum_{y=1}^{2N_R}\left[(\kappa_{v_y}^I)^2 + (\kappa_{v_y}^Q)^2\right], \quad v \in [1:3] \tag{B.33}$$

Note that $\kappa_{v_y}^I, \kappa_{v_y}^Q\mathcal{N}(0, \sigma_{\kappa_v}^2)$, where $\sigma_{\kappa_v}^2 = \frac{\tau}{12}|d_v|^2$.

References

[1] ETSI EN 302 307-1, "Digital Video Broadcasting (DVB), second generation framing structure, channel coding and modulation systems for broadcasting, interactive services, news gathering and other broadband satellite applications, Part I: DVB-S2." ETSI, Tech. Rep., 2014.

[2] Draft ETSI EN 302 307-2 V1.1.1 , "Digital video broadcasting (DVB), second generation framing structure, channel coding and modulation systems for broadcasting, interactive services, news gathering and other broadband satellite applications, part II: S2-Extensions (DVB-S2X)," ETSI, Tech. Rep., 2014-10.

[3] M. Eroz, L.-N. Lee, N. Loghin, U. De Bie, F. Simoens, and D. Delaruelle, "New DVB-S2X constellations for improved performance on the satellite channel," *International Journal of Satellite Communications and Networking*, vol. 34, no. 3, pp. 351–360, May 2016.

[4] D4.1: Satellite Network Mission Requirements, "Broadband Access via Integrated Terrestrial and Satellite Systems (BATS)," European Project, Avanti PLLC, Tech. Rep., 2012.

[5] P. Ferrand, M. Maso, and V. Bioglio, "High-Rate Regular APSK Constellations," *IEEE Transactions on Communications*, vol. 67, no. 3, pp. 2015–2023, Dec. 2018.

[6] L. Giugno, M. Luise, and V. Lottici, "Adaptive pre-and post-compensation of nonlinear distortions for high-level data modulations," *IEEE Transactions on wireless communications*, vol. 3, no. 5, pp. 1490–1495, Oct. 2004.

[7] R. De Gaudenzi, A. G. i Fabregas, and A. Martinez, "Performance analysis of turbo-coded APSK modulations over nonlinear satellite channels," *IEEE transactions on wireless communications*, vol. 5, no. 9, pp. 2396–2407, Sep. 2006.

[8] K. P. Liolis and N. S. Alagha, "On 64-APSK constellation design optimization," in *2008 10th International Workshop on Signal Processing for Space Communications*, Oct. 2008, pp. 1–7.

[9] R. Muller, U. Wachsmann, and J. B. Huber, "Multilevel coding for peak power limited complex Gaussian channels," in *Proceedings of IEEE International Symposium on Information Theory*, Jun. 1997, p. 103.

[10] L. Dai, Z. Wang, and Z. Yang, "Next-generation digital television terrestrial broadcasting systems: Key technologies and research trends," *IEEE Communications Magazine*, vol. 50, no. 6, pp. 150–158, Jun. 2012.

[11] F. Yang, K. Yan, Q. Xie, and J. Song, "Non-equiprobable APSK constellation labeling design for BICM systems," *IEEE Communications Letters*, vol. 17, no. 6, pp. 1276–1279, May 2013.

[12] Y. Koizumi, Y. Suzuki, M. Kojima, and H. Sujikai, "Evaluation of Prototype Transmitter and Receiver with 64APSK Coded Modulation in Non-Linear Channel," in *2019 IEEE International Conference on Consumer Electronics (ICCE)*, Jan. 2019, pp. 1–2.

[13] F. Kayhan and G. Montorsi, "Constellation design for channels affected by phase noise," in *2013 IEEE International Conference on Communications (ICC)*, Jun. 2013, pp. 3154–3158.

[14] D. He, Y. Shi, Y. Guan, Y. Xu, Y. Wang, W. Zhang, and H. Yin, "Improvements to APSK constellation with gray mapping," in *2014 IEEE International Symposium on Broadband Multimedia Systems and Broadcasting*, Jun. 2014, pp. 1–4.

[15] D. Yoda and H. Ochiai, "Decision Region Optimization and Metric-Based Compensation of Memoryless Nonlinearity for APSK Systems," *IEEE Transactions on Broadcasting*, vol. 64, no. 2, pp. 281–292, Jan. 2018.

[16] W. Sung, S. Kang, P. Kim, D.-I. Chang, and D.-J. Shin, "Performance analysis of APSK modulation for DVB-S2 transmission over nonlinear channels," *International Journal of Satellite Communications and Networking*, vol. 27, no. 6, pp. 295–311, Nov. 2009.

[17] P. Arapoglou, K. Liolis, M. Bertinelli, A. Panagopoulos, P. Cottis, and R. De Gaudenzi, "MIMO over satellite: A review." *IEEE communications surveys tutorials*, vol. 13, no. 1, pp. 27–51, May 2010.

[18] M. K. Arti and M. R. Bhatnagar, "Beamforming and combining in hybrid satellite-terrestrial cooperative systems," *IEEE Communications Letters*, vol. 18, no. 3, pp. 483–486, Apr. 2010.

[19] M. Arti, "Channel estimation and detection in hybrid satellite–terrestrial communication systems," *IEEE Transactions on Vehicular Technology*, vol. 65, no. 7, pp. 5764–5771, Jul. 2015.

[20] A. I. Pérez-Neira, C. Ibars, J. Serra, A. Del Coso, J. Gómez-Vilardebó, M. Caus, and K. P. Liolis, "MIMO channel modeling and transmission techniques for multi-satellite and hybrid satellite–terrestrial mobile networks," *Physical Communication*, vol. 4, no. 2, pp. 127–139, Jun. 2011.

[21] ETSI Standard EN 302 755, "Digital Video Broadcasting (DVB); Frame Structure Channel Coding and Modulation for a Second Generation Digital Terrestrial Television Broadcasting System (DVB-T2)," ETSI, Tech. Rep., Nov. 2011.

[22] ETSI Standard EN 303 105, "Digital Video Broadcasting (DVB); Next Generation Broadcasting System to Handheld, Physical Layer Specification (DVB-NGH)," ETSI, Tech. Rep., Jun. 2013.

[23] H. Xu, K. Govindasamy, and N. Pillay, "Uncoded space-time labeling diversity," *IEEE Communications Letters*, vol. 20, no. 8, pp. 1511–1514, Jun. 2016.

[24] Y. Huang and J. A. Ritcey, "Optimal constellation labeling for iteratively decoded bit-interleaved space-time coded modulation," *IEEE Transactions on Information Theory*, vol. 51, no. 5, pp. 1865–1871, Apr. 2005.

[25] S. Ejaz, Y. FengFan, and H. Xu, "Labeling Diversity for 2 x 2 WLAN Coded-Cooperative Networks." *Radioengineering*, vol. 24, 2015.

[26] M. Krasicki, "Essence of 16-QAM labelling diversity," *Electronics Letters*, vol. 49, no. 8, pp. 567–569, Apr. 2013.

[27] B. Dlodlo and H. Xu, "Trellis code-aided high-rate M-QAM space-time labeling diversity using a unitary expansion," *International Journal of Communication Systems*, vol. 31, no. 11, e3590, Jul. 2018.

[28] H. Samra, Z. Ding, and P. M. Hahn, "Symbol mapping diversity design for multiple packet transmissions," *IEEE Transactions on Communications*, vol. 53, no. 5, pp. 810–817, May 2005.

[29] K. G. Seddik, A. S. Ibrahim, and K. R. Liu, "Trans-modulation in wireless relay networks," *IEEE Communications Letters*, vol. 12, no. 3, pp. 170–172, Mar. 2008.

[30] N. Pillay and H. Xu, "Uncoded space-time labeling diversity—Application of media-based modulation with RF mirrors," *IEEE Communications Letters*, vol. 22, no. 2, pp. 272–275, Nov. 2017.

[31] D. Ayanda, H. Xu, and N. Pillay, "Uncoded M-ary quadrature amplitude modulation space-time labeling diversity with three transmit antennas," *International Journal of Communication Systems*, vol. 31, no. 18, e3818, Dec. 2018.

[32] D. Ayanda and H. Xu, "A Unified Error Analysis of Uncoded Space-Time Labeling Diversity with Three Transmit Antennas in Rician Fading Channels," in *2019 IEEE 2nd Wireless Africa Conference (WAC)*, Aug. 2019, pp. 1–5.

[33] T. Quazi and S. S. Patel, "USTLD mapper design for APSK constellations over satellite links," *Transactions on Emerging Telecommunications Technologies*, vol. 30, no. 7, p. e3586, Jun. 2019.

[34] S. S. Patel, T. Quazi, and H. Xu, "A Genetic Algorithm for Designing Uncoded Space-Time Labelling Diversity Mappers," in *2018 IEEE International Workshop on Signal Processing Systems (SiPS)*, Oct. 2018, pp. 1–6.

[35] C. Loo, "A statistical model for a land mobile satellite link," *IEEE transactions on vehicular technology*, vol. 34, no. 3, pp. 122–127, Aug. 1985.

[36] M. K. Simon and M.-S. Alouini, *Digital communication over fading channels*. John Wiley & Sons, 2005, vol. 95.

[37] H. Keshavarz, L.-L. Xie, and R. R. Mazumdar, "User capacity of Rician and Nakagami fading broadcast channels," in *IEEE GLOBECOM 2008-2008 IEEE Global Telecommunications Conference*. IEEE, 2008, pp. 1–5.

[38] S. Papaharalabos, D. Benmayor, P. T. Mathiopoulos, and P. Fan, "Performance comparisons and improvements of channel coding techniques for digital satellite broadcasting to mobile users," *IEEE Transactions on Broadcasting*, vol. 57, no. 1, pp. 94–102, Oct. 2010.

[39] H. Gao, J. Jiao, S. Wu, S. Gu, and Q. Zhang, "Performance analysis of cooperative relaying communications for space information networks," in *2017 9th International Conference on Wireless Communications and Signal Processing (WCSP)*. IEEE, 2017, pp. 1–6.

[40] M. A. Khodeir and M. Jawarneh, "Approximate symbol error rate for M-ary phase shift keying (M-PSK) using maximum ratio combining (MRC) technique over fading channels," in *2013 Science and Information Conference*. IEEE, 2013, pp. 99–103.

[41] E. Kucharska, “Heuristic Method for Decision-Making in Common Scheduling Problems,” *Applied Sciences*, vol. 7, no. 10, p. 1073, 2017.

Part IV

Paper C

Paper C

Symbol Mapping Design and Error Analysis of Cross-QAM Uncoded Space-Time Labeling Diversity with Three Transmit Antennas

1 Abstract

Uncoded space-time labeling diversity (USTLD) is a recent scheme that improves the error performance of space-time block code by using labeling mappers to transmit information bits. In this scheme, square quadratic amplitude modulation (QAM) has been widely used due to its high power and bandwidth efficiency. However, square QAM does not provide satisfying requirements for a system where the number of bits per symbol is odd. In this scenario, the peak and the average power of transmission can be reduced by using cross QAMs (XQAMs) instead. Hence, authors in this paper investigate the design of XQAM labeling mappers for three transmit antennas USTLD scheme over independent and identically distributed (i.i.d) Nakagami-*m* fading channels. The analytical average bit error probability (ABEP) are derived based on pairwise error probability. This expression is validated by Monte Carlo simulation results, which converge accurately at high signal-to-noise ratio. Since channels are not i.i.d in practical sense, the authors further investigate XQAM USTLD scheme in correlated channels. The ABEP for the proposed system are derived and served to validate the Monte-Carlo simulation results. Finally, the authors demonstrate the effects of correlation by comparing BER results of correlated channels with that of i.i.d channels.

2 Introduction

Uncoded space-time labeling diversity (USTLD) is a recently proposed multiple-input, multiple-output (MIMO) techniques for two transmit antennas scheme similar to Alamouti [1]. In this scheme, the authors use symmetric-based heuristic algorithm to design signal constellations for M-QAM and M-PSK USTLD modulation schemes for two different bits-to-constellation point mappers in two time slots.

More recently, authors in [2] proposed a new genetic algorithm for labeling mapper design for square quadrature amplitude modulation (QAM), circular M-ary phase shift keying (M-PSK) and A-PSK in USTLD with two transmit antennas. The proposed scheme matches the best heuristic designs for 16-QAM and 64-QAM USTLD in [1]. Other authors have applied heuristic algorithm for labeling mapper design to circular 16-APSK and 64-APSK in USTLD with two transmit antennas [3] which are DVB-S2X standard compatible for digital broadcasting channels.

In order to further improve USTLD for transmit antenna diversity gain in downlink channels, Ayanda et al. [4] proposed USTLD scheme with three transmit antennas using heuristic algorithm. In this approach, the authors propose 16-QAM and 64-QAM techniques for the second and third mappers in USTLD scheme. Morever, the authors further extend the heuristic algorithm for mapper design to high density 256-QAM and 1024-QAM USTLD schemes which have become promising modulation schemes for next-generation wireless communication [5].

Obviously, recently proposed USTLD schemes with three transmit antennas in the literature [4] [5] are designed more for square QAM where the number of bits per symbol is even. Square QAM schemes are broadly employed in wireless communication as a result of its high power and bandwidth efficiency. However, for a scheme where the number of bits per symbol is odd, cross QAM (XQAM) is a preferred signal constellation scheme which achieves greater power efficiency over square QAM by reducing the average energy of the signal set [6].

As a result, XQAM has found use in adaptive modulation schemes where the constellation size m increments from 2^m to 2^{m+1} and allows for more granularity [7]. XQAM has also been used in blind equalization that minimize the dispersion of the equalizer output with respect to single or multiple cross-shaped zero error contour(s) [8]- [9]. XQAM with constellations from 5 bits to 15 bits have been used in ADSL [10] and VDSL [11] while 32-XQAM and 128-XQAM have been adopted in practical systems in DVB-C [12] [13] as well.

Authors in [14] derived approximate and generic analytical expressions for bit error rate (BER) of

X-QAM signal constellations under Smith-style pseudo-Gray coding. The numerical results compared the approximate BER expressions with Smith's approximation and have found that Smith's approximation is a simple and close approximation, especially for high signal-to-noise ratio (SNR) values, over AWGN channels.

Furthermore, exact analytical expressions for the average symbol error probability (SEP) of 32-XQAM signal constellation in AWGN has been derived in the literature [15] as an improvement over the existing scheme [14]. The authors then derive exact closed-form expressions for the average SEP of 32-XQAM in slow and flat Nakagami -*m* fading with maximal ratio combining (MRC) diversity.

Closed-form theoretical expressions for average SEP and bit error probability (BEP) of arbitrary M-ary XQAM signaling with MRC diversity reception over independent but not necessarily identical $\eta - \mu$ fading channels have been derived in the literature [16]. The authors presented results for Rayleigh and Nakagami-*m* channels based on finite sum of trigonometric functions and the analytical expressions tightly match the Monte Carlo simulation outputs.

In addition, the effect of channel correlation was taken into consideration in the error performance analysis of XQAM for single-input multiple-output (SIMO) scheme in [17]. The authors derived arbitrarily closed-form analytical expressions in the form of Gaussian Q-function and moment generating function (MGF) over dual correlated Rayleigh, Nakagami-*m*, Nakagami-*n* and Nakagami-*q* fading channels. Monte Carlo simulation outputs tightly match the derived analytical expressions.

In the context of USTLD, XQAM for two transmit antennas USTLD with improved bandwidth efficiency has recently been proposed in Rayleigh fading channels [18]. The proposed system is a combination of USTLD with XQAM and MPSK modulation that improved data rate by introducing extra bits to a USTLD system via a 16PSK phase component.

Motivated by transmit antennas diversity gain of USTLD with three transmit antennas over the existing USTLD scheme [4], this study presents labeling mapper designs for 32-XQAM and 128-XQAM USTLD scheme with three transmit antennas using heuristic algorithm over independent and identically distributed (i.i.d) Nakagami-*m* fading channels. A closed-form bound on the average bit error probability (ABEP) of the proposed scheme in Nakagami-*m* distribution for i.i.d channels are formulated.

Moreover, in channels where the conditions for i.i.d are not satisfied, the channels become correlated. Hence, it is necessary to investigate the impacts of channel correlation on BER of XQAM in three transmit antennas USTLD scheme which is another major contribution of this study. A closed-form

error analysis based on characteristic function is derived for Nakagami-*m* fading channels which converges accurately at high SNR.

The remainder of this paper is organized as follows: The model description of the proposed XQAM signal modulation techniques for three transmit antennas USTLD schemes for both uncorrelated and correlated Nakagami-*m* channels are presented in Section 3. In Section 4, approximate analytical expressions for error performance are derived for both uncorrelated and correlated channels. Section 5 discusses the proposed labeling mapper design for 32-XQAM and 128-XQAM using heuristic algorithm. Section 6 presents the numerical results that demonstrate the tightness and validity of the analytical results. Section 7 is the conclusion for the study.

Notation: Throughout this paper, bold lowercase are used for vectors, while uppercase letters are used for matrices. The operators $[\cdot]^T$, $(\cdot)^H$, $\|\cdot\|_F$ and $|\cdot|$ respectively correspond to transpose, Hermitian transpose, Frobenius norm and Euclidean norm. $|\cdot|^{-1}$ is the inverse of a matrix. $\Gamma(\cdot)$ is the Gamma function and $\otimes$ is the Kronecker product. $E(\cdot)$ is the expectation operator and $Q(\cdot)$ is the Gaussian Q-function. $J_0(\cdot)$ is the modified Bessel function of the first kind of order zero. *vec*$(\cdot)$ and *tr*$(\cdot)$ are vector operator and trace element, respectively. *argmin*$_w(\cdot)$ is the minimum of the argument with respect to *w*. *rank*$(\cdot)$ is the rank of a matrix with respect to the dimension of the vector space generated by its columns.

3 System Model

In this section, the authors present system models for both uncorrelated and correlated Nakagami-*m* fading channels.

3.1 Uncorrelated Channel Modeling

Consider a USTLD MIMO system equipped with $N_T = 3$ and N_R transmit and receive antennas, respectively as shown in **Figure C.1**. Message bits is split into three $r = \log_2 M$-tuple vectors $\mathbf{r}_i = [r_{i,1}\, r_{i,2} \cdots r_{i,r}]$, $i \in [1:3]$, which are injected into Mapper 1, Mapper 2 and Mapper 3 simultaneously. Mappers $\Omega_k^M(\mathbf{r}_i)$, $i \in [1:3]$ and $k \in [1:3]$ map bit stream $\mathbf{r}_i$ into *M*-QAM constellation points in the Argand plane that produces $x_{q_i}^k = \Omega_k^M(\mathbf{r}_i)$. q_i is an index of $\mathbf{r}_i$ given as $q_i = 1 + \sum_{k=1}^{r} 2^{k-1} r_{i,k}$. In the USTLD system, Mapper 1 Ω_1^M represents a Gray coded mapper, while Mapper 2 and Mapper 3 are the optimized labeling mappers designed to maximize the minimum Euclidean distance [4]. The authors assume that $E(|x_{q_i}^k|^2) = 1$.

After the mapping, antennas 1, 2 and 3 simultaneously transmit the modulated symbols $x_{q_1}^1$, $x_{q_2}^1$ and

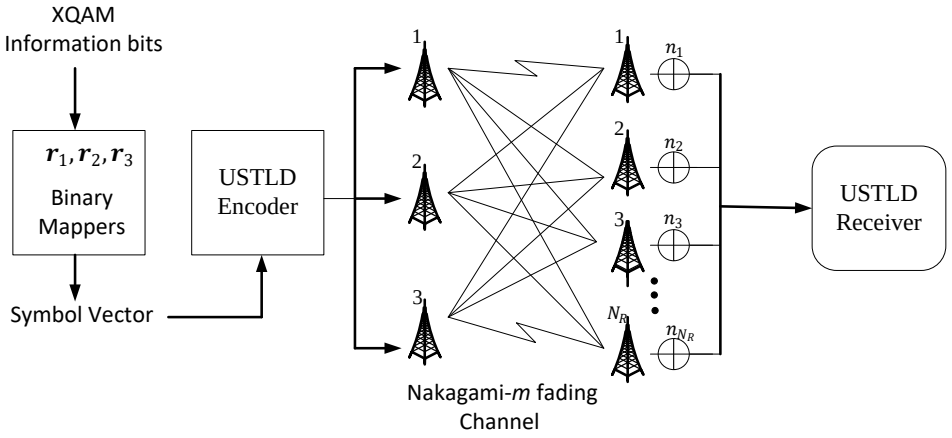

Figure C.1: System model of the proposed XQAM-USTLD

$x_{q_3}^1$ in time slot 1. Symbols $x_{q_2}^2$, $x_{q_3}^2$ and $x_{q_1}^2$ are simultaneously transmitted by antennas 1, 2 and 3 in time slot 2 and in time slot 3, antennas 1, 2 and 3 simultaneously transmit $x_{q_3}^3$, $x_{q_1}^3$ and $x_{q_2}^3$, respectively. Accordingly, the received signal vectors $\mathbf{y}_1$, $\mathbf{y}_2$ and $\mathbf{y}_3$ over Nakagami-*m* fading channels in time slots 1, 2 and 3 may be given as:

$$\mathbf{y}_1 = \sqrt{\frac{\rho}{3}}(\mathbf{h}_1^1 x_{q_1}^1 + \mathbf{h}_1^2 x_{q_2}^1 + \mathbf{h}_1^3 x_{q_3}^1) + \mathbf{n}_1 \tag{C.1a}$$

$$\mathbf{y}_2 = \sqrt{\frac{\rho}{3}}(\mathbf{h}_2^1 x_{q_2}^2 + \mathbf{h}_2^2 x_{q_3}^2 + \mathbf{h}_2^3 x_{q_1}^2) + \mathbf{n}_2 \tag{C.1b}$$

$$\mathbf{y}_3 = \sqrt{\frac{\rho}{3}}(\mathbf{h}_3^1 x_{q_3}^3 + \mathbf{h}_3^2 x_{q_1}^3 + \mathbf{h}_3^3 x_{q_2}^3) + \mathbf{n}_3 \tag{C.1c}$$

where $\mathbf{y}_k = [y_{1,k}\ y_{2,k}\ \cdots\ y_{N_R,k}]^T$ is the $N_R \times 1$ dimensional received signal vector. $\frac{\rho}{3}$ is the average SNR at the receive antenna. The $N_R \times 1$ channel gain matrix $\mathbf{h}_k^i$ is modeled as fast frequency-flat Nakagami-*m* fading channel. In this scenario, the channel remains constant during each time slot and takes on independent values in time slot 1, time slot 2 and time slot 3, respectively. The channel fading vector for the k^{th} transmit antennas is defined as $\mathbf{h}_k^i = [h_k^{1,i}\, h_k^{2,i}\ \cdots\ h_k^{N_R,i}]^T$. $\mathbf{n}_k \in C^{N_R \times 1}$ is an $N_R \times 1$ additive white Gaussian noise (AWGN) vector. Both entries of $\mathbf{h}_k^i$ and $\mathbf{n}_k$ are independent and identically distributed (i.i.d) complex Gaussian random variables (RVs) distributed according to $CN(0, 1)$.

3.2 Correlated Channel Modeling

Spatial correlation takes place in channels where there exist closed physical separation in the antennas spacing. In this instance, the wavelength is half of the transmission carrier. For the correlated channel,

Kronecker correlation model is adopted to describe the relationship between correlated channel matrix ($\bar{\bar{\mathbf{h}}}_k^i$) and uncorrelated channel matrix, $\mathbf{h}_k^i \in C^{N_R \times 1}$, with entries $CN(0,1)$ which can be expressed as [19]:

$$\bar{\bar{\mathbf{h}}}_k^i = \left[\mathbf{R}_{N_R}^{\frac{1}{2}}\right] \mathbf{h}_k^i \left[x_{q_k}^i\right]^{\frac{T}{2}} \tag{C.2}$$

where $\mathbf{R}_{N_R}$ represents the channel correlation matrices at the receiver with dimension $N_R \times N_R$. In order to exploit full antenna diversity based on the arbitrarily correlated channel at the receiver, the transmit antennas are assumed to be uncorrelated at half-wavelength of the carrier transmission [20]. Therefore, $x_{q_k}^i$ is taken as an identity matrix and (C.2) reduces to:

$$\bar{\bar{\mathbf{h}}}_k^i = \left[\mathbf{R}_{N_R}^{\frac{1}{2}}\right] \mathbf{h}_k^i \tag{C.3}$$

The normalized correlation matrix $\mathbf{R}_{N_R}$ at the receiver is given as [21]:

$$\mathbf{R}_{N_R} = \begin{bmatrix} 1 & \rho_{1,2} & \cdots & \rho_{1,N_R} \\ \rho_{2,1} & 1 & \cdots & \rho_{2,N_R} \\ \vdots & \vdots & \ddots & \vdots \\ \rho_{N_R,1} & \rho_{N_R,2} & \cdots & 1 \end{bmatrix} \tag{C.4}$$

where $\rho_{i,k}, \;\; i,k \in [1 : N_R]$ is the correlation coefficient of an electric-field component observed in a homogeneous scattering environment given in the form of [22] [23]:

$$\rho_{i,k} = J_0\Big(2\pi \frac{d}{\lambda}\Big) \tag{C.5}$$

where d denotes antenna spacing and λ corresponds to the wavelength of the transmission carrier frequency of a mobile system.

3.3 Maximum Likelihood Detection (ML)

In this study, the authors assume perfect knowledge of the channel at the receiver. The optimal ML detector for i.i.d receiver may be defined as:

$$[\hat{q}_1,\ \hat{q}_2,\ \hat{q}_3] = \underset{q_1,q_2,q_3 \in [1:M]}{\operatorname{argmin}} \Big(\Big\| \mathbf{y}_1 - (\mathbf{h}_1^1 x_{q_1}^1 + \mathbf{h}_1^2 x_{q_2}^1 + \mathbf{h}_1^3 x_{q_3}^1) \Big\|_F^2 + \Big\| \mathbf{y}_2 - (\mathbf{h}_2^1 x_{q_2}^2 + \mathbf{h}_2^2 x_{q_3}^2 + \mathbf{h}_2^3 x_{q_1}^2) \Big\|_F^2 + \Big\| \mathbf{y}_3 - (\mathbf{h}_3^1 x_{q_3}^3 + \mathbf{h}_3^2 x_{q_1}^3 + \mathbf{h}_3^3 x_{q_2}^3) \Big\|_F^2 \Big) \tag{C.6}$$

4 Error Performance Analysis

This section presents a closed-form theoretical ABEP of three transmit antennas USTLD scheme in the form of conditional pairwise error probability (PEP) and the trapezoidal approximation to Q-function.

The analysis is based on the assumption that only one triad of information bits is erroneously detected while the other two triads of information bits are correctly detected [4].

4.1 Uncorrelated Error Analysis

It is assumed that two triads of symbol bits, $x^i_{q_u}$, $u \in [2:3]$, $i \in [1:3]$ are correctly detected in the at high SNR, while $x^i_{q_1}$ is detected with errors. (C.1a) - (C.1c) can be further expressed as:

$$\mathbf{y}_1 = \sqrt{\frac{\rho}{3}}\mathbf{h}^1_1 x^1_{q_1} + \mathbf{n}_1 \tag{C.7a}$$

$$\mathbf{y}_2 = \sqrt{\frac{\rho}{3}}\mathbf{h}^3_2 x^2_{q_1} + \mathbf{n}_2 \tag{C.7b}$$

$$\mathbf{y}_3 = \sqrt{\frac{\rho}{3}}\mathbf{h}^2_3 x^3_{q_1} + \mathbf{n}_3 \tag{C.7c}$$

Based on the transmit model in (C.7a) - (C.7c), the theoretical union bound expression is given as:

$$P_{ABEP}(\rho) \leq \frac{1}{Mr}\sum_{q_1=1}^{M}\sum_{\hat{q}_1 \neq q_1}^{M} \Delta(q_1, \hat{q}_1) P(\mathbf{X} \rightarrow \hat{\mathbf{X}}) \tag{C.8}$$

where *M*= 32-XQAM or 128-XQAM, $r = \log_2 M$, $\Delta(q_1, \hat{q}_1)$ denotes the number of bits erroneously detected for the given pairwise error probability (PEP) event. $P(\mathbf{X} \rightarrow \hat{\mathbf{X}})$ corresponds to the PEP when $\mathbf{X}$ is transmitted and $\hat{\mathbf{X}}$ is detected, represented as $\mathbf{X} = [x^1_{q_1} x^2_{q_1} x^3_{q_1}]$ and $\hat{\mathbf{X}} = [x^1_{\hat{q}_1}\ x^2_{\hat{q}_1}\ x^3_{\hat{q}_1}]$. The conditional PEP, $P(\mathbf{X} \rightarrow \hat{\mathbf{X}}|\mathbf{h}^1_1,\ \mathbf{h}^3_2,\ \mathbf{h}^2_3)$, may be formulated as:

$$\begin{aligned} P(\mathbf{X} \rightarrow \hat{\mathbf{X}}|\mathbf{h}^1_1,\ \mathbf{h}^3_2,\ \mathbf{h}^2_3) =& P\Bigg(\left\| \mathbf{y}_1 - \sqrt{\frac{\rho}{3}}\mathbf{h}^1_1 x^1_{\hat{q}_1} \right\|^2_F + \left\| \mathbf{y}_2 - \sqrt{\frac{\rho}{3}}\mathbf{h}^3_2 x^2_{\hat{q}_1} \right\|^2_F + \left\| \mathbf{y}_3 - \sqrt{\frac{\rho}{3}}\mathbf{h}^2_3 x^3_{\hat{q}_1} \right\|^2_F \\ <& \left\| \mathbf{y}_1 - \sqrt{\frac{\rho}{3}}\mathbf{h}^1_1 x^1_{q_1} \right\|^2_F + \left\| \mathbf{y}_2 - \sqrt{\frac{\rho}{3}}\mathbf{h}^3_2 x^2_{q_1} \right\|^2_F + \left\| \mathbf{y}_3 - \sqrt{\frac{\rho}{3}}\mathbf{h}^2_3 x^3_{q_1} \right\|^2_F \Bigg) \end{aligned} \tag{C.9}$$

The PEP can be given as (refer to Appendix C):

$$P(\mathbf{X} \rightarrow \hat{\mathbf{X}}|\mathbf{h}^1_1,\ \mathbf{h}^3_2,\ \mathbf{h}^2_3) = Q\left(\sqrt{\sum_{k=1}^{3} \delta_k} \right) \tag{C.10}$$

where $\delta_1 = \frac{\rho}{6}\|\mathbf{h}^1_1\|^2_F |d_1|^2$, $\delta_2 = \frac{\rho}{6}\|\mathbf{h}^3_2\|^2_F |d_2|^2$ and $\delta_3 = \frac{\rho}{6}\|\mathbf{h}^2_3\|^2_F |d_3|^2$. Note that $d_k = x^k_{q_1} - x^k_{\hat{q}_1}$, $k \in [1:3]$. δ_k can be simplified in terms of v^{th}-received antennas as:

$$\delta_k = \frac{\rho}{6}|d_k|^2 \sum_{v=1}^{N_R} |h^{v,1}_k|^2 \tag{C.11}$$

For MRC with N_R diversity branches, the combiner output is given as: $\gamma_k = \sum_{v=1}^{N_R} \gamma_v$, where γ_v is the instantaneous SNR given as: $\gamma_v = \frac{\rho}{6}|h_k^{v,1}|^2$. The average SNR is then computed as:

$$\bar{\gamma}_v = E[\gamma_v] = \frac{\rho}{6} E[|h_k^{v,1}|^2] \tag{C.12a}$$

$$\bar{\gamma}_v = \frac{\rho}{6} \tag{C.12b}$$

The probability density function (pdf) in Nakagami-*m* distribution may be defined as [22]:

$$f_{\delta_k}(\delta_k) = \left(\frac{m}{\bar{\gamma}_v}\right)^{mN_R} \frac{\delta_k^{mN_R-1}}{\Gamma(mN_R)} \exp\left(-\frac{m}{\bar{\gamma}_v}\delta_k\right) \quad \delta_k \geq 0,\, \bar{\gamma}_v \geq 0,\, m \geq 0 \tag{C.13}$$

The PEP in uncorrelated channel may be given as:

$$P(\mathbf{X} \to \hat{\mathbf{X}}) = \int_0^\infty \int_0^\infty \int_0^\infty P(\mathbf{X} \to \hat{\mathbf{X}}|\mathbf{h}_1^1,\, \mathbf{h}_2^3,\, \mathbf{h}_3^2) \prod_{k=1}^{3} f_{\delta_k}(\delta_k) d\delta_k \tag{C.14}$$

by applying trapezoidal approximation to Q-function, we obtain:

$$P(\mathbf{X} \to \hat{\mathbf{X}}|\mathbf{h}_1^1,\, \mathbf{h}_2^3,\, \mathbf{h}_3^2) = \frac{1}{2n}\left[\frac{1}{2}\prod_{k=1}^{3} \exp\Big(-\frac{\delta_k}{2}\Big) + \sum_{\ell=1}^{n-1}\prod_{k=1}^{3} \exp\Big(-\frac{\delta_k}{2\sin^2\left(\frac{\ell\pi}{2n}\right)}\Big)\right] \tag{C.15}$$

where n is the total number of iterations. Based on moment generating function (MGF), the PEP can be written as:

$$P(\mathbf{X} \to \hat{\mathbf{X}}) = \frac{1}{2n}\left[\frac{1}{2}\prod_{k=1}^{3} M_{\delta_k}\Big(\frac{1}{2}\Big) + \sum_{\ell=1}^{n-1}\prod_{k=1}^{3} M_{\delta_k}\left(\frac{1}{2\sin^2(\frac{\ell\pi}{2n})}\right)\right] \tag{C.16}$$

where $M_{\delta_k}(\cdot)$ is the MGF. By expressing the MGF as $M_{\delta_k}(s)E(e^{-s\gamma})$ [22], the MGF of Nakagami-*m* fading channel may be expressed as:

$$\mathbf{M}_{\delta_k}(\delta_k) = \left(1 + \frac{\bar{\gamma}}{m}\delta_k\right)^{-mN_R} \tag{C.17}$$

Hence, the PEP can be verified as:

$$P(\mathbf{X} \to \hat{\mathbf{X}}) = \frac{1}{2n}\left[\frac{1}{2}\prod_{k=1}^{3}\left(\frac{m}{m + \left(\frac{\rho}{6}\right)d_k}\right)^{mN_R} + \sum_{\ell=1}^{n-1}\prod_{k=1}^{3}\left(\frac{m}{m + \left(\frac{\rho}{6}\right)d_k\frac{1}{\sin^2\left(\frac{\ell\pi}{2n}\right)}}\right)^{mN_R}\right] \tag{C.18}$$

4.2 The special case of m = 1 for Nakagami-m in i.i.d channels

Nakagami-m fading distribution is a generalized fading distribution that captures Rayleigh distribution as a special case (that is, m=1). Thus, by substituting m=1 into (C.18), we arrive at:

$$P(\mathbf{X} \to \hat{\mathbf{X}}) = \frac{1}{2n}\left[\frac{1}{2}\prod_{k=1}^{3}\left(\frac{1}{1 + \left(\frac{\rho}{6}\right)d_k}\right)^{N_R} + \sum_{\ell=1}^{n-1}\prod_{k=1}^{3}\left(\frac{1}{1 + \left(\frac{\rho}{6}\right)d_k\frac{1}{\sin^2\left(\frac{\ell\pi}{2n}\right)}}\right)^{N_R}\right] \tag{C.19}$$

Note that (C.19) is the closed-form expression for PEP in Rayleigh fading distribution as verified in [4] using Real Analysis technique [21].

4.3 Correlated Error Analysis

In this subsection, we carry out analytical analysis in correlated Nakagami-*m* channels. Following the analysis for error performance in uncorrelated fading channel in (C.8), the PEP in the correlated channel can be written as:

$$P(\mathbf{X} \to \hat{\mathbf{X}}) = \int_0^\infty \int_0^\infty \int_0^\infty P(\mathbf{X} \to \hat{\mathbf{X}} | \bar{\bar{\mathbf{h}}}_1^1,\ \bar{\bar{\mathbf{h}}}_2^3,\ \bar{\bar{\mathbf{h}}}_3^2) \prod_{k=1}^{3} f_{\bar{\bar{\delta}}_k}(\bar{\bar{\delta}}_k) d\bar{\bar{\delta}}_k \tag{C.20}$$

where $\bar{\bar{\delta}}_k$ are the RVs for correlated channels. By applying eigenfilter-based signal analysis approach [23], the pdf of the average SNR for correlated channels with i^{th} received antennas can be expressed as:

$$f_{\bar{\bar{\delta}}_k}(\bar{\bar{\delta}}_k) = \left(\frac{m}{\beta_{i,i}\bar{\gamma}_k}\right)^{mN_R} \frac{\bar{\bar{\delta}}_k^{\,mN_R-1}}{\Gamma(mN_R)} \exp\left(-\frac{m}{\beta_{i,i}\bar{\gamma}_k}\bar{\bar{\delta}}_k\right) \quad \bar{\bar{\delta}}_k \geq 0,\ \bar{\gamma}_k \geq 0,\ m \geq 0 \tag{C.21}$$

where $\beta_{i,i}$ denotes the eigenvalue of the i^{th} received antennas and $\bar{\gamma}_k$ is the average SNR. The MGF for correlated Nakagami-*m* fading channel may be given as [22]:

$$\mathbf{M}_{\bar{\bar{\delta}}_k}(s) = \int_0^\infty s^{s\bar{\bar{\delta}}_k} f_{\bar{\bar{\delta}}_k}(\bar{\bar{\delta}}_k) d\bar{\bar{\delta}}_k \tag{C.22}$$

Using characteristic function of Hermitian quadratic forms and based on the concept of a virtual channel and a diagonalizing argument [21] - [24], the MGF can be further expressed as:

$$\mathbf{M}_{\bar{\bar{\delta}}_k}(s) = \left| \boldsymbol{I}_{N_R N_T} - s\big(\mathbf{R}_{\bar{\bar{\mathbf{H}}}_k}^{\frac{1}{2}}\big)^H \big(\boldsymbol{I}_{N_R} \otimes d_k d_k^H\big) \mathbf{R}_{\bar{\bar{\mathbf{H}}}_k}^{\frac{1}{2}} \right|^{-1} \tag{C.23}$$

where $\boldsymbol{I}$ is the identity matrix of order $N_R \times N_T$. Since $\big(\mathbf{R}_{\bar{\bar{\mathbf{H}}}_k}^{\frac{1}{2}}\big)^H \cdot \mathbf{R}_{\bar{\bar{\mathbf{H}}}_k}^{\frac{1}{2}} = \mathbf{R}_{\bar{\bar{\mathbf{H}}}_k}$ and $\mathbf{R}_{\bar{\bar{\mathbf{H}}}_k} = \mathbf{R}_{N_T} \otimes \mathbf{R}_{N_T}$, (20) becomes:

$$\begin{aligned}
\mathbf{M}_{\bar{\bar{\delta}}_k}(s) &= \left| \boldsymbol{I}_{N_R N_T} - s(\mathbf{R}_{N_R} \otimes \mathbf{R}_{N_T})(\boldsymbol{I}_{N_R} \otimes d_k d_k^H) \right|^{-1} \\
&= \left| \boldsymbol{I}_{N_R N_T} - s\mathbf{R}_{N_R} \otimes \big(d_k d_k^H \mathbf{R}_{N_T}\big) \right|^{-1} \\
\mathbf{M}_{\bar{\bar{\delta}}_k}(s) &= \prod_{i=1}^{N_R} \big(1 - s\nabla_{k,k}\beta_{i,i}\big)^{-1}
\end{aligned} \tag{C.24}$$

The non-zero eigenvalue of $d_k d_k^H \mathbf{R}_{N_T}$ is denoted by $\nabla_{k,k}$ and the eigenvalue of $\mathbf{R}_{N_R}$ is $\beta_{i,i}$. In order to exploit full antenna diversity, the channel must remain fixed over N_T transmit symbol durations [20]. In this case, $\nabla_{k,k}$ becomes unitary and $d_k d_k^H = \sum_{k=1}^{3} \left| x_{q_1}^k - x_{\hat{q}_1}^k \right|^2$. Thus (21) becomes:

$$\mathbf{M}_{\bar{\bar{\delta}}_k}(s) = \prod_{i=1}^{N_R} \big(1 - s\beta_{i,i}\big)^{-1} \tag{C.25}$$

Hence, the PEP in correlated Nakagami-*m* fading channel can be verified as:

$$P(\mathbf{X} \to \hat{\mathbf{X}}) = \frac{1}{2n}\left[\frac{1}{2}\prod_{k=1}^{3}\prod_{i=1}^{N_R}\left(\frac{m}{m + (\frac{\rho}{6})d_k\beta_{i,i}}\right)^m + \sum_{\ell=1}^{n-1}\prod_{k=1}^{3}\prod_{i=1}^{N_R}\left(\frac{m}{m + (\frac{\rho}{6})d_k\beta_{i,i}\frac{1}{\sin^2(\frac{\ell\pi}{2n})}}\right)^m\right] \tag{C.26}$$

5 Design of the Labeling Mappers

The output in (C.18) shows that, at high SNRs, ABEP is dominated by the product Euclidean distance, $\prod_{k=1}^{3} d_k$. In this study, we extend the optimization metric to mapper design in [4] to three transmit antennas XQAM USTLD scheme given by:

$$(\Omega_2^M, \Omega_3^M) = argmax\Big\{ \min_{x_{q_1}^k \neq \hat{x}_{q_1}^k} \prod_{k=1}^{3} d_k \Big\} \tag{C.27}$$

As shown in **Figure C.2** and **Figure C.3** for 32-XQAM and 128-XQAM, respectively, the optimal decision regions are not square. The 32-XQAM constellations can be constructed by 8×8 square block array with the 4 corner blocks deleted. Likewise, 128-XQAM constellations can be designed by 16×16 square block array with the 7th and 8th rows in the 4 corner blocks deleted.

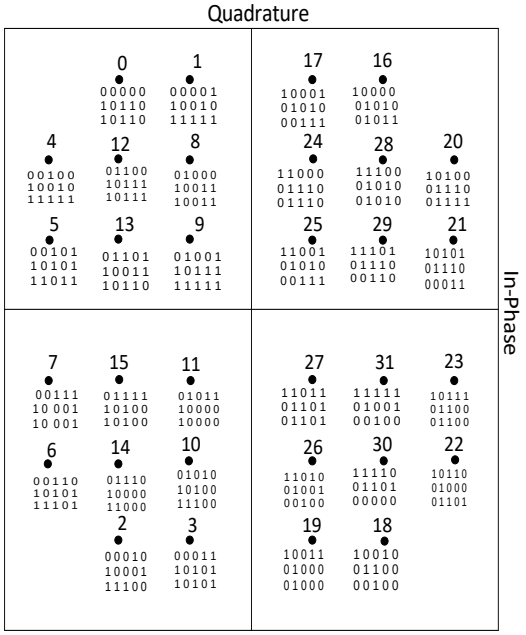

Figure C.2: 32-XQAM constellations and optimized mappers for three transmit antennas USTLD scheme

A heuristic algorithm is then applied using the existing square-QAM USTLD with three transmit antennas for 8×8 matrix [4] and 16×16 matrix constellation points [5] to 32-XQAM and 128-XQAM for the second and third mappers. This is achieved by rearraging the rows and then the columns of the matrix to ensure that any two adjacent rows (columns) in the source constellation matrix are non-adjacent [4]. In 32-XQAM USTLD, for instance, heuristic algorithms are applied for the second and third mappers whereby constellation points 4 and 13 are swapped with opposite constellation points

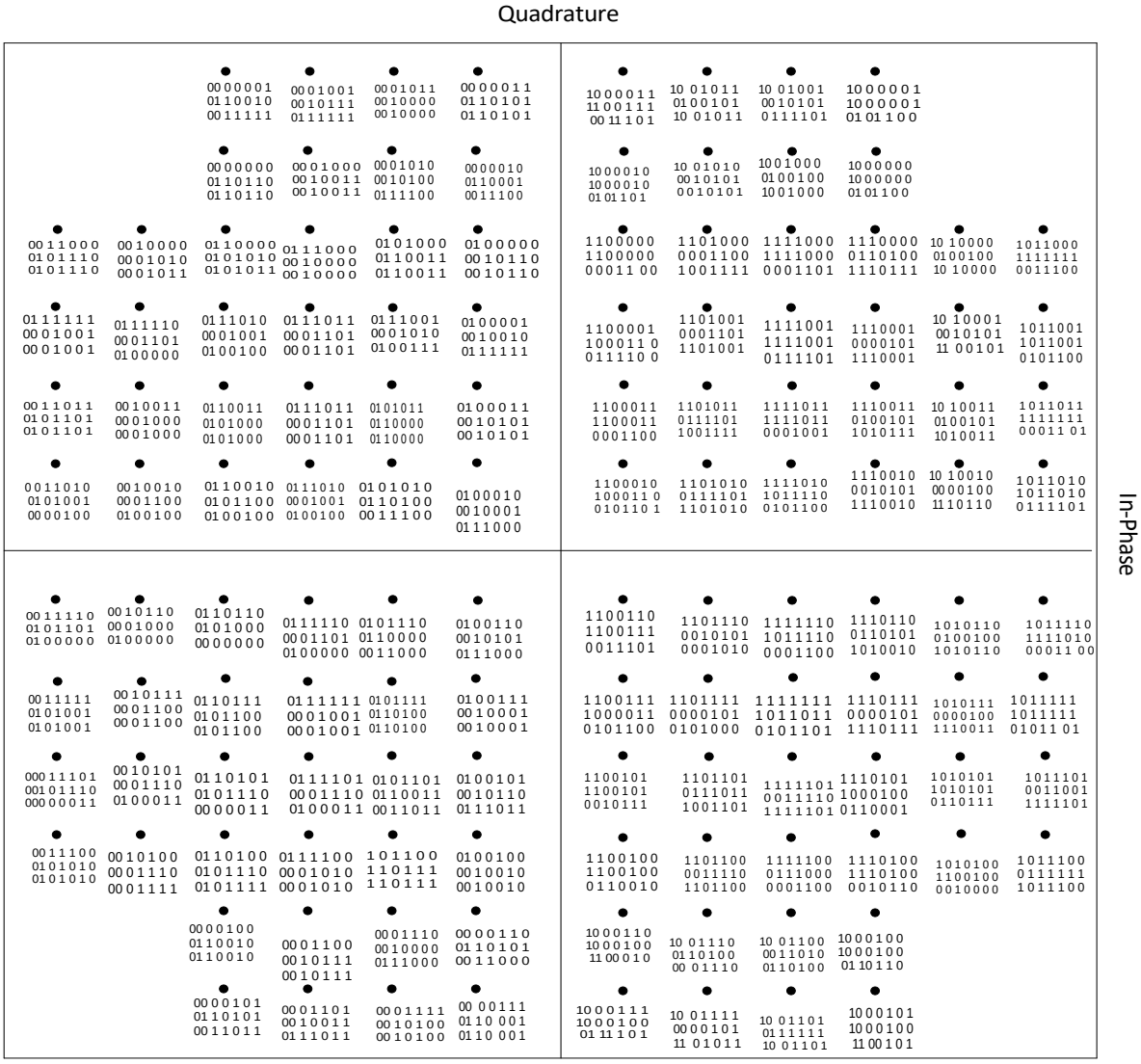

Figure C.3: 128-XQAM constellation and optimized mapper for three transmit antennas USTLD scheme

31 and 22. On the other hand, constellation points 20 and 29 are swapped with constellation points 15 and 6.

6 Numerical Results and Discussion

In this section, Monte Carlo simulation results of the proposed XQAM USTLD schemes in both uncorrelated and correlated Nakagami-*m* fading channels are presented with $M = 32$ and $M = 128$. We set the number of iterations $n = 10$ and $N_R = 4$. In both proposed modulation schemes, we assume a complete channel state information at the receiver.

The first simulations are performed in i.i.d fading channels to validate the tightness of the proposed closed-form error performance in (C.18) and (C.19). In addition, extensive simulations are carried out to validate theoretical BER expressions in the correlated fading channel in (C.27).

6.1 BER validation in uncorrelated USTLD Nakagami-m channel

This sub-section demonstrates theoretical ABEP outputs for three transmit antennas USTLD schemes in uncorrelated Nakagami-m fading channel as verified in (C.18) and (C.19). The ABEP is analyzed in order to show the tightness of Monte Carlo simulation outputs with the theoretical results. **Figure C.4** shows results for 32-XQAM and 128-XQAM. At BER of 10^{-6}, the proposed USTLD scheme shows a tight match for the theory with simulation for $m = 1$, $m = 2$ and $m = 4$. Moreover, there is SNR gain of 1 dB for $m = 4$ over $m = 2$ and likewise SNR gain of 2 dB for $m = 2$ over $m = 1$ in 32-XQAM. Similar results could be observed in 128-XQAM with approximately 1 dB gain for $m = 4$ over $m = 2$ and SNR gain of 3 dB for $m = 2$ over $m = 1$.

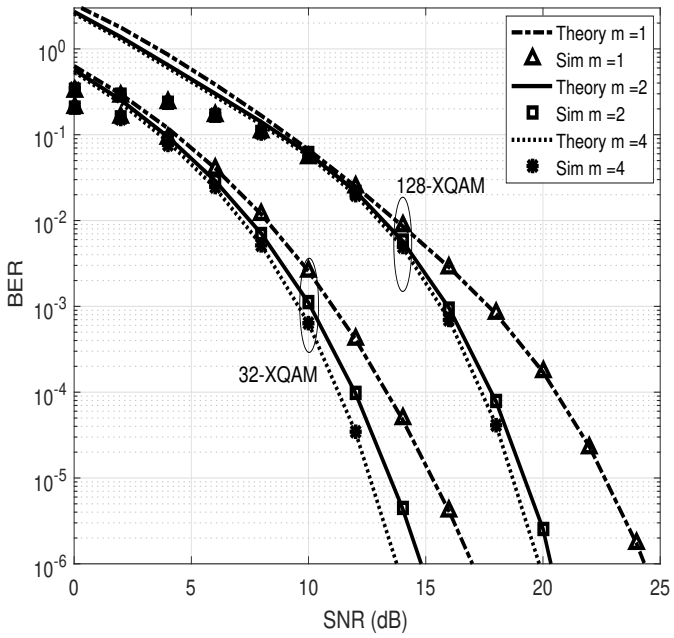

Figure C.4: Validation of BER for CrossQAM modulation with *M*=32, 128-XQAM, in i.i.d Nakagami-*m* fading channel

6.2 Average BER in correlated channels with antenna spacing

This sub-section demonstrates the impact of antenna spacing on the average BER of a correlated USTLD system in (C.27). The configuration of the antennas at the receiver is varied as a result of physical distance of separation between them and this determines the severity of correlation. Generally, the study assumes a linear array of antennas configurations with a uniform angle of arrival

distribution in a correlation model. **Figure C.5** shows the average BER with varied antenna spacings of $d = 0.2\lambda$ and $d = 0.4\lambda$ at a BER of 10^{-6}. Simulation results are provided to validate the analytical expression for the two different antenna spacings, which agree well with the the theoretical BER expressions at high SNR.

In both 32-XQAM and 128-XQAM, simulation outputs show that higher errors which correspond to more correlated channel take place for a closed set antenna spacing of $d = 0.2\lambda$, and then followed by and $d = 0.4\lambda$ that correspond to the lower channel correlation. BER output for $d = 0.2\lambda$ is degraded by approximately 1 dB when compared to $d = 0.4\lambda$ for 32-XQAM and approximately 0.8 dB in 128-XQAM. This output for $d = 0.4\lambda$ as the lower channel correlation can be insightfully observed from the fact that the spacing is close to half a wavelength, which is the assumed condition for i.i.d.

Figure C.6 compares the effects of channel correlation on BER of the proposed USTLD scheme over i.i.d channel. For 32-XQAM, 1.5 dB gain could be observed in i.i.d channel over correlated channel with antenna spacing, $c = 0.2\lambda$ and for 128-XQAM, 3.5 dB gain could be observed in i.i.d channel over correlated channel with similar conditions.

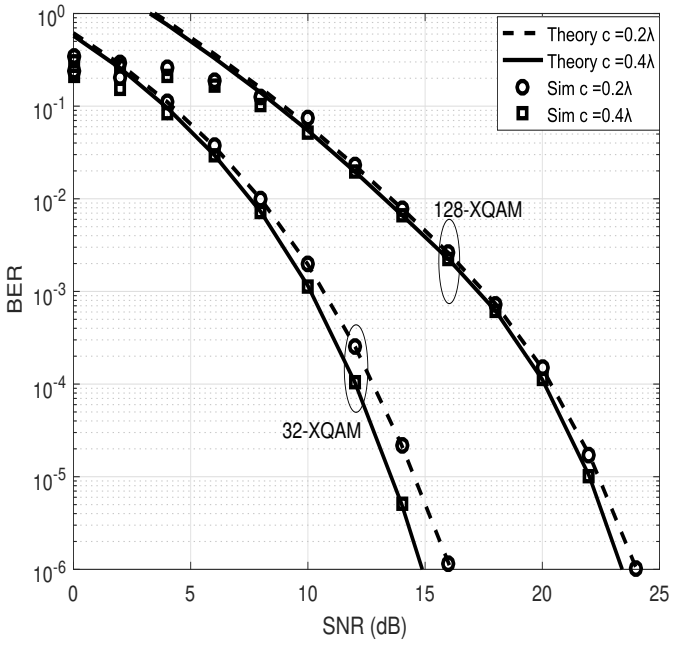

Figure C.5: Validation of BER for CrossQAM modulation with *M*=32, 128XQAM, *m*=2 in Correlated Nakagami-m fading channel

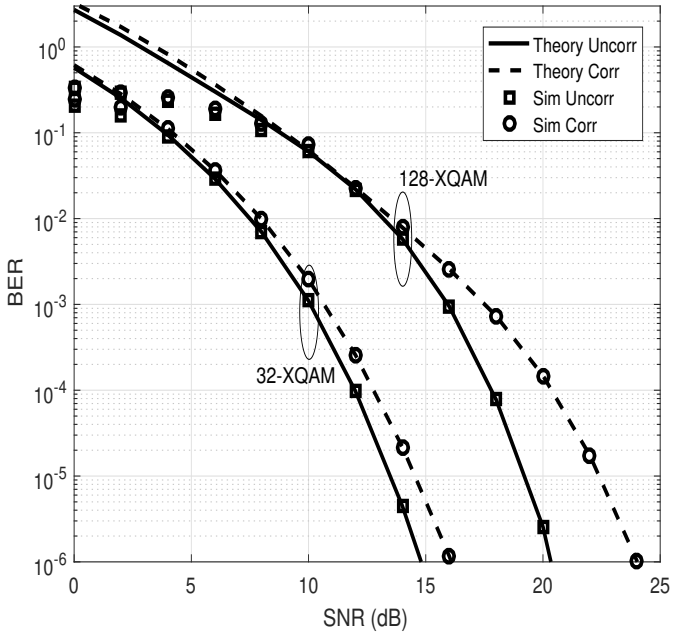

Figure C.6: BER Comparison for CrossQAM modulation with M=32, 128-XQAM, m=2, $c = 0.2\lambda$ in i.i.d and Correlated Nakagami-m fading channel

7 Conclusion

This paper introduced labeling mapper design of USTLD with three transmit antennas for 32-XQAM and 128-XQAM modulation schemes. A heuristic algorithm that employed features of square QAM is adapted for XQAM constellation design. The authors proposed closed-form expressions and asymptotically tight bounds for bit error rates and average conditional probability in an i.i.d Nakagami-m fading channels. In addition, we investigated XQAM USTLD scheme in an arbitrarily correlated Nakagami-m fading channel. A closed-form error analysis based on characteristic function was derived for the correlated channels which converged accurately at high SNR. In addition, impact of channel correlation were demonstrated by comparing the BER results with BER of i.i.d channels.

8 Appendix C

The conditional PEP on $\mathbf{h}_1^1$, $\mathbf{h}_2^3$ and $\mathbf{h}_3^2$ is given as:

$$\begin{aligned} P(\mathbf{X} \to \hat{\mathbf{X}}|\mathbf{h}_1^1,\ \mathbf{h}_2^3,\ \mathbf{h}_3^2) =& P\Bigg(\left\|\mathbf{y}_1 - \sqrt{\frac{\rho}{3}}\mathbf{h}_1^1 x_{\hat{q}_1}^1\right\|_F^2 + \left\|\mathbf{y}_2 - \sqrt{\frac{\rho}{3}}\mathbf{h}_2^3 x_{\hat{q}_1}^2\right\|_F^2 + \left\|\mathbf{y}_3 - \sqrt{\frac{\rho}{3}}\mathbf{h}_3^2 x_{\hat{q}_1}^3\right\|_F^2 \\ <& \left\|\mathbf{y}_1 - \sqrt{\frac{\rho}{3}}\mathbf{h}_1^1 x_{q_1}^1\right\|_F^2 + \left\|\mathbf{y}_2 - \sqrt{\frac{\rho}{3}}\mathbf{h}_2^3 x_{q_1}^2\right\|_F^2 + \left\|\mathbf{y}_3 - \sqrt{\frac{\rho}{3}}\mathbf{h}_3^2 x_{q_1}^3\right\|_F^2 \end{aligned} \tag{C.28}$$

Based on the assumption that $(x_{q_1}^1, x_{q_1}^2, x_{q_1}^3)$ are detected in error while other symbols are detected correctly, (C.28) becomes:

$$\begin{aligned} P(\mathbf{X} \to \hat{\mathbf{X}}|\mathbf{h}_1^1,\ \mathbf{h}_2^3,\ \mathbf{h}_3^2) =& P\Bigg(\left\|\sqrt{\frac{\rho}{3}}\mathbf{h}_1^1(x_{q_1}^1 - x_{\hat{q}_1}^1) + \mathbf{n}_1\right\|_F^2 + \left\|\sqrt{\frac{\rho}{3}}\mathbf{h}_2^3(x_{q_1}^2 - x_{\hat{q}_1}^2) + \mathbf{n}_2\right\|_F^2 \\ &+ \left\|\sqrt{\frac{\rho}{3}}\mathbf{h}_3^2(x_{q_1}^3 - x_{\hat{q}_1}^3) + \mathbf{n}_3\right\|_F^2 < \left\|\mathbf{n}_1\right\|_F^2 + \left\|\mathbf{n}_2\right\|_F^2 + \left\|\mathbf{n}_3\right\|_F^2 \Bigg) \end{aligned} \tag{C.29}$$

Let $\mathbf{A} = \sqrt{\frac{\rho}{3}}\mathbf{h}_1^1(x_{q_1}^1 - x_{\hat{q}_1}^1)$, $\mathbf{B} = \sqrt{\frac{\rho}{3}}\mathbf{h}_2^3(x_{q_1}^2 - x_{\hat{q}_1}^2)$, and $\mathbf{C} = \sqrt{\frac{\rho}{3}}\mathbf{h}_3^2(x_{q_1}^3 - x_{\hat{q}_1}^3)$. By expanding the square of the Frobenius as a binomial expressions yields:

$$\begin{aligned} P(\mathbf{X} \to \hat{\mathbf{X}}|\mathbf{h}_1^1,\ \mathbf{h}_2^3,\ \mathbf{h}_3^2) =& P\Big(\|\mathbf{A}\|_F^2 + 2Re\{\mathbf{n}_1^H\mathbf{A}\} + \|\mathbf{n}_1\|_F^2 + \|\mathbf{B}\|_F^2 + 2Re\{\mathbf{n}_2^H\mathbf{B}\} + \|\mathbf{n}_2\|_F^2 \\ &+ \|\mathbf{C}\|_F^2 + 2Re\{\mathbf{n}_3^H\mathbf{C}\} + \|\mathbf{n}_3\|_F^2 < \|\mathbf{n}_1\|_F^2 + \|\mathbf{n}_2\|_F^2 + \|\mathbf{n}_3\|_F^2 \Big) \end{aligned} \tag{C.30}$$

$$= P\Big(Re\{\mathbf{n}_1^H\mathbf{A}\} + Re\{\mathbf{n}_2^H\mathbf{B}\} + Re\{\mathbf{n}_3^H\mathbf{C}\} > \frac{\|\mathbf{A}\|_F^2 + \|\mathbf{B}\|_F^2 + \|\mathbf{C}\|_F^2}{2} \Big) \tag{C.31}$$

Let $d_k = x_{q_1}^k - x_{\hat{q}_1}^k$, further simplification gives:

$$\begin{aligned} P(\mathbf{X} \to \hat{\mathbf{X}}|\mathbf{h}_1^1,\ \mathbf{h}_2^3,\ \mathbf{h}_3^2) =& P\Bigg(Re\Bigg\{\mathbf{n}_1^H\sqrt{\frac{\rho}{3}}\mathbf{h}_1^1 d_1\Bigg\} + Re\Bigg\{\mathbf{n}_2^H\sqrt{\frac{\rho}{3}}\mathbf{h}_2^3 d_2\Bigg\} + Re\Bigg\{\mathbf{n}_3^H\sqrt{\frac{\rho}{3}}\mathbf{h}_3^2 d_3\Bigg\} \\ &> \frac{1}{2}\Bigg\{ \left\|\sqrt{\frac{\rho}{3}}\mathbf{h}_1^1 d_1\right\|_F^2 + \left\|\sqrt{\frac{\rho}{3}}\mathbf{h}_2^3 d_2\right\|_F^2 + \left\|\sqrt{\frac{\rho}{3}}\mathbf{h}_3^2 d_3\right\|_F^2 \Bigg\} \Bigg) \end{aligned} \tag{C.32}$$

Let $\tilde{n}_1 = \mathbf{n}_1^H\sqrt{\frac{\rho}{3}}\mathbf{h}_1^1 d_1$, $\tilde{n}_2 = \mathbf{n}_2^H\sqrt{\frac{\rho}{3}}\mathbf{h}_2^3 d_2$ and $\tilde{n}_3 = \mathbf{n}_3^H\sqrt{\frac{\rho}{3}}\mathbf{h}_3^2 d_3$. Given $\mathbf{h}_1^1$, $\mathbf{h}_2^3$ and $\mathbf{h}_3^2$, then $\tilde{n}_1$, $\tilde{n}_2$ and $\tilde{n}_3$ are Gaussian RVs with independent entries according to:

$$\tilde{n}_1 \sim CN(0, \frac{\rho}{3}\left\|\mathbf{h}_1^1\right\|_F^2 |d_1|^2) \tag{C.33}$$

$$\tilde{n}_2 \sim CN(0, \frac{\rho}{3}\left\|\mathbf{h}_2^3\right\|_F^2 |d_2|^2) \tag{C.34}$$

$$\tilde{n}_3 \sim CN(0, \frac{\rho}{3}\left\|\mathbf{h}_3^2\right\|_F^2 |d_3|^2) \tag{C.35}$$

Let the decision variable $\tilde{n}$ be defined as:

$$\tilde{n} = \tilde{n}_1 + \tilde{n}_2 + \tilde{n}_3 \tag{C.36}$$

The decision variable $\tilde{n}$ is distributed according to:

$$\tilde{n} \sim CN(0, \frac{\rho}{3}\left\|\mathbf{h}_1^1\right\|_F^2 |d_1|^2 + \frac{\rho}{3}\left\|\mathbf{h}_2^3\right\|_F^2 |d_2|^2 + \frac{\rho}{3}\left\|\mathbf{h}_3^2\right\|_F^2 |d_3|^2) \tag{C.37}$$

Note that $Re\{\tilde{n}\} = Re\{\tilde{n}_1\} + Re\{\tilde{n}_2\} + Re\{\tilde{n}_3\}$, where $Re\{\tilde{n}\}$ is distributed according to:

$$Re\{\tilde{n}\} \sim \mathcal{N}(0, \frac{\rho}{6}\left\|\mathbf{h}_1^1\right\|_F^2 |d_1|^2 + \frac{\rho}{6}\left\|\mathbf{h}_2^3\right\|_F^2 |d_2|^2 + \frac{\rho}{6}\left\|\mathbf{h}_3^2\right\|_F^2 |d_3|^2) \tag{C.38}$$

Thus, (C.32) becomes:

$$P(\mathbf{X} \to \hat{\mathbf{X}}|\mathbf{h}_1^1,\ \mathbf{h}_2^3,\ \mathbf{h}_3^2) = P\left(Re\{\tilde{n}\} > \frac{1}{2}\left\{\frac{\rho}{3}\left\|\mathbf{h}_1^1\right\|_F^2 |d_1|^2 + \frac{\rho}{3}\left\|\mathbf{h}_2^3\right\|_F^2 |d_2|^2 + \frac{\rho}{3}\left\|\mathbf{h}_3^2\right\|_F^2 |d_3|^2\right\}\right) \tag{C.39}$$

It is to be noted that for a Gaussian RVs *W* with zero mean and unit variance, the expression becomes:

$$\begin{aligned} P(W > w) &= \frac{1}{\sqrt{2\pi}} \int_w^\infty e^{\frac{-t^2}{2}} dt \\ &= Q(w) \end{aligned} \tag{C.40}$$

Hence,

$$P(\mathbf{X} \to \hat{\mathbf{X}}|\mathbf{h}_1^1,\ \mathbf{h}_2^3,\ \mathbf{h}_3^2) = Q\left(\frac{\left\{\frac{\rho}{6}\left\|\mathbf{h}_1^1\right\|_F^2 |d_1|^2 + \frac{\rho}{6}\left\|\mathbf{h}_2^3\right\|_F^2 |d_2|^2 + \frac{\rho}{6}\left\|\mathbf{h}_3^2\right\|_F^2 |d_3|^2\right\}}{\sqrt{\frac{\rho}{6}\left\|\mathbf{h}_1^1\right\|_F^2 |d_1|^2 + \frac{\rho}{6}\left\|\mathbf{h}_2^3\right\|_F^2 |d_2|^2 + \frac{\rho}{6}\left\|\mathbf{h}_3^2\right\|_F^2 |d_3|^2}}\right) \tag{C.41}$$

$$= Q\left(\sqrt{\frac{\rho}{6}\|\mathbf{h}_1^1\|_F^2 |d_1|^2 + \frac{\rho}{6}\|\mathbf{h}_2^3\|_F^2 |d_2|^2 + \frac{\rho}{6}\|\mathbf{h}_3^2\|_F^2 |d_3|^2}\right) \tag{C.42}$$

Let $\delta_1 = \frac{\rho}{6}\|\mathbf{h}_1^1\|_F^2 |d_1|^2$, $\delta_2 = \frac{\rho}{6}\|\mathbf{h}_2^3\|_F^2 |d_2|^2$, $\delta_3 = \frac{\rho}{6}\|\mathbf{h}_3^2\|_F^2 |d_3|^2$. Hence:

$$P(\mathbf{X} \to \hat{\mathbf{X}}|\mathbf{h}_1^1,\ \mathbf{h}_2^3,\ \mathbf{h}_3^2) = Q\left(\sqrt{\delta_1 + \delta_2 + \delta_3}\right) \tag{C.43}$$

$$= Q\left(\sqrt{\sum_{k=1}^{3} \delta_k}\right)$$

where δ_k are central chi-squared RVs with $2N_R$ degrees of freedom, defined as:

$$\delta_k = \sum_{y=1}^{2N_R} \left[(\kappa_{k_y}^I)^2 + (\kappa_{k_y}^Q)^2\right], \quad k \in [1:3] \tag{C.44}$$

Note that $\kappa_{k_y}^I, \kappa_{k_y}^Q \mathcal{N}(0, \sigma_{\kappa_k}^2)$, where $\sigma_{\kappa_k}^2 = \frac{\rho}{12}|d_k|^2$.

References

[1] H. Xu, K. Govindasamy, and N. Pillay, "Uncoded space-time labeling diversity," *IEEE Communications Letters*, vol. 20, no. 8, pp. 1511–1514, Jun. 2016.

[2] S. S. Patel, T. Quazi, and H. Xu, "A Genetic Algorithm for Designing Uncoded Space-Time Labelling Diversity Mappers," in *2018 IEEE International Workshop on Signal Processing Systems (SiPS)*, Oct. 2018, pp. 1–6.

[3] T. Quazi and S. S. Patel, "USTLD mapper design for APSK constellations over satellite links," *Transactions on Emerging Telecommunications Technologies*, vol. 30, no. 7, e3586, Jun. 2019.

[4] D. Ayanda, H. Xu, and N. Pillay, "Uncoded M-ary quadrature amplitude modulation space-time labeling diversity with three transmit antennas," *International Journal of Communication Systems*, vol. 31, no. 18, e3818, Dec. 2018.

[5] D. Ayanda, H. Xu, and S. Mughal, "High-Density *M*-QAM Mapper Design for Uncoded Space-Time Labeling Diversity with Three Transmit Antenna over Nakagami-*m* fading channel," in *2019 IEEE AFRICON, Ghana (in press)*, Sept. 2019.

[6] J. Smith, "Odd-bit quadrature amplitude-shift keying," *IEEE Transactions on Communications*, vol. 23, no. 3, pp. 385–389, Mar. 1975.

[7] S. Panigrahi and T. Le-Ngoc, "Fine-granularity loading schemes using adaptive Reed-Solomon coding for discrete multitone modulation systems," in *IEEE International Conference on Communications, 2005. ICC 2005. 2005*, vol. 2, May 2005, pp. 1352–1356.

[8] K. V. Cartwright, "Blind phase recovery in cross QAM communication systems with eighth-order statistics," *IEEE Signal Processing Letters*, vol. 8, no. 12, pp. 304–306, Dec. 2001.

[9] S. Colonnese, G. Panci, S. Rinauro, and G. Scarano, "Blind carrier frequency offset estimation for cross QAM constellations," in *2007 4th International Symposium on Wireless Communication Systems*. Oct., 2007, pp. 241–245.

[10] R. G. ITU-T, "992.5 Asymmetric digital subscriber line (ADSL) transceivers-Extended bandwidth ADSL (ADSL2+)," Geneva, Mar. 2005.

[11] ITU-T Standard G.992.1., "Very High Speed Digital Subscriber Line Transceivers." Mar. 2004.

[12] E. ETSI, "Digital Video Broadcasting (DVB); Framing structure, channel coding and modulation for digital terrestrial television," *ETSI EN*, vol. 300, no. 744, p. V1, 2004.

[13] I. Kallfass, A. Tessmann, J. Antes, D. Lopez-Diaz, M. Kuri, H. Massler, T. Zwick, and A. Leuther, "Wireless DVB-C transmission at 220 GHz using active single-chip receive and transmit MMICs," in *2011 IEEE MTT-S International Microwave Symposium*, Jun. 2011, pp. 1–4.

[14] P. K. Vitthaladevuni, M.-S. Alouini, and J. C. Kieffer, "Exact BER computation for cross QAM constellations," *IEEE Transactions on Wireless Communications*, vol. 4, no. 6, pp. 3039–3050, Dec. 2005.

[15] N. C. Beaulieu and Y. Chen, "Closed-form expressions for the exact symbol error probability of 32-cross-QAM in AWGN and in slow Nakagami fading," *IEEE Communications Letters*, vol. 11, no. 4, pp. 310–312, Apr. 2007.

[16] H. Yu, G. Wei, F. Ji, and X. Zhang, "On the Error Probability of Cross-QAM With MRC Reception Over Generalized \$\eta$-\$\mu$ Fading Channels," *IEEE Transactions on Vehicular Technology*, vol. 60, no. 6, pp. 2631–2643, May 2011.

[17] M. W. Kamdar and H. Xu, "Performance Analysis of Cross QAM with MRC Over Dual Correlated Nakagami-*m*,-*n*, and-*q* Channels," *Wireless Personal Communications*, vol. 84, no. 4, pp. 3015–3030, Oct. 2015.

[18] M. W. Kamdar, "Error Performance Analysis of Cross QAM and Space-Time Labeling Diversity for Cross QAM," Ph.D. dissertation, Discipline of Electrical, Electronic and Computer Engineering, University of KwaZulu-Natal, Apr. 2019.

[19] A. Hedayat, H. Shah, and A. Nosratinia, "Analysis of space-time coding in correlated fading channels," *IEEE Transactions on Wireless Communications*, vol. 4, no. 6, pp. 2882–2891, Dec. 2005.

[20] V. Tarokh, N. Seshadri, and A. R. Calderbank, "Space-time codes for high data rate wireless communication: Performance criterion and code construction," *IEEE transactions on information theory*, vol. 44, no. 2, pp. 744–765, Mar. 1998.

[21] R. A. Horn and C. R. Johnson, *Matrix analysis*. Cambridge university press, 2012.

[22] M. K. Simon and M.-S. Alouini, *Digital communication over fading channels*. John Wiley & Sons, 2005.

[23] P. O. Akuon and H. Xu, "Optimal error analysis of receive diversity schemes on arbitrarily correlated rayleigh fading channels," *IET Communications*, vol. 10, no. 7, pp. 854–861, May 2016.

[24] U. Fernández-Plazaola, E. Martos-Naya, J. F. Paris, and J. T. Entrambasaguas, "Comments on Proakis analysis of the characteristic function of complex Gaussian quadratic forms," *arXiv preprint arXiv:1212.0382*, Dec. 2012.

Part V

Conclusion

1 Conclusion

The main research contributions and outcomes presented in this thesis may be summarized as follows:

Paper A proposed an enhanced USTLD scheme with three transmit antennas in Rayleigh fading channels. A heuristic algorithm was applied to design the second and third mappers for square quadratic amplitude modulation (QAM). Monte Carlo simulation results demonstrated superior error performance compared with the conventional two transmit USTLD. In addition, OP complexity reduction technique was proposed which achieved lower computational complexity of 51% and 96.5% for 16QAM and 64QAM, respectively.

Paper B proposed labeling mapper design for USTLD scheme with three transmit antennas using APSK modulation. The proposed APSK transmission scheme for A-USTLD were based on adaptation of square QAM USTLD scheme to concentric ring structures of 16-APSK, 32-APSK and 64-APSK for A-USTLD scheme using heuristic algorithm. In particular, A-USTLD scheme are standard compatible with DVB-S2 and its latest extension (DVB-S2X) over Rician fast frequency-flat fading and quasi-static frequency-flat fading channels. An analytical bound for the average BEP for the proposed A-USTLD scheme was also derived, and the accuracy of the theoretical results was verified by Monte Carlo simulation results for both fast fading and quasi-static fading Rician channels. In addition, A-USTLD scheme was capable of achieving error performance gain of 1.2 dB and 2.8 dB at a BER 10^{-6} for 16-APSK and 64-APSK, respectively when compared to USTLD scheme with two transmit antennas.

Paper C proposed XQAM USTLD scheme with three transmit antennas for both i.i.d Nakagami-*m* and correlated Nakagami-*m* fading channels. A Mathematical optimization algorithm for the design of the second and third mappers were proposed using heuristic algorithm. In addition, analytical expressions for the ABEP of XQAM USTLD over i.i.d Nakagami-*m* and correlated Nakagami-*m* fading channels were derived and the accuracy of the theoretical expressions were verified by Monte Carlo simulation results. Moreover, a comparison between i.i.d and correlated Nakagami-*m* fading channels with shape factor $m = 2$ and $N_R = 4$, led to the following findings: (i) i.i.d channels achieved 1.5 dB gain at a BER of 10^{-6} as compared to correlated channels with antenna spacing 0.2 λ for 32-XQAM USTLD scheme; (ii) i.i.d channels exhibited 3.5 dB gain at a BER of 10^{-6} as compared to correlated channels with antenna spacing 0.2 λ for 128-XQAM USTLD scheme.

2 Future Research

USTLD schemes with three transmit antennas presented in this thesis can be further improved and extended to other areas of wireless communications. This study identified the following areas or topics of interest for possible future work.

2.1 Higher Order Mapper Design for USTLD Scheme

USTLD schemes with three transmit antennas are the main contributions of this research to the literature. To this end, a heuristic algorithm for designing the second and third labeling mappers are adopted. Motivated by transmit antenna diversity gain, future research should focus on improvement of this thesis by investigating higher order USTLD schemes such as 4×4 scheme as well as investigating other optimization algorithms such as genetic algorithm for such future ideas.

2.2 Optimization Algorithm using Artificial Intelligence Concept

In USTLD scheme with three transmit antennas, the mappers are manually designed from a bits-to-symbol constellation map based on hand crafted heuristic algorithm. Application of Artificial intelligence concept especially deep learning for mapper designs should be investigated in the future research.

2.3 Large Scale Fading for USTLD Scheme with Transmit Antennas

In this thesis, small scale fading that describes the signal level at the receiver after encountering obstacles for USTLD scheme with three transmit antennas are investigated. In practice, these channel models do not cover various types of fading [1]. Large scale fading is characterized by average path loss and shadow fading as a result of signal attenuation due to signal propagation over large distances and diffraction around large objects. Thus, large scale fading provides generalized fading that holds the promise to offer higher data rates and good quality of service for next-generation wireless systems [2] [3]. Hence, future research should investigate large scale fading for USTLD scheme with three transmit antennas.

2.4 Further Application of USTLD Scheme to Digital Broadcasting

The Digital Video Broadcasting (DVB) standards cover all aspects of digital television from transmission through interfacing, conditional access and interactivity for digital video, audio and data [4]. In this thesis, USTLD transmission scheme are developed for both the conventional standard DVB-S2 system and the latest extension approved in 2014 identified as DVB-S2X.

Motivated by the added additive modulation and coding (MODCOD)s scheme for DVB-S2X as an improvement over the conventional DVB-S2 standard, DVB-S2X is a technological standard that promotes high spectrum efficiency and offers the ability to operate with very-low carrier-to-noise and carrier-to-interference ratios for consumer electronics [4]. Hence, high-density APSK transmission schemes for USTLD with three transmit antennas become more attractive as possible future research for the latest DVB-S2X standard [5]. Besides, maximizing mutual information criteria for the transmission amplitude and phase should be further investigated in order to achieve lower peak-to-average power ratio.

2.5 Application of USTLD Scheme to Hybrid Satellite-Terrestrial MIMO

Hybrid Satellite-Terrestrial Communication for MIMO scheme has developed rapidly in the recent time due to the practical advantages for high speed data rate, wide coverage and ability to relief the terrestrial traffic congestion in urban areas [6], [7], [8] .

Motivated by the successful application of MIMO scheme for hybrid Satellite-Terrestrial networks as one of the most important enabling technologies for the future space-ground integrated technologies, future research should focus at applications of USTLD scheme for hybrid Satellite-Terrestrial network using generalized fading due to obstacles and shadowing between the satellite and terrestrial resulting in masking effect that led to difficulties in LOS communication components [8]. On the other hand, a combination of both large scale fading for satellite land mobile and small scale fading for terrestrial networks can be applied to MIMO scheme for hybrid Satellite-Terrestrial communication [9]. Hence, USTLD scheme should be investigated in this research focus for possible future ideas.

2.6 Application of Index Modulation for USTLD Scheme with three Transmit Antennas

Media-based modulation (MbM) with radio frequency (RF) mirror is a new technique in wireless communication system that has attracted significant attentions in the literature [10] [11] [12] [13]. In such literature, researchers have identified the following practical application of MbM to wireless communication systems: improves error performance by converting static multi-path fading channels into additive white Gaussian noise (AWGN); increases the number of channel realisations without requiring extra power; and significantly improves error performance by selecting a subset of channel realisations.

Motivated by the superior error performance application of recently proposed USTLD scheme and MbM with RF mirrors for two transmit antennas [14] over the conventional USTLD scheme [15],

future research should be aimed at investigating both MbM with RF mirrors for USTLD scheme with three transmit antennas.

2.7 Impact of Channel Estimation Error on USTLD Scheme with three Transmit Antennas

In this research, USTLD scheme with three transmit antennas have been introduced by assuming a known perfect channel state information (CSI) at the receiver. In practical wireless communication systems, a degradation in error performance is unavoidable when these systems are subjected to imperfect CSI [16] and hence impacted negatively link reliability. Future research should investigate various channel estimation error approaches for USTLD scheme with three transmit antennas.

References

[1] J. M. Moualeu, D. B. da Costa, W. Hamouda, U. S. Dias, and R. A. de Souza, "Performance Analysis of Digital Communication Systems Over $\alpha -\kappa$-μ Fading Channels," *IEEE Communications Letters*, vol. 23, no. 1, pp. 192–195, Oct. 2018.

[2] X. Li, S. Jin, H. A. Suraweera, J. Hou, and X. Gao, "Statistical 3-D beamforming for large-scale MIMO downlink systems over Rician fading channels," *IEEE Transactions on Communications*, vol. 64, no. 4, pp. 1529–1543, Feb. 2016.

[3] T. Van Chien, C. Mollén, and E. Björnson, "Large-scale-fading decoding in cellular massive MIMO systems with spatially correlated channels," *IEEE Transactions on Communications*, vol. 67, no. 4, pp. 2746–2762, Dec. 2018.

[4] Draft ETSI EN 302 307-2 V1.1.1 , "Digital video broadcasting (DVB), second generation framing structure, channel coding and modulation systems for broadcasting, interactive services, news gathering and other broadband satellite applications, part II: S2-Extensions (DVB-S2X)," ETSI, Tech. Rep., 2014-Oct.

[5] D4.1: Satellite Network Mission Requirements, "Broadband Access via Integrated Terrestrial and Satellite Systems (BATS)," European Project, Avanti PLLC, Tech. Rep., 2012.

[6] T. Wei, W. Feng, Y. Chen, C.-X. Wang, N. Ge, and J. Lu, "Hybrid satellite-terrestrial communication networks for the maritime internet of things: key technologies, opportunities, and challenges," *arXiv preprint arXiv:1903.11814*, 2019.

[7] L. Gao, S. Zhang, Z. Liu, J. Lin, S. Wang, and C. Xing, "An overview of multi-antenna technologies for space-ground integrated networks," *Science China Information Sciences*, vol. 59, no. 12, p. 121301, Dec. 2016.

[8] K. An, M. Lin, T. Liang, J.-B. Wang, J. Wang, Y. Huang, and A. L. Swindlehurst, "Performance analysis of multi-antenna hybrid satellite-terrestrial relay networks in the presence of interference," *IEEE Transactions on Communications*, vol. 63, no. 11, pp. 4390–4404, Aug. 2015.

[9] L. Yang and M. O. Hasna, "Performance analysis of amplify-and-forward hybrid satellite-terrestrial networks with cochannel interference," *IEEE Transactions on Communications*, vol. 63, no. 12, pp. 5052–5061, Oct. 2015.

[10] A. K. Khandani, "Media-based modulation: A new approach to wireless transmission," in *2013 IEEE International Symposium on Information Theory*. IEEE, 2013, pp. 3050–3054.

[11] ——, "Media-based modulation: Converting static Rayleigh fading to AWGN," in *2014 IEEE International Symposium on Information Theory*. IEEE, 2014, pp. 1549–1553.

[12] E. Seifi, M. Atamanesh, and A. K. Khandani, "Media-based MIMO: A new frontier in wireless communications," *arXiv preprint arXiv:1507.07516*, 2015.

[13] B. S. Adejumobi and N. Pillay, "RF mirror media-based space-time block coded spatial modulation techniques for two time-slots," *IET Communications*, vol. 13, no. 15, pp. 2313–2321, Jun. 2019.

[14] N. Pillay and H. Xu, "Uncoded space-time labeling diversity—Application of media-based modulation with RF mirrors," *IEEE Communications Letters*, vol. 22, no. 2, pp. 272–275, Nov. 2017.

[15] H. Xu, K. Govindasamy, and N. Pillay, "Uncoded space-time labeling diversity," *IEEE Communications Letters*, vol. 20, no. 8, pp. 1511–1514, Jun. 2016.

[16] J. Chung, S. Park, and S. Lee, "Effect of channel estimation errors on the performance of MIMO-OFDM systems in correlated fading channels," in *2006 Canadian Conference on Electrical and Computer Engineering*. IEEE, 2006, pp. 478–481.